Bioactive glycerophospholipids and their role in modulating neuronal vulnerability following cerebral ischemia

Andrew James Syrett

Thesis submitted to the

Faculty of Graduate and Postdoctoral Studies

In partial fulfillment of the requirements

For the MSc degree in Biochemistry

Biochemistry, Microbiology and Immunology

Faculty of Medicine

University of Ottawa

© Andrew James Syrett, Ottawa, Canada, 2012

Abstract.

Stroke is a devastating and debilitating condition resulting from a blockage or hemorrhage in the vasculature of the brain. Despite extensive research, the etiology and pathophysiology of the disease at the level of the cell membrane are poorly understood, and effective treatment has been elusive. Though much research has shown marked increases in lipid metabolism following stroke, the impact of these changes have often been overlooked given the technical challenges associated with identifying regionally specific changes in degenerating tissue. The advent of lipidomics – a systems biology approach to the large-scale profiling of individual lipid species in tissues – has renewed interest in understanding the role of membrane lipids and their metabolites in the cell and in ischemic injury. In this thesis, I have used an unbiased LC-ESI-MS-based lipidomic approach to profile the small molecular weight glycerophosphocholine second messenger lipidome in anterior and posterior regions of cortex and striatum in the forebrain of wild-type and platelet activating factor receptor (PAFR) null-mutant mice before and after middle cerebral artery occlusion (MCAO). From these profiles, I have outlined the potential use of lipid second messenger distribution as topographic landmarks to identify functional subdomains within neural tissue. Further, I have demonstrated that ischemia does not simply disrupt lipid second messenger metabolism globally but produces regionally specific changes in discrete species and that these changes are altered by the loss of lipid regulatory effectors (i.e., PAFR null mutation). Based on the lipid species identified in this profile of healthy and ischemic tissue, I proposed that tight regulation of PC(O-22:6/2:0) homeostasis by PAFR-expressing microglia is

required for proper dopaminergic signaling in prefrontal cortex. Finally, I have outlined a model whereby increased PAF synthesis following ischemia contributes the inflammatory response by promoting blood-brain barrier permeability, microglial activation and immune cell infiltration in a PAFR-dependent manner.

Acknowledgements

First and foremost, I would like to extend my most heartfelt thanks to my supervisor, Dr. Steffany Bennett. Her enthusiasm and passion for biomedical research are infectious. As an undergraduate student in the Neural Regeneration Laboratory, her support and commitment were instrumental in my success and continuation into graduate studies. As an M.Sc student, her availability and constant support were instrumental in the success of this project. I am also indebted to my Thesis Advisory Committee members, Dr Daniel Figeys, Dr. Ruth Slack and Dr. Jianjun Li for their guidance and expertise without which this project would not have been possible. I would also like to thank my co-mentors and peers in the CIHR Training Program in Neurodegenerative Lipidomics for sharing their knowledge and expertise.

To my colleagues at NRL, past and present – without you, this journey would have been simply a cog in the wheel of life. Your bottomless support and endless friendship have made my five years in the lab some of the best of my life. I was truly blessed to have working colleagues that I am proud to call my best friends.

Lastly, I need to thank my family for their constant support. Mom and Dad, you have provided me with a foundation upon which to grow as a person, and you deserve so much credit in my success. Ian, your support and friendship have been so helpful – I am lucky to be able to call you my brother. Finally, I would like to thank all of my friends for their constant companionship and encouragement.

List of Abbreviations.

4-VO	four-vessel occlusion
AA	arachidonic acid
Acetyl-CoA	acetyl Coenzyme A
ANOVA	analysis of variance
ATP	adenosine Triphosphate
CBF	cerebral blood flow
COX-2	cyclooxygenase-2
cPLA2	cytosolic phospholipase A2
D(1), D(2)	dopamine receptors 1, 2
DHA	docosahexaenoic acid
DNA	deoxyribonucleic acid
ESI	electrospray ionization
HIV	Human immunodeficiency virus
HPLC	high performance liquid chromatography
LC	liquid chromatography
LC-ESI-MS	high performance liquid chromatography electrospray ionization tandem mass spectrometry
LPC	lysophosphatidylcholine
LPCAT	lysophosphatidylcholine acyl-transferase
MALDI	matrix-assisted laser desorption ionization
MCA	middle cerebral artery
MCAO	middle cerebral artery occlusion
MS	mass spectrometry
NMDA	N-methyl-D-aspartate
NPD1	Neuroprotectin D1
PA	peak area
PAF	platelet-activating factor
PAF-AH	platelet-activating factor acetylhydrolase
PAFR	platelet-activating factor receptor
PA_N	normalized peak area
PPT1	palmitoyl protein thioesterase-1
PtdCho	phosphatidylcholine
PtdH	phosphatidic acid
PtdIns	thosphatidylinositol
sPLA2	secretory phospholipase A2
TIA	transient ischemic attack
TNF-a	tumor necrosis factor alpha
ToF	time-of-flight
tPA	tissue plasminogen activator

Table of Contents

Thesis Abstract ..... **i**
Acknowledgements ..... **iii**
List of Abbreviations ..... **iv**
Table of Contents ..... **v**
List of Figures ..... **viii**
List of Tables ..... **xi**
1. Introduction ..... **i.**
1.1 What is stroke? 1
1.2 Animal models of cerebral ischemia 3
1.3 Stroke pathophysiology 5
1.4 Different mechanisms of injury underlie damage in the ischemic core and surrounding penumbra 7
1.5 Aberrant membrane metabolism results from loss of calcium homeostasis following ischemic injury 7
1.6 Lipid second messenger biogenesis 9
1.7 Lipidomics 13
1.8 Lipidomic approaches to the study of stroke pathophysiology 21
1.9 Lipid second messenger biology 22
1.10 Objectives and hypothesis 23
2. Materials & methods **25**
2.1 MCAO-reperfusion 25
2.2 Lipid extraction 26
2.3 Sample preparation and LC-ESI-MS 27
2.4 Data analysis 27
2.5 Heatmap analysis 28
2.6 Statistical analysis 29
3. Results **30**
3.1 Glycerophospholipid second messenger profiles are regionally specific and display an anterior-posterior gradient in the uninjured C57Bl/6 striatum and frontal cortex. 30
3.1.1 Lipid differences between anterior and posterior regions of uninjured frontal cortex 30
3.1.2 Lipid differences between anterior and posterior regions of uninjured striatum in the forebrain 38
3.1.3 Lipid differences between anterior regions of uninjured cortex and striatum in the forebrain 45
3.1.4 Lipid differences between posterior regions of uninjured cortex and striatum in the forebrain 53
3.2 MCAO disrupts glycerophosphocholine metabolism with regional specificity in C57Bl/6 striatum and frontal cortex 61
3.2.1 Lipid differences between anterior and posterior regions of ischemic frontal cortex 61
3.2.2 Lipid differences between anterior and posterior regions of ischemic striatum 66

3.2.3 Lipid differences between anterior regions of ischemic striatum and frontal cortex 71
3.2.4 Lipid differences between posterior regions of ischemic striatum and frontal cortex 76
3.3 PAFR null-mutation alters glycerophospholipid metabolism in uninjured brain and following MCAO 76
3.3.1 Effect of PAFR null-mutation on anterior-posterior gradients of glycerophosphocholine second messenger lipids in the uninjured frontal cortex 81
3.3.2 Effect of PAFR null-mutation on anterior-posterior gradients of glycerophosphocholine second messenger lipids in the uninjured striatum 81
3.3.3 Effect of PAFR null-mutation on medial-lateral gradients of glycerophosphocholine second messenger lipids between anterior regions the uninjured striatum and frontal cortex 84
3.3.4 Effect of PAFR null-mutation on medial-lateral gradients of glycerophosphocholine second messenger lipids between posterior regions of the uninjured striatum and frontal cortex 89
3.4 MCAO altered glycerophospholipid metabolism in PAFR$^{-/-}$ mice 92
3.4.1 Lipid differences between anterior and posterior regions of ischemic frontal cortex in PAFR$^{-/-}$ mice 92
3.4.2 Lipid differences between anterior and posterior regions of ischemic frontal striatum in PAFR$^{-/-}$ mice 97
3.4.3 Lipid differences between anterior regions of ischemic frontal striatum and cortex in PAFR$^{-/-}$ mice 102
3.4.4 Lipid differences between posterior regions of ischemic frontal striatum and cortex in PAFR$^{-/-}$ mice 102
3.5 Region-specific differences in discrete glycerophosphocholine second messenger lipid abundance in frontal cortex and striatum between C57Bl/6 and PAFR null-mutant mice following MCAO 107
3.5.1 Lipid differences in anterior frontal cortex between wild-type C57Bl/6 and PAFR$^{-/-}$ following MCAO 107
3.5.2 Lipid differences in posterior frontal cortex between wild-type C57Bl/6 and PAFR$^{-/-}$ following MCAO 116
3.5.3 Lipid differences in anterior striatum between wild-type C57Bl/6 and PAFR$^{-/-}$ following MCAO 116
3.5.4 Lipid differences in posterior striatum between wild-type C57Bl/6 and PAFR$^{-/-}$ following MCAO 116
4. Discussion 128
4.1 Summary 128
4.2 Defining functional domains in brain architecture through lipid topography 128
4.3 Is crosstalk between neurotoxicity and neuroprotection mediated by specific lipid second messengers in the posterior frontal cortex following MCAO 134
4.4 PAFR null-mutant animals are deficient in PAF clearance 137
4.5 Conclusion 140

5. References 144
6. Appendix 1 154

List of Figures

Figure 1.1 The Land's Cycle 11
Figure 1.2 Lipid analysis by mass spectrometry 18
Figure 3.1.1a Global differences in glycerophosphocholine second messenger lipid abundance between anterior and posterior regions of uninjured wild-type frontal cortex 32
Figure 3.1.1b Heatmap clustering of relative glycerophosphocholine lipid second messenger abundance between anterior and posterior regions of uninjured wild-type frontal cortex 34
Figure 3.1.1c Anterior-posterior gradients of glycerophosphocholine lipid second messenger abundance in uninjured wild-type frontal cortex 36
Figure 3.1.2a Global differences in glycerophosphocholine second messenger lipid abundance between anterior and posterior regions of uninjured wild-type striatum 40
Figure 3.1.2b Heatmap clustering of relative glycerophosphocholine lipid second messenger abundance between anterior and posterior regions of uninjured wild-type striatum 42
Figure 3.1.2c Anterior-posterior gradients of glycerophosphocholine lipid second messenger abundance in uninjured wild-type striatum 44
Figure 3.1.3a Global differences in glycerophosphocholine second messenger lipid abundance between anterior regions of uninjured wild-type frontal cortex and striatum 47
Figure 3.1.3b Heatmap clustering of relative glycerophosphocholine lipid second messenger abundance between anterior regions of uninjured wild-type frontal cortex and striatum 49
Figure 3.1.3c Medial-lateral gradients of glycerophosphocholine lipid second messenger abundance between anterior regions of uninjured wild-type frontal cortex and striatum 51
Figure 3.1.4a Global differences in glycerophosphocholine second messenger lipid abundance between anterior and posterior regions of uninjured wild-type frontal cortex 55
Figure 3.1.4b Heatmap clustering of relative glycerophosphocholine lipid second messenger abundance between posterior regions of uninjured wild-type frontal cortex and striatum 57
Figure 3.1.4c Medial-lateral gradients of glycerophosphocholine lipid second messenger abundance between posterior regions of uninjured wild-type frontal cortex and striatum 59
Figure 3.2.1a Heatmap clustering of relative glycerophosphocholine lipid second messenger abundance between anterior and posterior regions of wild-type frontal cortex following MCAO 63
Figure 3.2.1b Differences in glycerophosphocholine lipid second messenger abundance between anterior and posterior frontal cortex in uninjured wild-type mice and following MCAO 65
Figure 3.2.2a Heatmap clustering of relative glycerophosphocholine lipid second

messenger abundance between anterior and posterior regions of wild-type striatum following MCAO 68
Figure 3.2.2b Differences in glycerophosphocholine lipid second messenger abundance between anterior and posterior striatum in uninjured wild-type mice and following MCAO 70
Figure 3.2.3a Heatmap clustering of relative glycerophosphocholine lipid second messenger abundance between anterior regions of wild-type frontal cortex and striatum following MCAO..... 73
Figure 3.2.3b Differences in glycerophosphocholine lipid second messenger abundance between anterior regions of frontal cortex and striatum in uninjured wild-type mice and following MCAO..... 75
Figure 3.2.4a Heatmap clustering of relative glycerophosphocholine lipid second messenger abundance between posterior regions of wild-type frontal cortex and striatum following MCAO..... 78
Figure 3.2.4b Differences in glycerophosphocholine lipid second messenger abundance between posterior regions of frontal cortex and striatum in uninjured wild-type mice and following MCAO..... 80
Figure 3.4.1a Heatmap clustering of relative glycerophosphocholine lipid second messenger abundance between anterior and posterior regions of PAFR-/- frontal cortex following MCAO 94
Figure 3.4.1b Differences in glycerophosphocholine lipid second messenger abundance between anterior and posterior frontal cortex in uninjured PAFR-/- mice and following MCAO..... 96
Figure 3.4.2a Heatmap clustering of relative glycerophosphocholine lipid second messenger abundance between anterior and posterior regions of PAFR-/- striatum following MCAO 99
Figure 3.4.2b Differences in glycerophosphocholine lipid second messenger abundance between anterior and posterior striatum in uninjured PAFR-/- mice and following MCAO..... 101
Figure 3.4.3a Heatmap clustering of relative glycerophosphocholine lipid second messenger abundance between anterior regions of PAFR-/- frontal cortex and striatum following MCAO..... 104
Figure 3.4.3b Differences in glycerophosphocholine lipid second messenger abundance between anterior regions of frontal cortex and striatum in uninjured PAFR-/- mice and following MCAO..... 106
Figure 3.4.4a Heatmap clustering of relative glycerophosphocholine lipid second messenger abundance between posterior regions of PAFR-/- frontal cortex and striatum following MCAO..... 109
Figure 3.4.4b Differences in glycerophosphocholine lipid second messenger abundance between posterior regions of frontal cortex and striatum in uninjured PAFR-/- mice and following MCAO 111
Figure 3.5.1a Heatmap clustering of relative glycerophosphocholine lipid second messenger abundance in anterior regions of frontal cortex between wild-type and PAFR-/- mice following MCAO 113
Figure 3.5.1b Differences in glycerophosphocholine lipid second messenger abundance in anterior frontal cortex between uninjured wild-type and PAFR-/- mice and following MCAO..... 115

Figure 3.5.2a Heatmap clustering of relative glycerophosphocholine lipid second messenger abundance in posterior regions of frontal cortex between wild-type and PAFR-/- mice following MCAO 118
Figure 3.5.2b Differences in glycerophosphocholine lipid second messenger abundance in posterior frontal cortex between uninjured wild-type and PAFR-/- mice and following MCAO..... 120
Figure 3.5.3a Heatmap clustering of relative glycerophosphocholine lipid second messenger abundance in anterior regions of striatum between wild-type and PAFR-/- mice following MCAO..... 122
Figure 3.5.4a Heatmap clustering of relative glycerophosphocholine lipid second messenger abundance in posterior regions of striatum between wild-type and PAFR-/- mice following MCAO..... 125
Figure 3.5.4b Differences in glycerophosphocholine lipid second messenger abundance in posterior striatum between uninjured wild-type and PAFR-/- mice and following MCAO..... 127
Figure 4.1 Dopamine signaling in the prefrontal cortex..... 131
Figure 4.2 PAF accumulation in ischemic tissue promotes a PAFR-dependent response leading to increased inflammation..... 143
Figure A1.1a Heatmap clustering of relative glycerophosphocholine lipid second messenger abundance between anterior and posterior regions of uninjured PAFR-/- frontal cortex. 156
Figure A1.1b Anterior-posterior gradients of glycerophosphocholine lipid second messenger abundance in uninjured PAFR-/- frontal cortex..... 158
Figure A1.2a Heatmap clustering of relative glycerophosphocholine lipid second messenger abundance between anterior and posterior regions of uninjured PAFR-/- striatum 160
Figure A1.2b Anterior-posterior gradients of glycerophosphocholine lipid second messenger abundance in uninjured PAFR-/- striatum..... 162
Figure A1.3a Heatmap clustering of relative glycerophosphocholine lipid second messenger abundance between anterior regions of uninjured PAFR-/- frontal cortex and striatum 165
Figure A1.3b Medial-lateral gradients of glycerophosphocholine lipid second messenger abundance in anterior regions of uninjured PAFR-/- frontal cortex and striatum 167
Figure A1.4a Heatmap clustering of relative glycerophosphocholine lipid second messenger abundance between posterior regions of uninjured PAFR-/- frontal cortex and striatum 170
Figure A1.4b Medial-lateral gradients of glycerophosphocholine lipid second messenger abundance in posterior regions of uninjured PAFR-/- frontal cortex and striatum 172

List of Tables

Table 3.1.1 Lipid species that show significantly altered abundance between anterior and posterior regions of uninjured frontal cortex by paired t-test 38

Table 3.1.2 Lipid species that show significantly altered abundance between anterior and posterior regions of uninjured frontal striatum by paired t-test 45

Table 3.1.3 Lipid species that show significantly altered abundance between anterior regions of uninjured frontal cortex and striatum by paired t-test 53

Table 3.1.4 Lipid species that show significantly altered abundance between posterior regions of uninjured frontal cortex and striatum by paired t-test 61

Table 3.3.1 Relative abundance of glycerophosphocholine lipid second messenge species between anterior and posterior regions of uninjured cortex in wild-type and PAFR-/- animals 83

Table 3.3.2 Relative abundance of glycerophosphocholine lipid second messenger species between anterior and posterior regions of uninjured striatum in wild-type and PAFR-/- animals 86

Table 3.3.3 Relative abundance of glycerophosphocholine lipid second messenger species between anterior regions of uninjured frontal cortex and striatum in wild-type and PAFR-/- animals 88

Table 3.3.4 Relative abundance of glycerophosphocholine lipid second messenger species between posterior regions of uninjured frontal cortex and striatum in wild-type and PAFR-/- animals 91

Table A1.1 Lipid species that show significantly altered abundance between anterior and posterior regions of uninjured $PAFR^{-/-}$ frontal cortex by paired t-test 154

Table A1.2 Lipid species that show significantly altered abundance between anterior and posterior regions of uninjured $PAFR^{-/-}$ frontal striatum by paired t-test 163

Table A1.3 Lipid species that show significantly altered abundance between anterior regions of uninjured $PAFR^{-/-}$ frontal cortex and striatum by paired t-test 163

Table A1.4 Lipid species that show significantly altered abundance between posterior regions of uninjured $PAFR^{-/-}$ frontal cortex and striatum by paired t-test 168

1. Introduction.

1.1 What is stroke?

Cerebral ischemia, or “stroke”, is defined as an occlusion or hemorrhage of a blood vessel supplying blood and oxygen to the brain. This acute syndrome results in extensive loss of neurons leading to severe impairment of neurological function. The effects of stroke present staggering costs, both financially and emotionally. Care for stroke victims and survivors costs an estimated $2.7 billion annually, in physician services, hospital costs, lost wages and decreased productivity (HSF, 2006). Canadians suffer more than 50 000 strokes each year, resulting in over 14 000 deaths (HSF, 2006). Further, an additional 15 000 Canadians suffer transient ischemic attacks (TIA) – temporary occlusions of small arteries that do not produce appreciable tissue damage. While not resulting in severe neurological impairment, victims of TIA are five times more likely to suffer a symptomatic stroke in the two years that follow (HSF, 2006). In fact, 43% of stroke patients involved in a population-study in Oxford, UK, had suffered a TIA within 7 days of ischemic stroke presentation (Rothwell et al., 2011; Rothwell and Warlow, 2005). Further, TIA, lacunar and silent (asymptomatic) strokes are associated with increased prevalence of post-stroke dementias. Overall, recurrent strokes of any kind increase the likelihood of developing dementia two-fold (Gorelick et al., 2011).

Despite extensive research, the mechanisms underlying the etiology of the ischemic disease are poorly understood. On a physiological level, hemorrhagic stroke occurs when a blood vessel within the brain (intracerebral hemorrhage) or

underlying the arachnoid mater (subarachnoid hemorrhage) ruptures resulting in uncontrolled bleeding either in the brain, or in the space between the brain and the skull. Ischemic stroke occurs when a blood vessel within the brain is blocked by a clot either formed in the vessel directly (thrombolic stroke) or formed in a vessel elsewhere in the body that subsequently travels to a vessel in the brain (embolic stroke) (Krishnaswamy et al.,2010).

Therapeutic approaches to date have proven to be only passably successful. The most successful treatments require timely intervention. It is estimated that every minute a supratentorial stroke goes untreated, the victim loses 1.9 million neurons, 230 million synapses and 12 km of myelinated fibers – equivalent to 3.1 weeks of normal aging (Saver, 2006). In this light, the Canadian Best Practices For Stroke Care outlines a rapid intervention protocol whereby tissue plasminogen activator (tPA) – a potent thrombolytic enzyme – should be administered within 4.5 hours of ischemic stroke onset. Further, the effectiveness of tPA therapy decreases significantly with time, stressing the need for rapid intervention (Carpenter et al., 2011; Lees et al., 2010; Network, 2011). Unfortunately, patient non-compliance is one of the leading causes of decreased treatment efficacy. In Canada, the median hospital arrival time following symptom onset is 7 hours – outside the time window of tPA efficacy (Network, 2011). It is clear, then, that better understanding of the etiology and pathophysiology of the acute cerebrovascular syndrome is required to develop novel therapeutic approaches that may be effective beyond the acute phase of ischemic disease.

1.2 Animal models of cerebral ischemia.

There are two main approaches to modeling stroke pathophysiology in small rodents. Global ischemia is defined as a reduction of cerebral blood flow (CBF) throughout most or all of the brain, while focal ischemia is a reduction of cerebral blood flow in a specific area of the brain (Traystman, 2003). In both cases, cerebral blood flow is most often restricted either by cauterization (permanent ischemia) or by the use of a ligature or suture (transient ischemia) to block the passage of blood through a specific artery. Global ischemia is most often modeled in rats, and is commonly achieved using a four-vessel occlusion (4-VO) model first described by Pulsinelli and Brierley in 1979 – a two step process in which both the left and right vertebral arteries and the left and right common carotid arteries are occluded, restricting blood flow to the brain in its entirety (Pulsinelli and Brierley, 1979; Traystman, 2003). Global ischemia has proven difficult to model in mice - the 4-VO model results in high mortality rates, and high incidence of seizure (Traystman, 2003). Transient focal cerebral ischemia can be modeled experimentally in both rats and mice using one of two approaches – the endothelin-1 microinjection paradigm, or the middle cerebral artery occlusion paradigm. Endothelin-1 is an endogenous vasoconstrictive peptide produced during ischemia that can be injected into the vicinity of the middle cerebral artery (MCA) leading to significantly reduced CBF in the MCA and surrounding tissue. Following an acute period of severe CBF restriction, blood flow begins to slowly return to normal levels in a dose-dependent manner (Sharkey and Butcher, 1995; Sicard and Fisher, 2009). Alternatively, blood flow to the middle cerebral artery can be reliably restricted by the introduction of a

silicon-coated nylon filament into the arterial lumen of the internal carotid artery, and advancing it beyond the bifurcation of the middle cerebral artery (Hara et al., 1996; Whitehead et al., 2010). The intraluminal MCAO model is the most common model of transient focal ischemia in rats. Because of the relative ease with which mice can be genetically manipulated, the intraluminal MCAO model has been adapted for use in mice, however, it's use faces certain challenges (Sicard and Fisher, 2009). The extent of ischemic injury in mice is largely dependent on strain. C57Bl/6 mice demonstrate increased susceptibility to ischemic injury, resulting in reproducibly larger infarcts compared to the 129/Sv strain (Connolly et al., 1996). Because embryonic stem cells for the purpose of transgenic strain development are routinely obtained from 129/Sv mice, genetically modified strains must be back-bred into the C57Bl/6 strain for at least 12 generations (Connolly et al., 1996; Gerlai, 1996). The time required to generate these congenic strains, then, is an important limitation to the use of mice for stroke research. Further, the reproducibility of injury depends on a variety of physiological factors, including size, core temperature, cerebral blood flow, and cerebral vascular physiology (Belayev et al., 1999; Connolly et al., 1996). During the procedure, core temperature is monitored and maintained at 37°C and blood flow can be monitored by Laser Doppler Flowmetry. Kitagawa *et al.* have suggested that the cerebral vasculature, and more specifically the integrity of the posterior communicating artery and the circle of Willis are key determinants of MCA occlusion success (Belayev et al., 1999; Kitagawa et al., 1998). Moreover, the length of the occlusion is a key determinant of the extent of damage resulting from MCAO. Total infarct volume increases with an increase in occlusion time from 30 to 60 minutes, but does not increase significantly beyond 60 minutes. Ischemic injury

after 30 minutes of MCA occlusion is inconsistent, but primarily localized to parts of the striatum and lateral septum. After 60 minutes of occlusion, the injury is far more reproducible, and results in ischemic lesions extending to parts of the frontoparietal somatosensory cortex, striatum, ventral thalamus and hippocampus (Belayev et al., 1999; Kitagawa et al., 1998). In mice, MCA occlusion of all durations results in extensive neurological deficits immediately following surgery, but only mice that have undergone occlusions of 30 or 60 minutes show significant neurological impairment following 24 hours of reperfusion/survival (Belayev et al., 1999; Kitagawa et al., 1998). For these reasons, the 1-hour coated nylon filament MCAO paradigm is one of the most common mouse models of transient focal cerebral ischemia, as it results in extensive histopathological injury, yet permits neurological recovery after 24 hours of reperfusion.

1.3 Stroke pathophysiology.

Stroke etiology progresses in two phases (reviewed in (Mehta et al., 2007)). The first occurs acutely following the development of the blood vessel occlusion. The tissue immediately surrounding the occluded vessel, the ischemic core, undergoes a necrotic form of cell death resulting from the failure of energy production. Restriction of blood flow deprives neurons in the vicinity of the occlusion of the oxygen and glucose required as substrates to fuel the electron transport chain for the production of adenosine triphosphate (ATP) (Dirnagl et al., 1999; Lowry et al., 1964). In the absence of ATP, neurons lose their ability to regulate the ionic gradients, quickly depolarize (Silver and Erecinska, 1990) and suppress their electrical activity (Mayevsky and Chance, 1975; Williams and Grossman, 1970). At

the same time, intracellular Ca^{2+} levels increase as neurons lose their ability to sequester Ca^{2+} in their endoplasmic reticular and mitochondrial pools (Belousov et al., 1995; Katchman and Hershkowitz, 1993; Martin et al., 1994; Wojda et al., 2008). Intracellular accumulation of Ca^{2+} leads to the release of excitatory amino acids, including the excitotoxic neurotransmitter glutamate (Benveniste et al., 1984). This release is exacerbated by the absence of ATP, preventing the energy-dependent re-uptake of these excitatory amino acids at the pre-synaptic membrane leading to their accumulation in the synaptic cleft (Dirnagl et al., 1999). Extracellular glutamate can then bind and activate N-methyl-D-aspartate (NMDA) receptors on the post-synaptic membrane (Silver and Erecinska, 1990). NMDA receptors are members of the ionotropic glutamate receptor family of ligand-gated ion channels permeable to Na^{+} Ca^{2+} and K^{+}. In response to activation by extracellular glutamate, they allow a net influx of Ca^{2+} and efflux of K^{+} that exacerbates the accumulation of Ca^{2+} ions in both the pre- and post-synaptic neurons (Dingledine et al., 1999; Silver and Erecinska, 1990). As a result, Na^{+} and Cl^{-} ions are able to diffuse into the cell through monovalent ion channels. This movement of ions from the extracellular space into the cell creates an osmotic gradient, down which water passively diffuses. This influx of water leads to edema, which may ultimately rupture the cell membrane, releasing the contents into the extracellular space (Farooqui et al., 2007a; Majno and Joris, 1995; Mehta et al., 2007).

1.4 Different mechanisms of injury underlie damage in the ischemic core and surrounding penumbra.

The ischemic penumbra represents a physiologically distinct area surrounding the ischemic core that consists of initially viable tissue. While the ischemic core undergoes necrotic death as a result of edema stemming from energy depletion, the penumbral tissue is perfused by collateral vasculature, and can sustain ATP production temporarily. The penumbra, however, is not protected from the electrical stimulation of neurons in the ischemic core. As the neurons in the core depolarize, this signal is propagated throughout the surrounding tissue. Neurons in the penumbra, however, are still capable of producing some of the ATP required to stimulate repolarization. As a result, these same neurons can be further depolarized in response to increasing extracellular glutamate or K^+ levels (Dirnagl et al., 1999; Hossmann, 1996; Mehta et al., 2007), a process known as peri-infarct depolarization (Doyle et al., 2008). Prolonged rounds of depolarization-repolarization are energetically demanding, and can overcome the cell's ability to produce ATP from reduced collateral blood flow (Pinard et al., 2002). As a result, these peri-infarct depolarizations contribute to penumbral cell death and result in larger infarct areas (Mies et al., 1993).

1.5 Aberrant membrane metabolism results from loss of calcium homeostasis following ischemic injury.

Accumulation of intracellular Ca^{2+} in penumbral tissue is responsible, in part, for the expansion of ischemic injury. Sustained neuronal elevations in Ca^{2+} initiates

multiple cell death pathways associated with excitotoxicity (Dirnagl et al., 1999). Calcium-mediated activation of proteolytic enzymes, including members of the Ca^{2+}-dependent calpain and caspase families, leads to cleavage of microtubule-associated proteins, neurofilaments, actin and spectrin and, ultimately, cytoskeletal degradation (Banik et al., 1997; Fischer et al., 1991; Johnson et al., 1989; Potter et al., 1998). Further, intracellular accumulation of Ca^{2+} leads to the activation of multiple enzymes responsible for the hydrolysis of structural membrane lipids to bioactive second messengers.

Group IV phospholipase A_2 (cytosolic phospholipase A_2,cPLA_2) (Arai et al., 2001), Ca^{2+}-dependent phospholipases capable of cleaving arachidonic acid from the *sn*-2 position of membrane phospholipids are activated soon after the onset of ischemia. Secretory PLA_2 (sPLA_2, group I, II, III, V, X, XI PLA_2s) enzymes are also activated. sPLA_2 family member sPLA_2-IIA is involved in inflammatory processes, and like other PLA_2 enzymes, can act upon the *sn*-2 position of membrane phospholipids on the outer leaflet of neural membranes, or can be internalized by binding N-type receptors on the surface of neighbouring neurons (Lambeau et al., 1989; Matsuzawa et al., 1996; Rodriguez De Turco et al., 2002; Sun et al.; Sun et al., 2004). Following MCAO, increased levels of TNF-α and interleukin-1β lead to increased sPLA_2 IIA mRNA transcription in activated astrocytes within 30 minutes of occlusion, and again in penumbral tissue between 12 hours and 14 days after MCA occlusion, but interestingly, protein was not detected until 24 hours after reperfusion, and was restricted to the ischemic penumbra (Adibhatla and Hatcher, 2007; Lin et al., 2004). Increased membrane lipid metabolism by activated PLA_2s leads to

compromised membrane integrity and is a hallmark of early ischemic injury – intracellular accumulation of free fatty acids, including arachidonic acid, is seen within minutes of the onset of ischemia (Farooqui et al., 2007a; Majno and Joris, 1995; Raichle, 1983; Rehncrona et al., 1982). Further, $sPLA_2$-IIA released from activated astrocytes contributes to neuronal injury by compromising membrane integrity in penumbral tissue following 24 hours of reperfusion (Adibhatla and Hatcher, 2007).

1.6 Lipid second messenger biogenesis.

The prototypical structural membrane phospholipid contains a saturated fatty acid chain esterified to the *sn*-1 position of the glycerol backbone, a poly-unsaturated fatty acid esterified to the *sn*-2 position, and a phosphodiester-linked polar "head-group" at the *sn*-3 (including choline, ethanolamine, serine, inositol etc…). Hydrolysis of the acyl-linked arachidonic acid at the *sn*-2 position of a membrane phospholipid by an activated PLA_2 yields a free arachidonate ion, and a biologically active lysophospholipid (Figure 1.1). Though the fate of the free arachidonate moiety has been well described (Rink and Khanna, 2011), the fate of the lysophospholipid backbone is poorly understood. When the membranous precursor is a phosphatidylcholine, the resulting lysophosphatidylcholine (LPC) can exert myriad intra- and extra-cellular functions. LPC is capable of activating microglia (Schilling et al., 2004) and phospholipase D – a phospholipase capable of cleaving the *sn*-3 position of a phosphatidylcholine, producing phosphatidic acid – which itself can be metabolized to the bioactive lysophosphatidic acid (Gomez-Munoz et al., 1999). Further, the LPC isoform containing a docosahexaenoic acid

Figure 1.1. The Land's Cycle. A schematic representation of the enzymatic catabolism (blue arrows) of membranous phosphatidylcholine lipids to bioactive lysophosphatidylcholine (LPC) and platelet-activating factor (PAF) species. The reverse, anabolic process is depicted by red arrows.

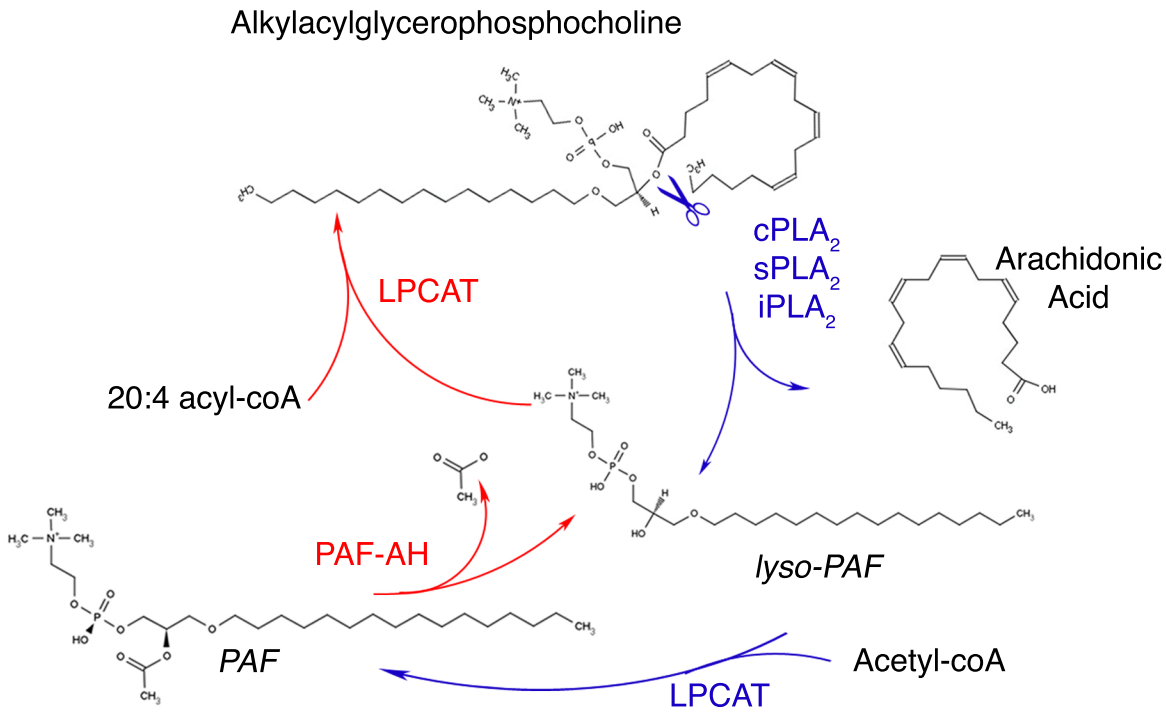
Alkylacylglycerophosphocholine
cPLA2
sPLA2
iPLA2
Arachidonic
Acid
LPCAT
20:4 acyl-coA
PAF-AH
lyso-PAF
PAF
Acetyl-coA
LPCAT

(DHA) moiety at the *sn*-2 position, 1-docosahexaenoyl-2-lysophosphatidylcholine, is the primary transport form of DHA in the blood (Bernoud et al., 1999; Lagarde et al., 2001). DHA, an essential ω-3 poly-unsaturated fatty acid, is highly abundant in ischemic tissue following stroke, and through the action of 15-lipoxygenase-1, can be converted to the potent anti-inflammatory autacoid neuroprotectin-D1 (NPD1). NPD1 has been shown to be neuroprotective and can dampen the severity of MCAO injury (Belayev et al., 2011). It is clear, then, that some LPC molecular species may be involved in mechanisms of neuroprotection, while others may exacerbate injury following cerebral ischemia.

Although the majority of membrane lipids display the canonical acyl linkages at both the *sn*-1 and *sn*-2 positions, there are a small percentage of membrane phospholipids that display subtle yet significant differences from this stereotype, and exhibit fundamentally different localizations and biophysical properties. Plasmalogens, defined by a vinyl ether at the *sn*-1 position and arachidonic acid at the *sn-2* are rare membrane lipids enriched in lipid rafts (Pike et al., 2002) Conversely, although lipids containing docosahexaenoic acid moieties (22:6) at the *sn*-2 position are most abundant in neural membranes, they seldom localize to ordered (raft) membrane domains (Wassall and Stillwell, 2008).

Ether-phospholipids, characterized by an ether linked alkyl chain at the *sn*-1 position of the glycerol backbone and ethanolamine or choline headgroups, represent more than 4% of total brain phospholipids (Braquet et al., 1989). Choline containing alkylacylglycerophosphocholine membrane lipids and plasmalogens are the precursors to a family of potent bioactive lipid second messengers known as

platelet-activating factors (PAF). If one of these relatively rare membrane lipids is the source of PLA_2 (plasmalogen-selective PLA_2 in the case of plasmalogens (Farooqui and Horrocks, 2001)) mediated arachidonic acid release, the resulting species is a *lyso*-PAF lipid that, in turn, can be converted by lysophosphatidylcholine acyltransferases (LPCAT1 and 2) back to an alkylacyl-linked structural membrane lipid or, using acetyl-CoA as substrate, to a bioactive PAF. This pathway is known as the Land's cycle (Figure 3). In fact, PAF levels have been shown to increase significantly in hippocampus, cortex and thalamus following transient focal ischemia in gerbils (Kumar et al., 1988; Lindsberg et al., 1990; Nishida and Markey, 1996). Elevated PAF levels have also been identified as an important mediator of neuronal death in other neurodegenerative conditions including encephalitis, HIV-dementia, meningitis (Bazan et al., 2002; Farooqui et al., 2006; Perry et al., 1998; Ryan et al., 2007).

1.7 Lipidomics.

Systems biology, or "omic" approaches have been used to produce profiles of proteins (the proteome), gene expression (the transcriptome), DNA sequences (the genome) protein-protein interactions (the interactome), and more recently, metabolites (the metabolome) present in a given cell type under a specific set of conditions. The newest addition to this list is the lipidome – the profile of all structural membrane lipids and their metabolites (Dennis, 2009). In the context of the brain, lipids represent greater than half of the mass of brain's dry weight and, historically, were considered limited in function (Brown and Murphy, 2009; Piomelli et al., 2007). Biological membranes were perceived as an organized collection of

inert phospholipids that served as a platform to support membrane proteins, and to separate the intracellular space from the extracellular environment (Brown and Murphy, 2009).

More recently there has been greater interest in understanding the important differences between the discrete membrane lipid molecular species and their metabolites (Axelsen and Murphy, 2010; Brand et al., 2010; Han et al., 2001; Igbavboa et al., 2002; Lohmann et al., 2010). This new "lipidomics" era in lipid biochemistry has been spurred on by the advent of new lipid identification and quantification techniques. New "soft" ionization techniques – including electrospray ionization (ESI) (Fenn et al., 1989) and matrix-assisted laser desorption ionization (MALDI) (Hillenkamp et al., 1991) - have facilitated the ionization of neutral classes of membrane lipids and their metabolites for mass spectrometry (MS) analysis. (Brown and Murphy, 2009). These technologies have allowed for the identification and quantification of discrete molecular species of membrane lipids and their second messenger metabolites, using two primary approaches. Individual methodologies are reviewed below. "Shotgun" lipidomics takes advantage of direct-injection MS to rapidly analyze whole lipid extracts without a time consuming chromatographic separation (Brown and Murphy, 2009; Dennis, 2009; Ejsing et al., 2009). Alternatively, a more traditional approach is to separate complex lipid samples by liquid chromatography (LC) into smaller subclasses to be analyzed individually. By analyzing samples in negative and/or positive ion modes and employing one of several scanning modes (precursor ion scan, product ion scan, neutral loss scan),

researchers can carefully select a target subclass of lipids for identification and quantification (Brown and Murphy, 2009).

ESI and MALDI are “soft” ionization techniques designed to deliver biomolecules into the gas phase without fragmentation. This is particularly important for the study of lipids, as their lability and nonvolatility hinder their ability to vaporize (Ivanova et al., 2004). For ESI applications, lipid samples must be suspended in a volatile solvent and passed through a narrow-bore capillary “tip” under a strong electric field. The electric field draws the solvent from the capillary forming a droplet of charged lipid molecules. The like-charged lipids repel one another, forcing the droplet to burst, producing smaller droplets containing fewer lipid molecules. This process continues until the ionized lipid molecules are in the gas phase, in an unsolvated state. For MALDI applications, lipid mixtures are crystallized with a “matrix” compound onto a MALDI plate. Matrix compounds vary, but are typically organic compounds selected based on their ability to absorb the energy from a UV laser (Fuchs et al., 2010). For a review of commonly used MALDI matrices for lipid analysis, see (Fuchs and Schiller, 2009). A pulsed N_2 laser beam is then directed at the MALDI plate containing the matrix/analyte co-crystal. The matrix absorbs the majority of the laser’s energy, vaporizing the matrix compound, forcing the crystallized analyte into the gas phase. In the vaporization process, an extreme excess of matrix protects the analyte from the laser’s energy, and is capable of transferring charge (typically H^+ or Na^+ ions) to neighbouring analyte molecules, producing “quasimolecular” ions ($[M+H^+]$ or $[M+Na^+]$) (Fuchs et al., 2010), that can then be analyzed by the mass spectrometer.

Like these new ionization techniques, there are also two main types of mass spectrometers used for the analysis of lipid samples – triple quadrupole (Q-Trap) and time-of-flight (ToF) mass spectrometers. Q-Trap mass spectrometers, typically associated with ESI ion sources, consist of three sets of four electrode rods arranged in a diamond pattern. The first quadrupole, Q1, an RF/DC "scanning cell", by applying an electrical potential across the four electrodes, allows for the passage of singly charged ions with a corresponding m/z ratio. By increasing the electrical potential in a stepwise fashion, Q1 scans all *m/z* ratios, allowing for the passage of all singly charged ions over time, in an *m/z* ratio dependent manner. Q2 acts as a collision cell, where N_2 molecules collide and fragment analytes that have passed through Q1. Like Q1, Q3 can be set to select for ions with specific *m/z*, or can be programmed to scan a range of *m/z* ratios. With these specifications, there are three main scanning modes applicable to ESI-MS analysis using Q-Trap mass spectrometers. Product ion scans are performed by selecting a precursor ion in Q1 and scanning the product ions in Q3 following fragmentation. Precursor ion scans are performed by selecting a diagnostic fragmentation product ion in Q3, and scanning precursor ions in Q1 (Figure 1.2). Neutral loss scans are designed to scan precursor ions in Q1 that produce a specific neutral fragment following collision. To do this, both Q1 and Q3 are programmed to scan a range of *m/z* ratios, but are offset from one another by the *m/z* corresponding to the neutral loss fragment. For a more detailed review of ESI-MS technology and methodology, see (Hou et al., 2008). ToF mass spectrometers, typically associated with MALDI ion sources, consist of a field-free-flight chamber, which sometimes contain a "reflectron" – a series of charged plates designed to deflect the flight path of ions in the gas phase.

Figure 1.2. Lipid analysis by mass spectrometry. A schematic representation of LC-ESI-MS technology (A) and the precursor ion scan mode used for the identification of small molecular weight glycerophosphocholine second messenger lipids (B). Quadrupole 1 (Q1) scans precursor ions (set at *m/z* 475 in this diagram), Q2 is a N_2 gas collision cell, and Q3 is fixed at *m/z* 184 to select for phosphocholine product ions.

A.

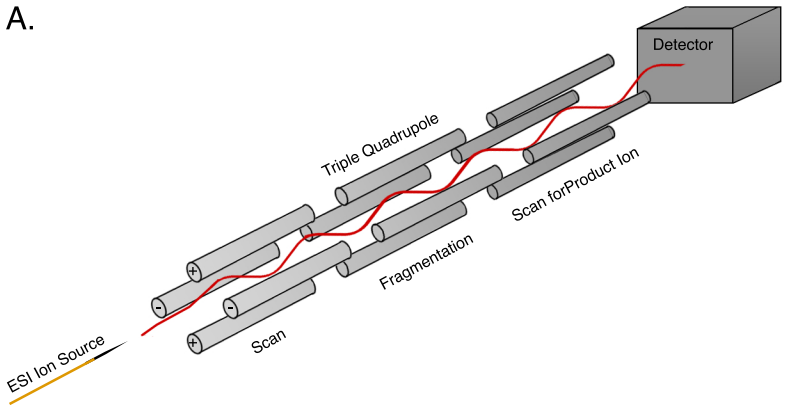
Detector
Triple Quadrupole
Scan forProduct Ion
Fragmentation
Scan
ESI Ion Source

B.

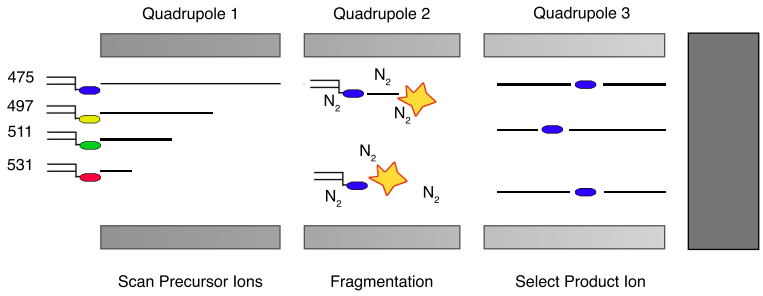
Quadrupole 1
Quadrupole 2
Quadrupole 3
475
497
511
531
N2
Scan Precursor Ions
Fragmentation
Select Product Ion

Ions produced by the pulsed laser are accelerated under strong electric field and then enter the ToF mass analyzer. Because the ions have identical kinetic energies, they travel through the vacuum of the field-free-flight chamber at mass-dependent velocities. The time of passage for a specific ion, then, corresponds to its *m/z* ratio (Hou et al., 2008).

Because HPLC separation systems can be coupled to ESI ion sources, ESI-MS is commonly used for the analysis of complex mixtures of lipids in solution. MALDI-ToF mass spectrometry, however, allows for the analysis of lipids directly from tissue – an application known as mass spectrometry imaging. By scanning the laser across a matrix-coated tissue section mounted on the MALDI plate in a stepwise manner, an image can be produced corresponding to the relative levels of particular analytes at specific locations within the tissue section. While both methodologies have advantages and limitations, they are not direct alternatives to one another, and in fact, are particularly useful when used in tandem. ESI-MS lends itself well to profiling lipids within a complex mixture of lipid extracted from tissue. MALDI-ToF imaging delivers higher spatial resolution of lipid levels in tissue, but is best suited the analysis of specific lipids, rather than profiling. It is advantageous, then, to first profile lipids from tissue using ESI-MS, and subsequently identify high-resolution spatial distribution of selected lipids within tissue sections by MALDI-ToF imaging.

These new techniques have allowed for the identification of novel lipid mediators and second messengers that may contribute to the etiology and pathophysiology of disease. One such messenger implicated through lipidomic

approaches, using ESI-MS/MS, in multiple neurodegenerative diseases and brain injury is arachidonic acid (Sanchez-Mejia et al., 2008). Free arachidonic acid (AA) is a potent inflammatory biomolecule, enriched at the *sn*-2 position of phosphatidylcholines (PtdCho), phosphatidylinositols (PtdIns) and phosphatidic acid (PtdH) (Farooqui et al., 2007b; Tillman and Cascio, 2003). Ca^{2+}-dependent activation of $sPLA_2$ and subsequent downstream $cPLA_2$ activation leads to arachidonate release and represents the early stages of the inflammatory response to ischemic injury (Samuelsson, 1983; Sun et al.). This newly released arachidonate follows the eicosanoid synthesis pathway, leading to a number of potent inflammatory cytokines including prostaglandins, prostacyclins, thromboxane and leukotrienes (Figure 2., see (Wang et al., 2007) for a review).

Until recently, it was not possible to identify modifications of discrete PAF and LPC molecular species or changes of members of other lipid classes. The lipidomics era of lipid biochemistry, however, has brought the technological advances reviewed above that enable us to identify and examine individual species with different carbon chain lengths. It is also now possible to distinguish between discrete lipid molecular species based on acyl chain and polar head group identity. This revolution has given insight into the immense number of distinct lipid species, and their unique functions (Brown and Murphy, 2009). To illustrate this, Callender *et al*, have used ESI-MS to identify twenty-eight discrete diacylglycerol molecular species (the product of phospholipase C-mediated membrane phospholipid cleavage), differing only in acyl chain-length and degree of unsaturation, that are each believed to have unique functions (Callender et al., 2007). Similarly, our lab

has used a lipidomic approach to identify specific PAF molecular species that accumulate in Alzheimer Disease tissue (Ryan et al., 2009).

1.8 Lipidomic approaches to the study of stroke pathophysiology.

Because stroke is a highly regionally and temporally-dynamic condition, the identification and localization of molecular changes following ischemia is challenging. As indicated above, developments in MS technology have facilitated the study of stroke pathophysiology on both global (millimeter) and micrometer scales (Jiang et al., 2010; Koizumi et al., 2010; Whitehead et al., 2010). MS analysis allows for a powerful systems biology approach to the broad-range identification of molecular profiles, and the identification of changes in these profiles under pathological conditions. MS-based techniques have been used to profile the proteome of human brain following stroke (Cuadrado et al., 2010), to identify novel protein changes in brain extracellular fluid in human stroke patients (Dayon et al., 2011). Proteomics has, in part, enabled lipidomics. MS is also widely used for the identification of lipids and changes in lipid profiles in tissue. As outlined previously, lipidomic studies have take two main approaches to MS-analysis: LC-ESI-MS and MALDI-ToF imaging. LC-ESI-MS, in precursor ion scan mode, is a powerful tool for the broad-range profiling of small molecular weight glycerophosphocholine second messengers from whole lipid extracts from tissue (Ryan et al., 2009; Whitehead et al., 2007). Conversely MALDI-ToF imaging allows for the localization and quantification of individual lipid species from tissue sections, but is best suited to study to particular lipids of interest (Hou et al., 2008; Whitehead et al., 2011).

1.9 Lipid second messenger biology.

PAF lipids elicit cellular responses by binding to their specific G-protein coupled receptors (platelet-activating factor receptor, PAFR) on the surface of neural and non-neural cells (Clark et al., 2000; Nakamura et al., 1991). In rat brain, PAFR expression has been reported in neurons and microglia, and localized to hypothalamus, cerebral cortex, hippocampus, cerebellum and more (Bito et al., 1993; Mori et al., 1996). PAFR is a 7-transmembrane receptor capable of interacting with several G-proteins, including Gαo, Gαi, Gβy and Gαq (Maclennan et al., 1996), thereby initiating a variety of signaling pathways, including calcium mobilization, kinase activation, phospholipase activation and phosphatidylinositol turnover (Maclennan et al., 1996). The PAF-mediated inflammatory response is also dependent on the PAF receptor, and contributes to neuronal damage following injury. In neuronal cells and brain, PAFR activation promotes the activation of inducible phospholipases including PLA_2 (Izumi and Shimizu, 1995) and cyclooxygenase-2 (COX-2) (Bazan and Allan, 1996; Bazan et al., 1991) – the activities of which lead to the production of arachidonic acid and prostaglandins respectively. These pro-inflammatory mediators contribute to the progression of ischemic injury as previously described.

Further, PAF lipids themselves are toxic and can contribute directly to neuronal (Ryan et al., 2008) and glial (Hostettler and Carlson, 2002) cell death when lipid levels exceed physiological concentrations (i.e., approximately 125 pM in cultured human neurons, and 250 pM in human brain). Members of our lab have elucidated a mechanism by which 1-*O*-hexadecyl-2-acetyl-*sn*-glycero-3-

phosphocholine, (PC(O-16:0/0:0)), promotes caspase-dependent neuronal apoptosis independently of its G-protein coupled receptor (PAFR) in human neurons in culture (Ryan et al., 2009). Further, we have shown that PAF species with different *sn*-1 chains signal different neurotoxic pathways (Ryan et al., 2008).

Both LPC and PAF lipids can execute their biological activities through G-protein coupled receptor-associated mechanisms. Interestingly, there is conflicting evidence that LPC may even have the ability to elicit downstream effects by binding to PAFR (Huang et al., 1999; Marathe et al., 2001). Nevertheless, recent studies have pointed to LPC as the high-affinity ligand for the orphan G2A G-protein coupled receptor (Lin and Ye, 2003). Further, like PAF-PAFR interaction, LPC binding to the G2A receptor leads to apoptosis in a human neuroblastoma cell line (Qin et al., 2009). Likely because of these effects, their lytic properties, and their tendency to promote membrane curvature, LPC levels are maintained at very low levels in brain by rapid consumption of free LPC by lysophospholipases, or reacylated to structural membrane lipids by LPCATs (Farooqui and Horrocks, 2006; Farooqui et al., 2000; van Meeteren and Moolenaar, 2007). Disruption of the regulation of LPC levels in brain, as is seen following cerebral ischemia, could lead to an exacerbation of the inflammatory reaction, perturbation and contortion of neuronal membranes, and ultimately result in more severe ischemic injury.

1.10. Objectives and hypothesis.

Small molecular weight glycerophosphocholine lipid second messengers and in particular, the bioactive pro-inflammatory PAF family of ether-linked

glycerophosphocholine lipids have been implicated in the progression of multiple neurodegenerative conditions. To date, it is understood that PAF lipids display increased abundance in ischemic tissue following stroke and likely contribute to the progression of the disease by promoting an inflammatory response involving activation of resident (and potentially bone-marrow derived) microglia, yet the impact of specific molecular species has been largely overlooked. I hypothesized that glycerophospholipid metabolites demonstrated altered metabolism in a PAF receptor-dependent manner following MCAO, leading to the accumulation of specific glycerophosphocholine second messenger molecular species. To test this hypothesis, I identified regional differences in glycerophosphocholine lipid second messenger abundance between anterior and posterior regions of frontal cortex and striatum from the uninjured (contralateral) hemisphere of uninjured C57Bl/6 mice. Next, I investigated the impact of MCAO on this spatial gradient by mapping regional differences in lipid abundance between these same regions in the ischemic (ipsilateral) hemisphere of C57Bl/6 mice subjected to one hour MCAO and 24 hours of reperfusion. Finally, to evaluate the impact of the PAF receptor on PAF (and other second messener glycerophosphocholine) homeostasis and metabolism, I compared the wild-type glycerophosphocholine second messenger lipidome to age-matched, congenic PAFR null-mutant animals subjected to 1 hour MCAO and 24 hours of reperfusion.

2. Materials and Methods

2.1 MCAO-reperfusion.

C57Bl/6J mice (22-24 g) (Charles River Laboratories Inc., Saint-Constant QC, Canada) were subjected to 1 hour middle cerebral artery occlusion using an intraluminal filament as previously described (Hara et al., 1996; Weaver et al., 2005), followed a by 24 hour reperfusion period. Under temporary isofluorane anaesthesia, mice were given an incision to expose the external carotid artery. Following 1 hour of occlusion, mice were reanaesthetized, the filament removed to restore blood flow and the incision was sutured. When animals recovered from anaesthesia, the extent of behavioural impairment was assessed using a modified 6-point scale as previously described (Weaver et al., 2005). Mice were suspended by the tail 10 cm above the bench surface, and behaviour was scored: 0, normal; 1, mild turning behaviour with or without inconsistent curling, with less than 50% attempts to curl to the contralateral side; 2, mild, consistent curling with more than 50% attempts to curl to the contralateral side; 3, strong and immediate consistent curling, held for more than 1-2 seconds, and mouse's nose nearly reaches tail; 4, severe curling progressing into barreling and loss of walking or righting reflex; 5, comatose or moribund. The same behavioural test was performed following 24 hours of reperfusion, prior to sacrifice. Under deep euthanyl anaesthesia, mice were sacrificed by decapitation. Brains were removed and cut into four 2 mm thick coronal sections using a zinc brain matrix. Under a dissection microscope, sections were dissected into striatum, cortex, hippocampus and thalamus, separated into

ipsilateral and contralateral sides. Dissected tissue was weighed and quickly flash frozen in liquid nitrogen and stored at -80°C.

2.2 Lipid extraction.

Glycerophospholipids were extracted from tissue using a modified Bligh & Dyer lipid extraction (Bligh and Dyer, 1959) as previously described (Whitehead et al., 2007). Briefly, tissue was homogenized using a 7 mm Tissue-Tearor (Biospec Products Inc., Bartlesville OK, USA) in 5 mL disposable borosilicate glass homogenization tubes (VWR International), containing 1 mL of 2% (v/v) glacial acetic acid in methanol. Prior to transfer, 25 µL of homogenate was collected and frozen for protein analysis. 41.3 µL of 10 µM PC(13:0/0:0) were added to tissue homogenates and homogenates were transferred to 10 mL glass conical tubes containing 3.2 mL of filtered 0.1 M sodium acetate. Homogenization tubes were rinsed with three sequential washes with 1 mL of acidified methanol, and wash solutions were added to tissue homogenates in the conical extraction tubes. Lipids were then extracted by adding 3.8 mL of chloroform, and the organic phase was retained in additional 10 mL conical borosilicate glass tubes following a two minute centrifugation at 2000 rpm at 4 °C. The aqueous phase was back-extracted three times by sequential addition of 2 mL of chloroform, centrifugation and organic phase recovery. Chloroform was evaporated under a stream of N_2 gas, and lipids were resuspended in 300 µL of 100% ethanol, and stored in 100 µL aliquots in 2 mL amber glass vials (BioLynx Chromatographic Specialties) under a N_2 atmosphere at -80 °C.

2.3 Sample preparation and LC-ESI-MS.

Lipid samples for LC-ESI-MS analysis were prepared in a 96-well auto-sampler plate, fitted with a pre-slit silicon cover mat (Agilent Technologies, Mississauga ON, Canada). Sample preparations included 5 µL of lipid extract, 2.5 µL of deuterated lipid standard mixture [1 ng/µL d_4-PC(O-16:0/0:0, 1 ng/µL d_4-PC(O-18:0/0:0), 0.5 ng/µL d_4-PC(O-16:0/2:0 and 0.5 ng/µL d_4-PC(O-18:0/2:0)] and 15.75 µL of 0.1% formic acid in H_20 (J.T. Baker). LC separation of lipids was accomplished using an 1100 HPLC system (Agilent Technologies, Mississauga ON, Canada). A 1100 autosampler was used to load 8 µL of sample mixture onto a 200 µm x 5 cm pre-column packed with Magic C18AQ beads (Michrom Bioresources, Inc., Auburn CA, USA) at a flow rate of 10 µL/min. Analytes were introduced into a 2000 Q-Trap mass spectrometer by electrospray ionization through a 75 µm x 5 cm PicoTip™ Emitter packed with Magic C18AQ beads. Lipid species were analyzed using an Enhanced MS Scan and Precursor Ion Scan (m/z 184) for the identification of small choline-containing lipid second messengers, as previously published (Whitehead et al., 2007).

2.4 Data analysis.

Lipid data was analyzed using the “Explore” module of Analyst® Software (Applied Biosystems). All peaks displayed on the 2-dimensional LC elution plot (retention-time vs. mass-to-charge ratio) are analyzed by integrating the area under the curve of the Extracted Ion Chromatograph (XIC). Peak area (PA) data for each peak was normalized to the peak area of the exogenous PC(13:0/0:0), and the wet

weight of the tissue (PA_N), and all PA_N data is Log_2 transformed to approximate a normally distributed population (Log_2PA_N).

2.5 Heatmap analysis

To represent lipid data from uninjured tissue in heatmaps, the mean Log_2PA_N data ($Log_2PA_{N\ Mean}$) for each species is subtracted from the Log_2PA_N for each individual in the population, and this is divided by the standard deviation of the $Log_2PA_{N\ Mean}$, giving the Log_2I^*.

$$Log_2PA_N = Log_2\left[\frac{\left(\frac{PA_{\ species}}{PA_{\ C13:0\ LPC}}\right)}{Wet\ Weight_{\ Tissue}}\right]$$

$$Log_2 I^* = \frac{\left(Log_2\ PA_N - Log_2\ PA_{N\,Mean}\right)}{SD\,Log_2\ PA_{N\,Mean}}$$

To represent lipid data from ischemic tissue, data is represented as the Log_2 of the ratio of the PA_N from ischemic tissue to the PA_N from uninjured tissue ($Log_2PA_{N\ Fold\ Change}$).

$$Log_2\ PA_{N\,Fold\ Change} = Log_2\left(\frac{PA_{N\,Injured}}{PA_{N\,uninjured}}\right)$$

Mean $Log_2PA_{N\ Fold\ Change\ Mean}$ is then subtracted from the $Log_2PA_{N\ Fold\ Change}$ for each species, and this is divided by the standard deviation of the $Log_2PA_{N\ Fold\ Change\ Mean}$, giving the $Log_2I^*_{Fold\ Change}$.

$$Log_2 I^*_{Fold\ Change} = \frac{\left(Log_2 PA_{N\,Fold\ Change} - Log_2 PA_{N\,Fold\ Change\ Mean}\right)}{SD\ Log_2 PA_{N\,Fold\ Change\ Mean}}$$

Log_2I^* data values are truncated, and the mean Log_2I^* data from the two conditions being compared are subtracted one from the other. Species that show a difference between mean Log_2I^* data of greater than 1 or less than -1 are considered significantly different.

2.6 Statistical analysis.

To test whether species identified by heatmap analysis are statistically significant, Log_2PA_N data is analyzed by paired t-test (regional differences in uninjured tissue), or by 2-way ANOVA with post-hoc Bonferroni (effect of ischemic injury on lipid metabolism).

3. Results.

3.1 Glycerophospholipid second messenger profiles are regionally specific and display an anterior-posterior gradient in the uninjured C57Bl/6 striatum and frontal cortex.

3.1.1 Lipid differences between anterior and posterior regions of uninjured frontal cortex.

To assess changes in glycerophosphocholine second messenger lipids across anterior-posterior regions in uninjured frontal cortex on a global level, Log_2PA_N data were analyzed in paired X,Y coordinate points (X, posterior; Y, anterior). Linear regression analysis then identified 15 lipid species in 3 animals that fell above (red dots), representing species with increased abundance in anterior regions of cortex, and another 14 species in 3 animals that fell below the 95% confidence interval (blue dots) representing species with increased abundance in posterior regions of cortex (Fig 3.1.1a). Next, $Log_2PA_N \times 10^6$ data was converted to Log_2A^* data, as described above. Using these new data, 39 identified lipid species were represented in a heatmap. Heatmap analysis revealed two species, PC(P-18:0/2:0) and PC(O-22:6/2:0), that showed at least one standard deviation difference between mean $Log_2PA_N \times 10^6$ data for the anterior and posterior regions of cortex (Fig 3.1.1b). Finally, $Log_2PA_N \times 10^6$ comparison revealed 12 lipid species (Table 3.1.1) with significantly altered abundance between anterior and posterior regions of frontal cortex (paired t-test, Fig 3.1.1c).

Figure 3.1.1a. Global differences in glycerophosphocholine second messenger lipid abundance between anterior and posterior regions of uninjured wild-type frontal cortex. Small molecular weight glycerophosphocholine second messengers were identified by LC-ESI-MS. Data shown represent log_2-transformed normalized peak area (Log_2PA_N) for each region plotted as (X,Y) coordinates. Dotted lines represent the 95% confidence interval identified by linear regression analysis. Species that fell above the interval (red dots) are more abundant in anterior frontal cortex, while those below (blue dots) are more abundant in posterior frontal cortex.

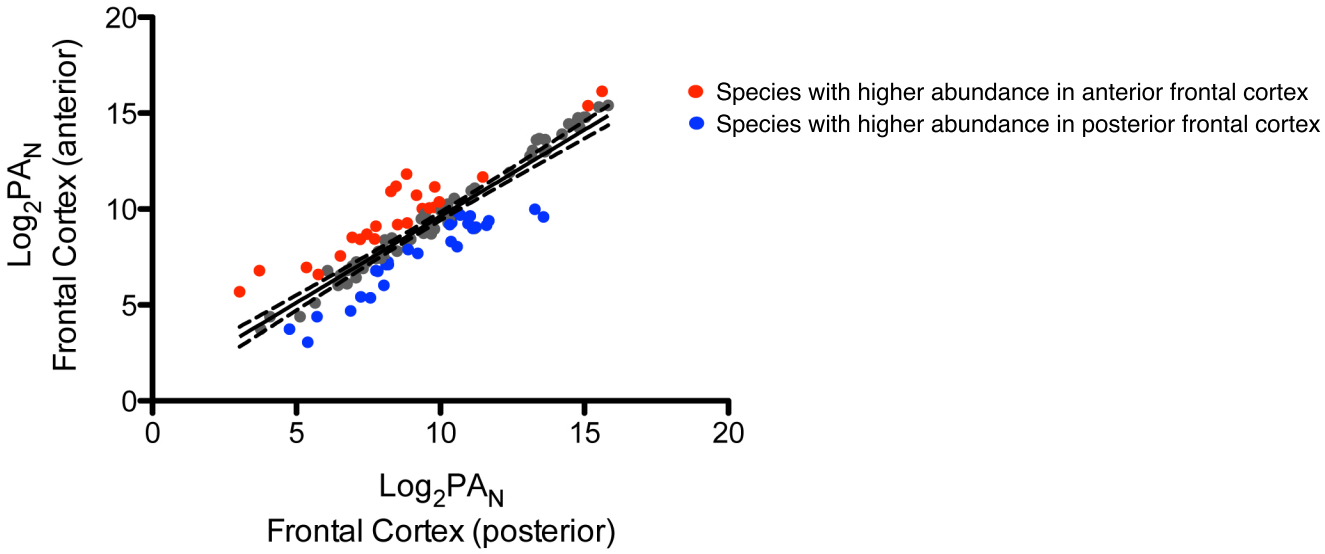
20
15
10
5
0
0
5
10
15
20
Log2PAN
Frontal Cortex (anterior)
Log2PAN
Frontal Cortex (posterior)
Species with higher abundance in anterior frontal cortex
Species with higher abundance in posterior frontal cortex

.

Figure 3.1.1b. Heatmap clustering of relative glycerophosphocholine lipid second messenger abundance between anterior and posterior regions of uninjured wild-type frontal cortex. Small molecular weight glycerophosphocholine second messengers were identified by LC-ESI-MS. Data represent the number of standard deviations (Log_2A^*) by which the abundance of a given species in a given animal differs from the mean abundance of the whole population. * denotes species that show at least 1 standard deviation from the mean. These were considered significant and were prioritized for a second level of statistical analysis.

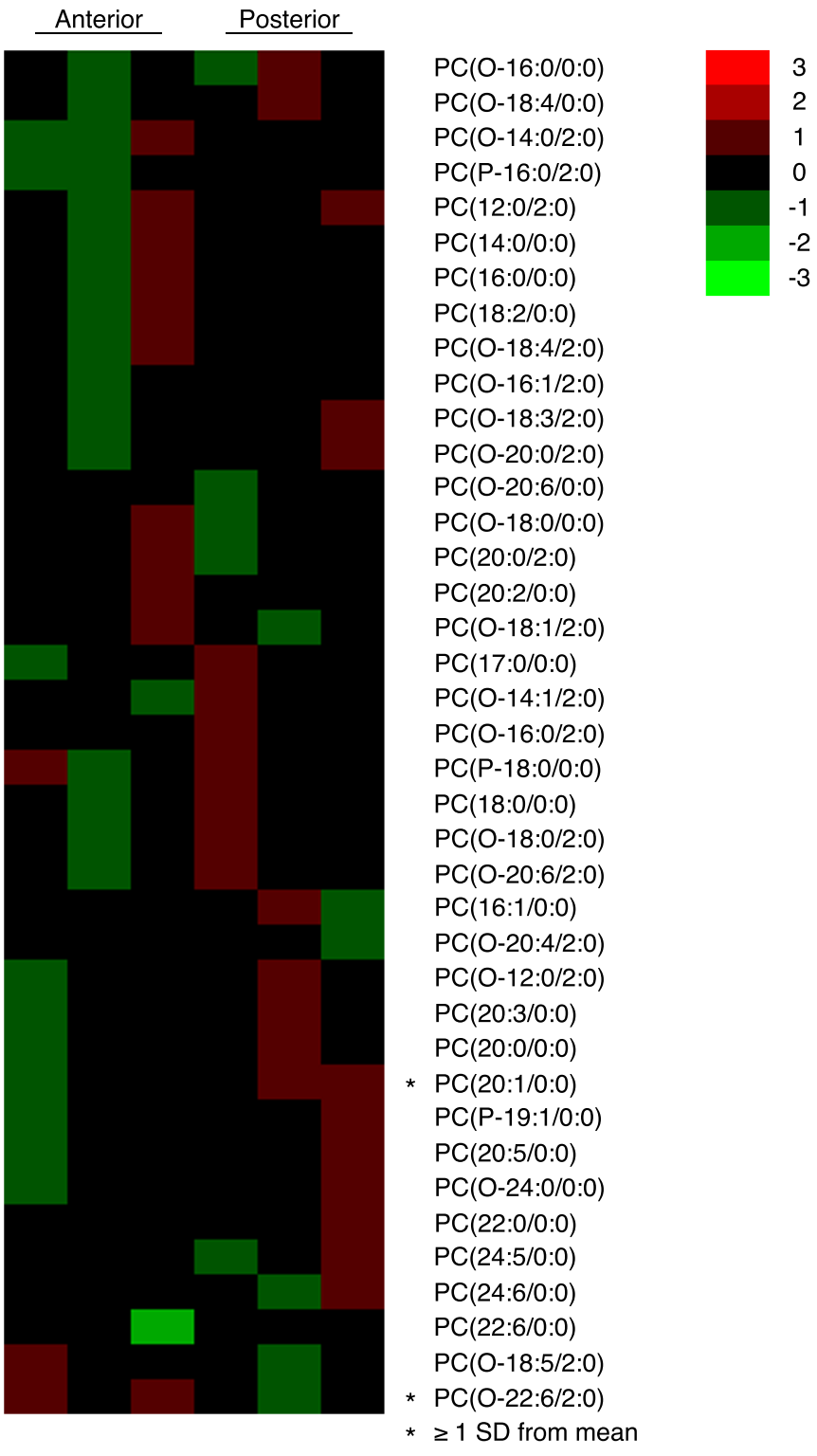
Anterior
Posterior
PC(O-16:0/0:0)
PC(O-18:4/0:0)
PC(O-14:0/2:0)
PC(P-16:0/2:0)
PC(12:0/2:0)
PC(14:0/0:0)
PC(16:0/0:0)
PC(18:2/0:0)
PC(O-18:4/2:0)
PC(O-16:1/2:0)
PC(O-18:3/2:0)
PC(O-20:0/2:0)
PC(O-20:6/0:0)
PC(O-18:0/0:0)
PC(20:0/2:0)
PC(20:2/0:0)
PC(O-18:1/2:0)
PC(17:0/0:0)
PC(O-14:1/2:0)
PC(O-16:0/2:0)
PC(P-18:0/0:0)
PC(18:0/0:0)
PC(O-18:0/2:0)
PC(O-20:6/2:0)
PC(16:1/0:0)
PC(O-20:4/2:0)
PC(O-12:0/2:0)
PC(20:3/0:0)
PC(20:0/0:0)
* PC(20:1/0:0)
PC(P-19:1/0:0)
PC(20:5/0:0)
PC(O-24:0/0:0)
PC(22:0/0:0)
PC(24:5/0:0)
PC(24:6/0:0)
PC(22:6/0:0)
PC(O-18:5/2:0)
* PC(O-22:6/2:0)
3
2
1
0
-1
-2
-3
* ≥ 1 SD from mean

Figure 3.1.1c. Anterior-posterior gradients of glycerophosphocholine lipid second messenger abundance in uninjured wild-type frontal cortex. Small molecular weight glycerophosphocholine second messengers were identified by LC-ESI-MS. Log_2-transformed normalized peak areas (Log_2PA_N) for lipid species exhibiting a regional difference by heatmap analysis were further analyzed in the anterior and posterior regions of frontal cortex by paired t-test. *p<0.05. **p<0.01. ***p<0.005

i. PC(O-12:0/2:0)

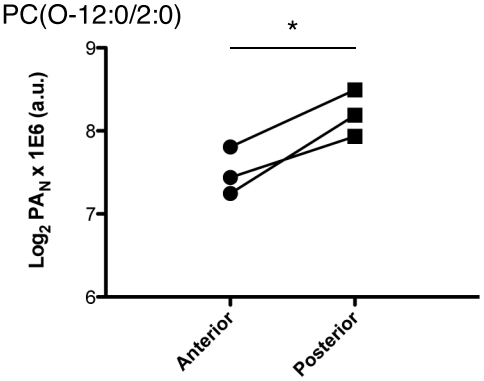

ii.PC(P-18:0/0:0)

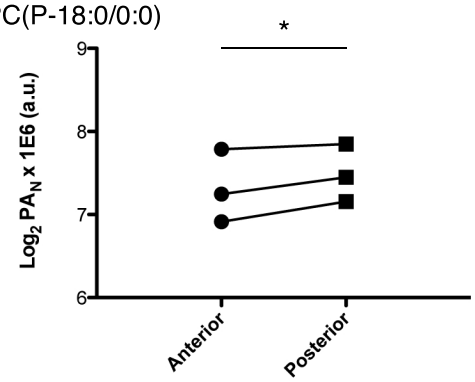

iii. PC(17:0/0:0)

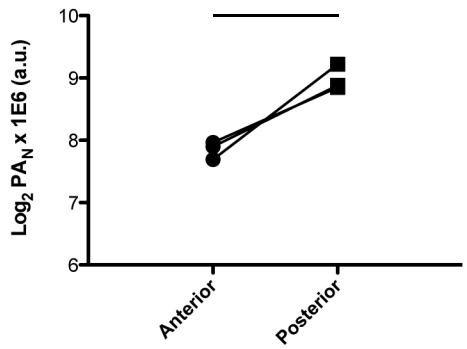

iv. PC(20:5/0:0)

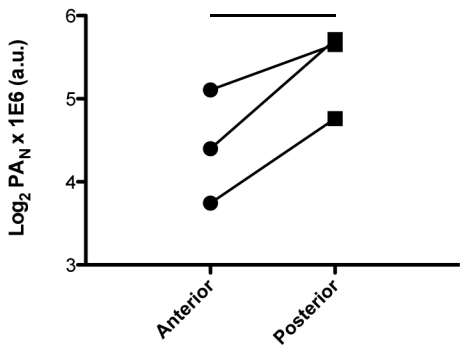

v. PC(O-18:3/2:0)

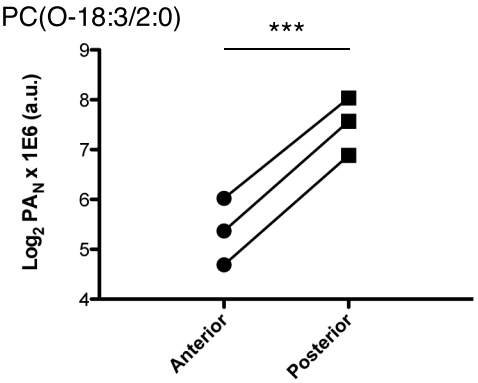

vi. PC(O-18:1/2:0)

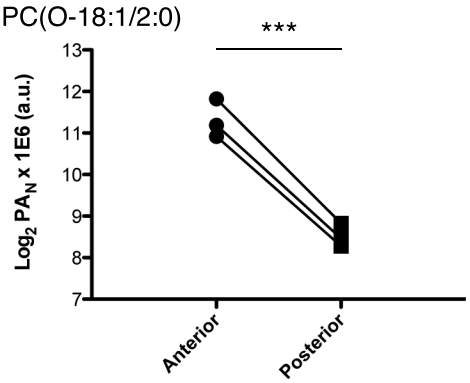

vii. PC(20:1/0:0)

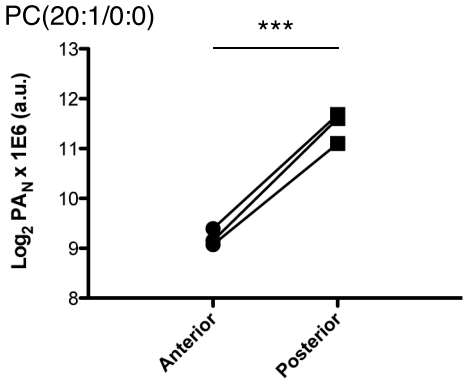

viii. PC(O-18:0/2:0)

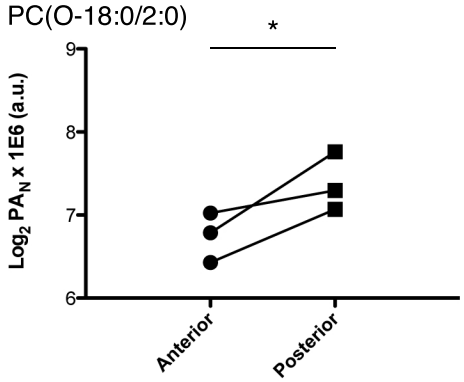

ix. PC(20:0/0:0)

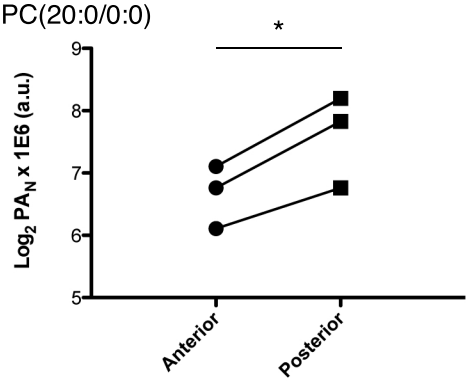

x. PC(O-20:6/2:0)

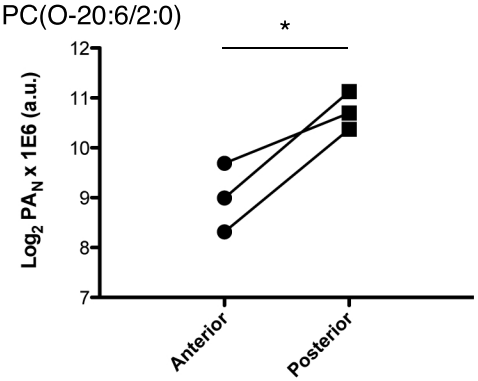

xi. PC(O-20:0/2:0)

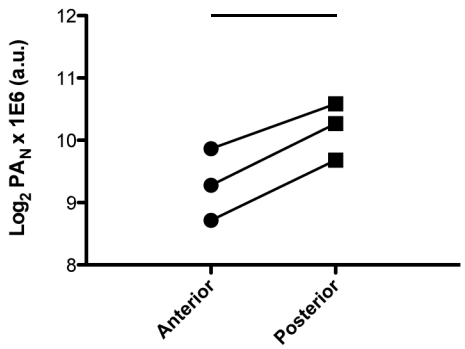

xii. PC(O-24:0/0:0)

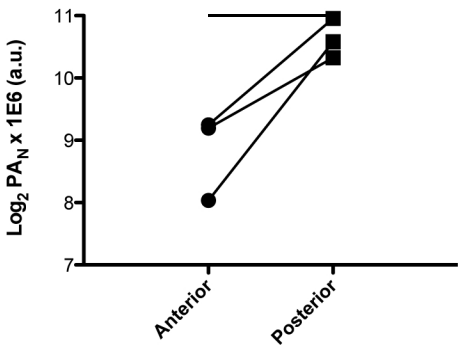

xiii. PC(O-22:6/2:0)

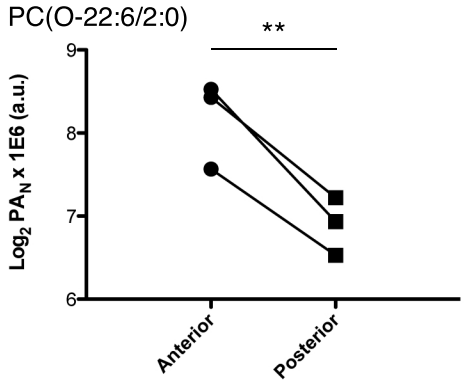

Lipid Species	Mean Log_2PA_N x 10^6		Paired t-test p-value
	Anterior	Posterior	
PC(O-12:0/2:0)	7.50E+00	8.21E+00	0.0160
PC(O-18:2/0:0)	7.32E+00	7.48E+00	0.0447
PC(O-16:0/1:0)	7.85E+00	8.98E+00	0.0149
PC(20:5/0:0)	4.42E+00	5.38E+00	0.0250
PC(O-18:3/2:0)	5.36E+00	7.50E+00	0.0004
PC(O-18:1/2:0)	1.13E+01	8.52E+00	0.0007
PC(P-18:0/2:0)	9.21E+00	1.15E+01	0.0015
PC(O-18:0/2:0)	6.75E+00	7.38E+00	0.0451
PC(20:0/0:0)	6.66E+00	7.60E+00	0.0111
PC(O-20:6/2:0)	9.00E+00	1.07E+01	0.0205
PC(O-20:0/2:0)	9.29E+00	1.02E+01	0.0047
PC(O-24:0/0:0)	8.82E+00	1.06E+01	0.0243
PC(O-22:6/2:0)	8.17E+00	6.89E+00	0.0080

Table 3.1.1. Lipid species that show significantly altered abundance between anterior and posterior regions of uninjured frontal cortex by paired t-test.

3.1.2 Lipid differences between anterior and posterior regions of uninjured striatum in the forebrain.

Linear regression analysis revealed global changes in glycerophosphocholine second messenger levels between anterior and posterior regions of the striatum in uninjured hemispheres of male C57Bl/6 mice. 17 species in 3 animals fell above the 95% confidence interval, representing lipids with increased abundance in anterior striatum (red dots), and 17 lipid species in 3 animals with increased abundance in posterior striatum (blue dots) (Fig 3.1.2a). Heatmap analysis revealed three species, PC(P-16:0/2:0), PC(20:3/0:0) and PC(O-18:1/2:0), that displayed greater than one standard deviation between the mean Log_2A^* data for anterior and posterior striatum (Fig 3.1.2b). Finally, paired t-test analysis revealed five lipid

Figure 3.1.2a. Global differences in glycerophosphocholine second messenger lipid abundance between anterior and posterior regions of uninjured wild-type striatum. Small molecular weight glycerophosphocholine second messengers were identified by LC-ESI-MS. Data shown represent log_2-transformed normalized peak area (Log_2PA_N) for each region plotted as (X,Y) coordinates. Dotted lines represent the 95% confidence interval identified by linear regression analysis. Species that fell above the interval (red dots) are more abundant in anterior striatum, while those below (blue dots) are more abundant in posterior striatum.

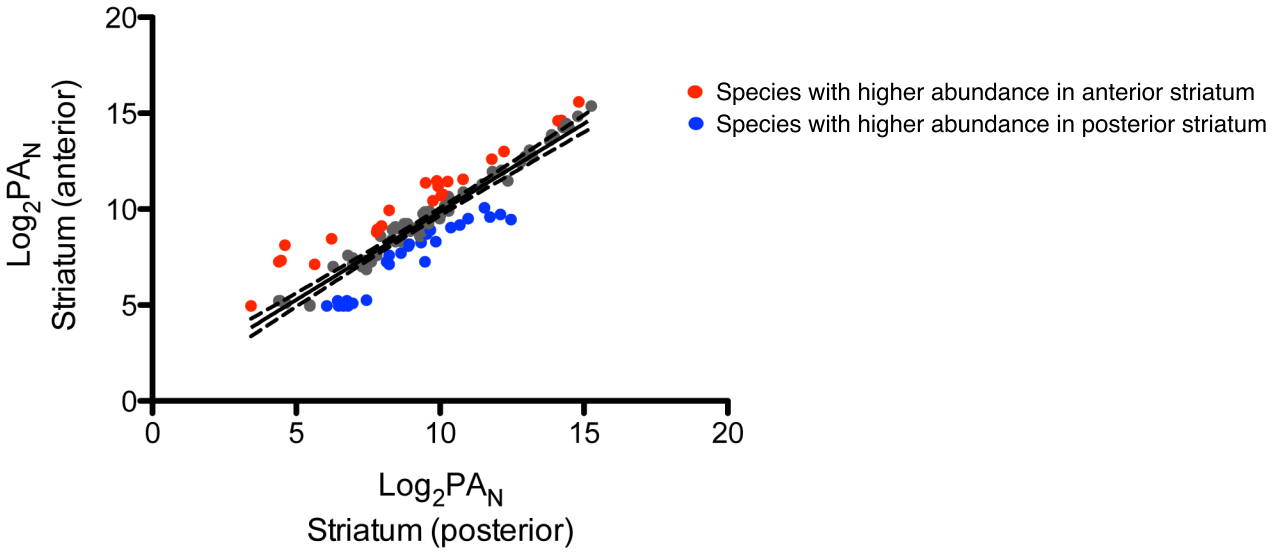
20
15
10
5
0
0
5
10
15
20
Log2PAN
Striatum (anterior)
Log2PAN
Striatum (posterior)
Species with higher abundance in anterior striatum
Species with higher abundance in posterior striatum

.

Figure 3.1.2b. Heatmap clustering of relative glycerophosphocholine lipid second messenger abundance between anterior and posterior regions of uninjured wild-type striatum. Small molecular weight glycerophosphocholine second messengers were identified by LC-ESI-MS. Data represent the number of standard deviations (Log_2A^*) by which the abundance of a given species in a given animal differs from the mean abundance of the whole population. * denotes species that show at least 1 standard deviation from the mean. These were considered significant and were prioritized for a second level of statistical analysis.

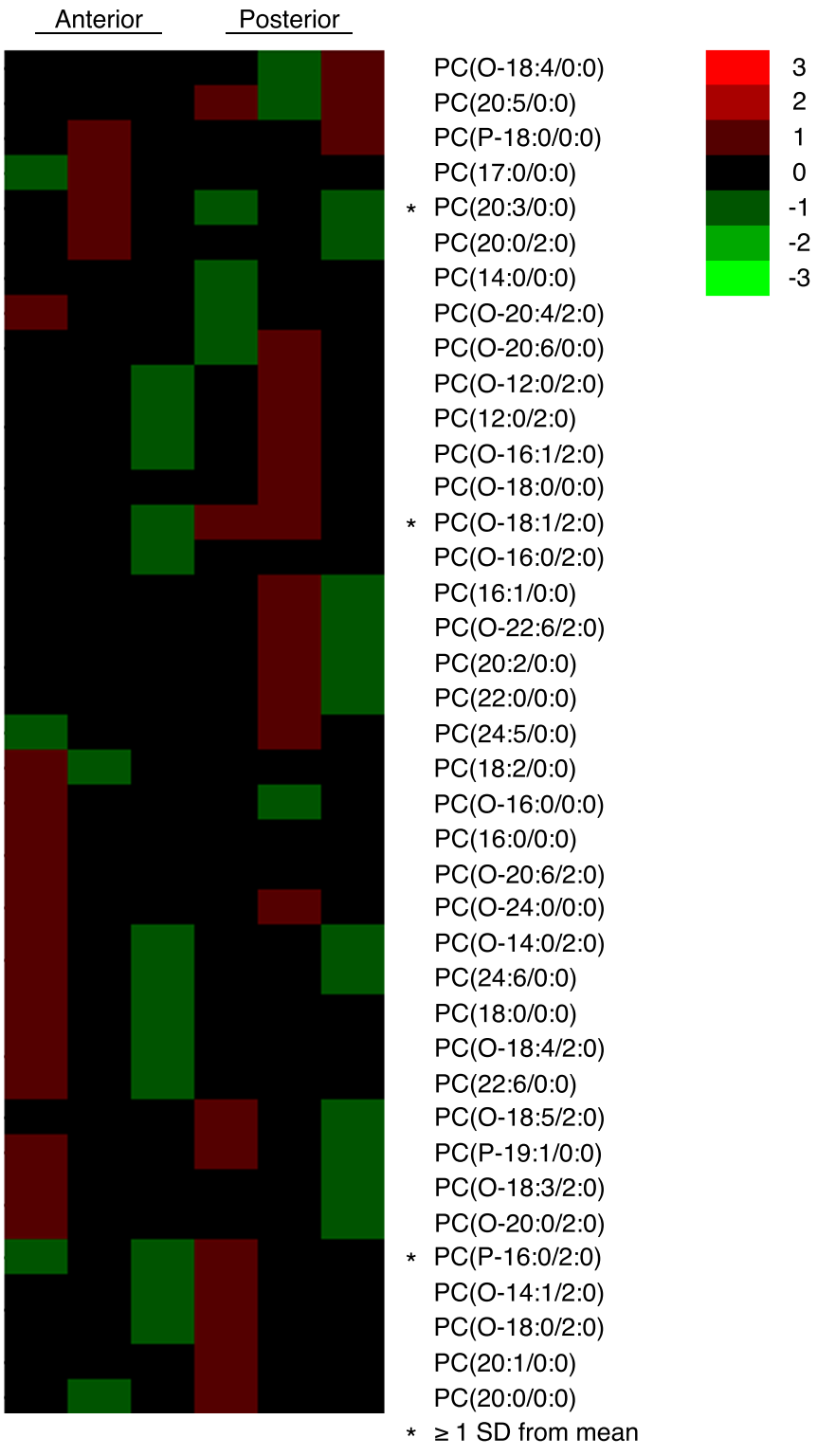
Anterior
Posterior
PC(O-18:4/0:0)
PC(20:5/0:0)
PC(P-18:0/0:0)
PC(17:0/0:0)
* PC(20:3/0:0)
PC(20:0/2:0)
PC(14:0/0:0)
PC(O-20:4/2:0)
PC(O-20:6/0:0)
PC(O-12:0/2:0)
PC(12:0/2:0)
PC(O-16:1/2:0)
PC(O-18:0/0:0)
* PC(O-18:1/2:0)
PC(O-16:0/2:0)
PC(16:1/0:0)
PC(O-22:6/2:0)
PC(20:2/0:0)
PC(22:0/0:0)
PC(24:5/0:0)
PC(18:2/0:0)
PC(O-16:0/0:0)
PC(16:0/0:0)
PC(O-20:6/2:0)
PC(O-24:0/0:0)
PC(O-14:0/2:0)
PC(24:6/0:0)
PC(18:0/0:0)
PC(O-18:4/2:0)
PC(22:6/0:0)
PC(O-18:5/2:0)
PC(P-19:1/0:0)
PC(O-18:3/2:0)
PC(O-20:0/2:0)
* PC(P-16:0/2:0)
PC(O-14:1/2:0)
PC(O-18:0/2:0)
PC(20:1/0:0)
PC(20:0/0:0)
* ≥ 1 SD from mean
3
2
1
0
-1
-2
-3

Figure 3.1.2c. Anterior-posterior gradients of glycerophosphocholine lipid second messenger abundance in uninjured wild-type striatum. Small molecular weight glycerophosphocholine second messengers were identified by LC-ESI-MS. Log_2-transformed normalized peak areas (Log_2PA_N) for lipid species exhibiting a regional difference by heatmap analysis were further analyzed in the anterior and posterior regions of striatum by paired t-test. *$p<0.05$. **$p<0.01$. ***$p<0.005$.

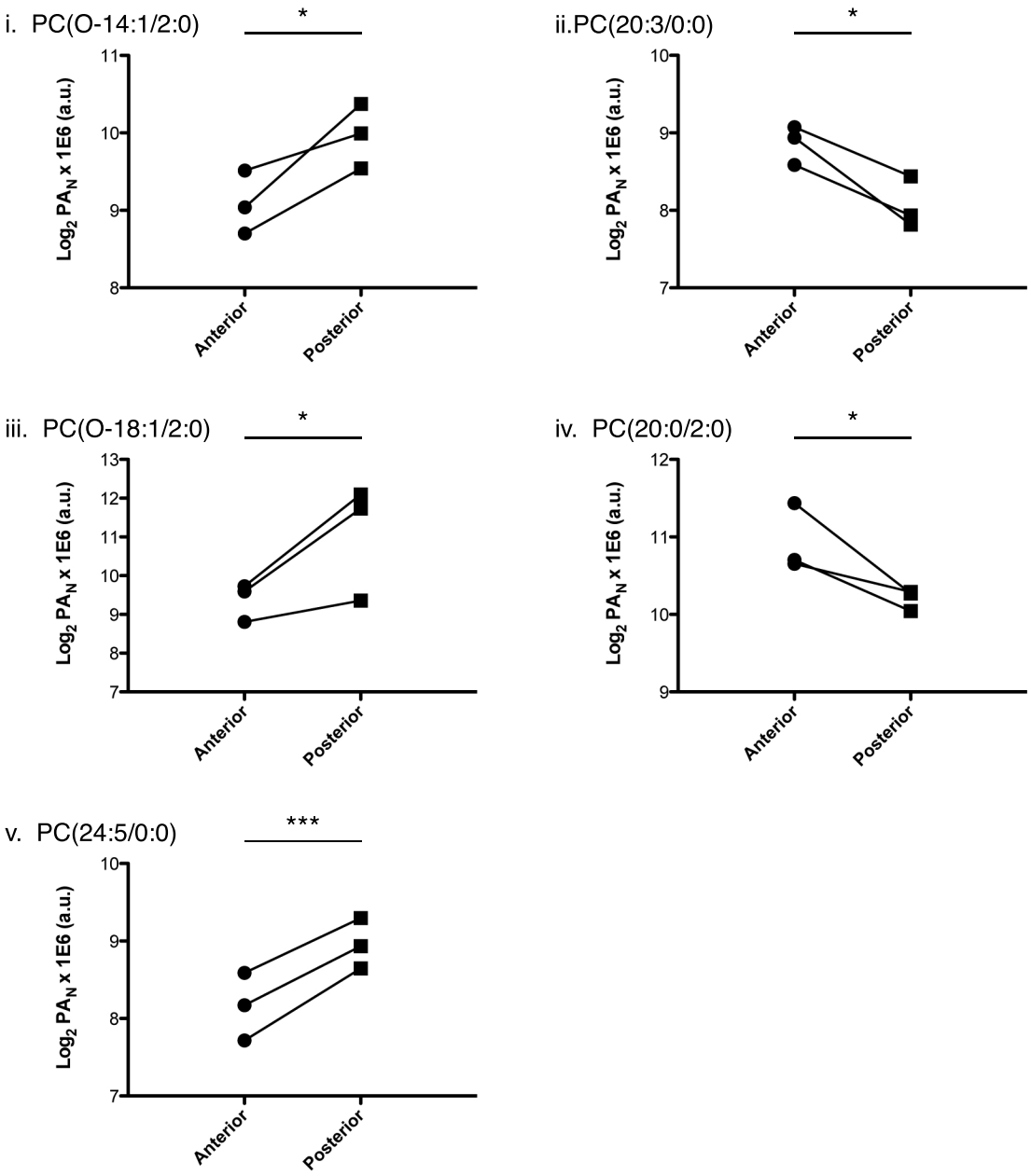
i. PC(O-14:1/2:0)
*
Log2 PAN x 1E6 (a.u.)
11
10
9
8
Anterior
Posterior
ii.PC(20:3/0:0)
*
Log2 PAN x 1E6 (a.u.)
10
9
8
7
Anterior
Posterior
iii. PC(O-18:1/2:0)
*
Log2 PAN x 1E6 (a.u.)
13
12
11
10
9
8
7
Anterior
Posterior
iv. PC(20:0/2:0)
*
Log2 PAN x 1E6 (a.u.)
12
11
10
9
Anterior
Posterior
v. PC(24:5/0:0)
***
Log2 PAN x 1E6 (a.u.)
10
9
8
7
Anterior
Posterior

species (table 3.1.2) with significantly altered abundance between anterior and posterior regions of uninjured striatum (Fig 3.1.2c).

Lipid Species	Mean Log_2PA_N x 10^6		Paired t-test p-value
	Anterior	Posterior	
PC(O-14:1/2:0)	9.08E+00	9.97E+00	0.0353
PC(20:3/0:0)	8.87E+00	8.06E+00	0.0187
PC(O-18:1/2:0)	9.37E+00	1.11E+01	0.0492
PC(20:0/2:0)	1.09E+01	1.02E+01	0.0445
PC(24:5/0:0)	8.16E+00	8.96E+00	0.0034

Table 3.1.2. Lipid species that show significantly altered abundance between anterior and posterior regions of uninjured frontal striatum by paired t-test.

3.1.3 Lipid differences between anterior regions of uninjured cortex and striatum in the forebrain.

Linear regression analysis between anterior regions of striatum (X-axis) and cortex (Y-axis), revealed 18 glycerophosphocholine second messenger lipid species with increased abundance in anterior cortical tissue (red dots) and 15 lipid species in 3 animals with increased abundance in anterior striatal tissue (blue dots) (Fig 3.1.3a). Three lipid species, PC(O-18:2/0:0), PC(O-18:0/2:0) and PC(20:0/0:0), displayed at least one standard deviation difference between mean Log_2A^* data by heatmap analysis (Fig 3.1.3b). Finally, nine lipid species (Table 3.1.3) showed significantly altered abundance between anterior regions of frontal cortex and striatum by paired t-test (Fig 3.1.3c).

Figure 3.1.3a. Global differences in glycerophosphocholine second messenger lipid abundance between anterior regions of uninjured wild-type frontal cortex and striatum. Small molecular weight glycerophosphocholine second messengers were identified by LC-ESI-MS. Data shown represent log_2-transformed normalized peak area (Log_2PA_N) for each region plotted as (X,Y) coordinates. Dotted lines represent the 95% confidence interval identified by linear regression analysis. Species that fell above the interval (red dots) are more abundant in anterior frontal cortex, while those below (blue dots) are more abundant in anterior striatum.

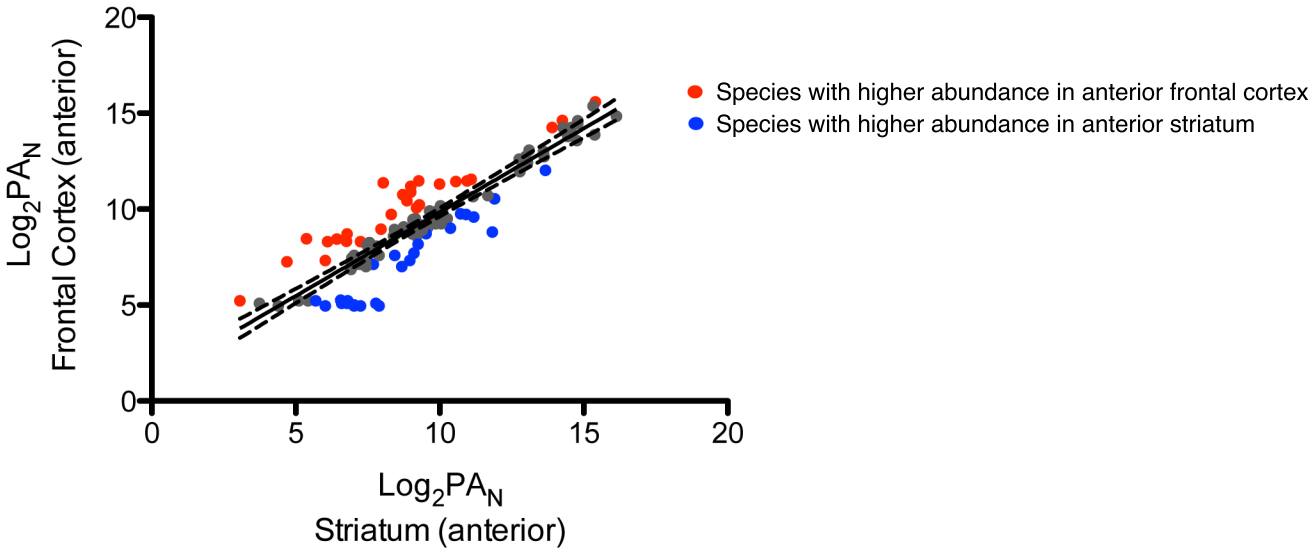
20
15
10
5
0
0
5
10
15
20
Log2PAN
Frontal Cortex (anterior)
Log2PAN
Striatum (anterior)
Species with higher abundance in anterior frontal cortex
Species with higher abundance in anterior striatum

.

Figure 3.1.3b. Heatmap clustering of relative glycerophosphocholine lipid second messenger abundance between anterior regions of uninjured wild-type frontal cortex and striatum. Small molecular weight glycerophosphocholine second messengers were identified by LC-ESI-MS. Data represent the number of standard deviations (Log_2A^*) by which the abundance of a given species in a given animal differs from the mean abundance of the whole population. * denotes species that show at least 1 standard deviation from the mean. These were considered significant and were prioritized for a second level of statistical analysis.

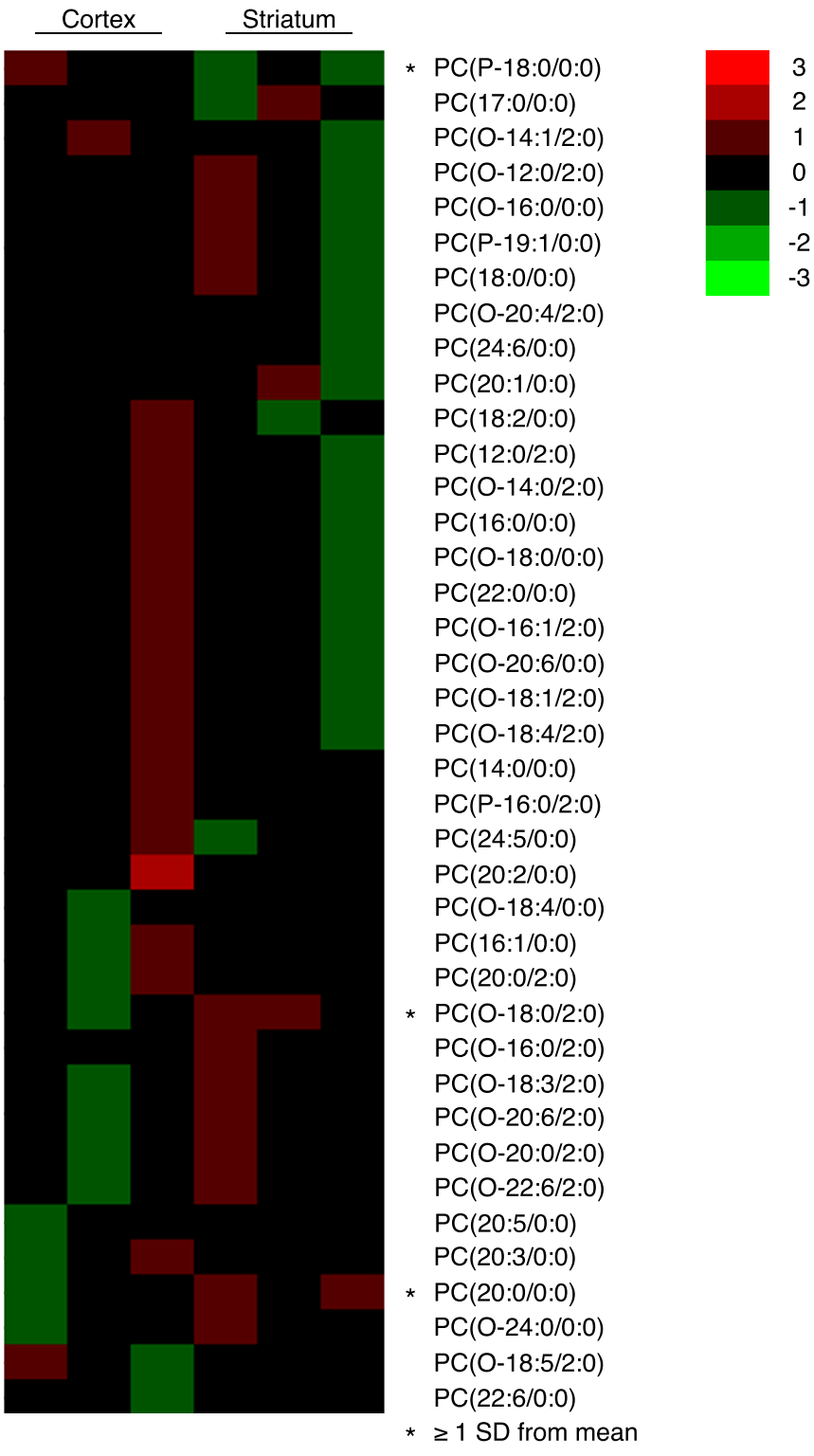
Cortex
Striatum
* PC(P-18:0/0:0)
PC(17:0/0:0)
PC(O-14:1/2:0)
PC(O-12:0/2:0)
PC(O-16:0/0:0)
PC(P-19:1/0:0)
PC(18:0/0:0)
PC(O-20:4/2:0)
PC(24:6/0:0)
PC(20:1/0:0)
PC(18:2/0:0)
PC(12:0/2:0)
PC(O-14:0/2:0)
PC(16:0/0:0)
PC(O-18:0/0:0)
PC(22:0/0:0)
PC(O-16:1/2:0)
PC(O-20:6/0:0)
PC(O-18:1/2:0)
PC(O-18:4/2:0)
PC(14:0/0:0)
PC(P-16:0/2:0)
PC(24:5/0:0)
PC(20:2/0:0)
PC(O-18:4/0:0)
PC(16:1/0:0)
PC(20:0/2:0)
* PC(O-18:0/2:0)
PC(O-16:0/2:0)
PC(O-18:3/2:0)
PC(O-20:6/2:0)
PC(O-20:0/2:0)
PC(O-22:6/2:0)
PC(20:5/0:0)
PC(20:3/0:0)
* PC(20:0/0:0)
PC(O-24:0/0:0)
PC(O-18:5/2:0)
PC(22:6/0:0)
* ≥ 1 SD from mean
3
2
1
0
-1
-2
-3

Figure 3.1.3c. Medial-lateral gradients of glycerophosphocholine lipid second messenger abundance between anterior regions of uninjured wild-type frontal cortex and striatum. Small molecular weight glycerophosphocholine second messengers were identified by LC-ESI-MS. Log_2-transformed normalized peak areas (Log_2PA_N) for lipid species exhibiting a regional difference by heatmap analysis were further analyzed in posterior regions of frontal cortex and striatum by paired t-test. *p<0.05. **p<0.01. ***p<0.005.

i. PC(O-14:1/2:0)

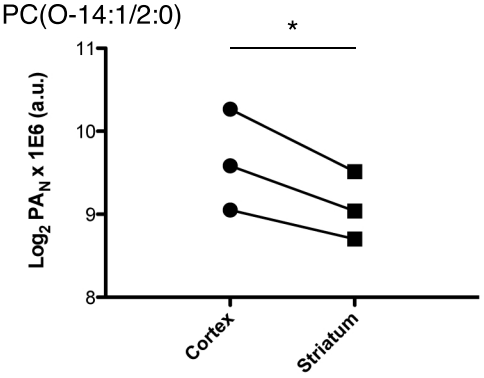

ii.PC(O-18:4/0:0)

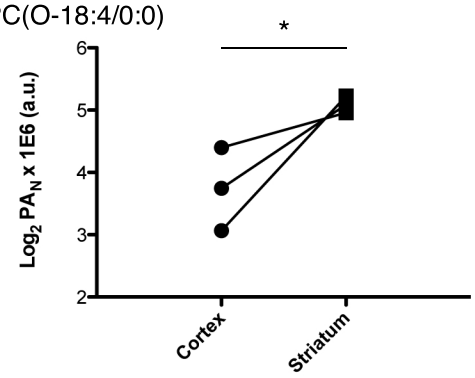

iii. PC(O-18:0/0:0)

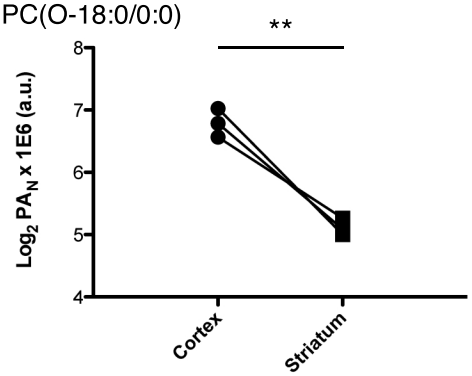

iv. PC(O-20:6/0:0)

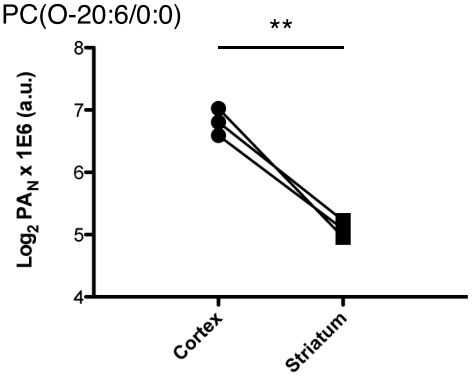

v. PC(O-18:4/2:0)

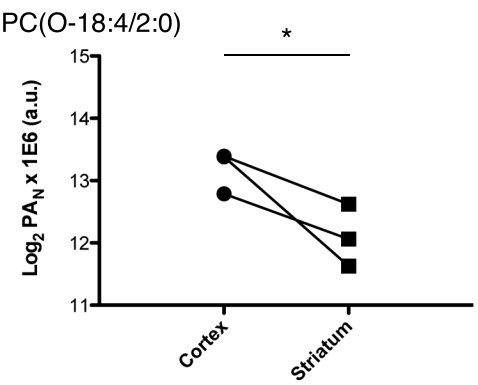

vi. PC(O-18:3/2:0)

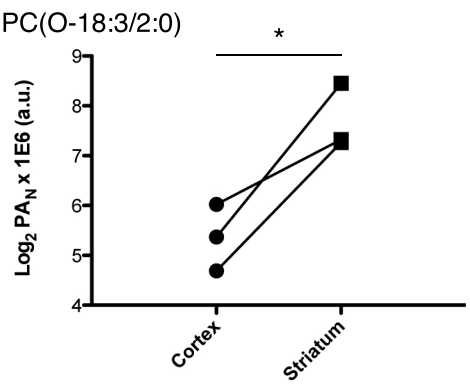

vii. PC(O-18:1/2:0)

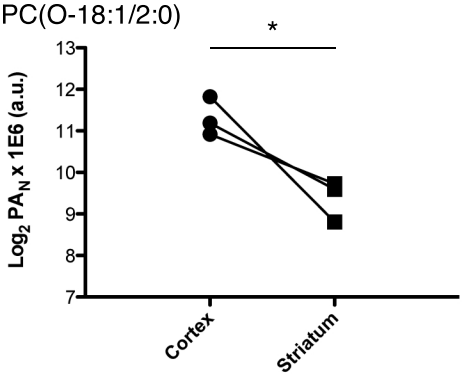

viii.PC(O-18:0/2:0)

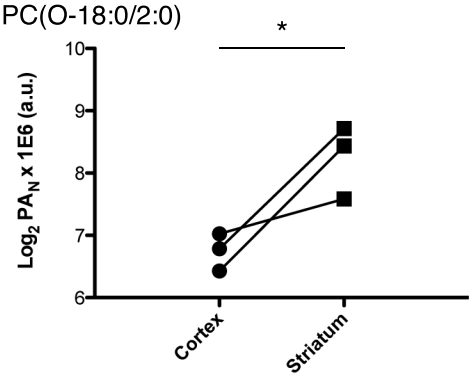

ix. PC(O-22:6/2:0)

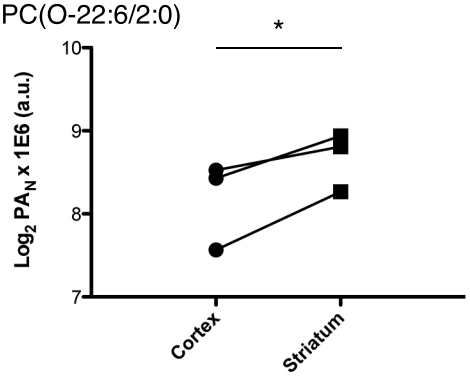

Lipid Species	Mean Log_2PA_N x 10^6		Paired t-test p-value
	Cortex	Striatum	
PC(O-14:1/2:0)	9.63E+00	9.08E+00	0.0209
PC(O-18:4/0:0)	3.74E+00	5.09E+00	0.0496
PC(O-18:0/0:0)	6.79E+00	5.12E+00	0.0077
PC(O-20:6/0:0)	6.81E+00	5.09E+00	0.0052
PC(O-18:4/2:0)	1.32E+01	1.21E+01	0.0420
PC(O-18:3/2:0)	5.36E+00	7.68E+00	0.0243
PC(O-18:1/2:0)	1.13E+01	9.37E+00	0.0364
PC(O-18:0/2:0)	6.75E+00	8.25E+00	0.0429
PC(O-22:6/2:0)	8.17E+00	8.67E+00	0.0275

Table 3.1.3. Lipid species that show significantly altered abundance between anterior regions of uninjured frontal cortex and striatum by paired t-test.

3.1.4 Lipid differences between posterior regions of uninjured cortex and striatum in the forebrain.

Linear regression analysis between posterior regions of striatum (X-axis) and cortex (Y-axis), revealed 23 glycerophosphocholine second messenger lipid species in 3 animals with increased abundance in posterior cortical tissue (red dots) and 17 lipid species in 3 animals with increased abundance in posterior striatal tissue (blue dots) (Fig 3.1.4a). Two lipid species, PC(O-14:0/2:0) and PC(20:4/0:0), displayed at least one standard deviation difference between mean Log_2A^* data by heatmap analysis (Fig 3.1.4b). Finally, eleven lipid species (Table 3.1.4) showed significantly altered abundance between posterior regions of frontal cortex and striatum by paired t-test (Fig 3.1.4c).

Figure 3.1.4a. Global differences in glycerophosphocholine second messenger lipid abundance between anterior and posterior regions of uninjured wild-type frontal cortex. Small molecular weight glycerophosphocholine second messengers were identified by LC-ESI-MS. Data shown represent log_2-transformed normalized peak area (Log_2PA_N) for each region plotted as (X,Y) coordinates. Dotted lines represent the 95% confidence interval identified by linear regression analysis. Species that fell above the interval (red dots) are more abundant in posterior frontal cortex, while those below (blue dots) are more abundant in posterior striatum.

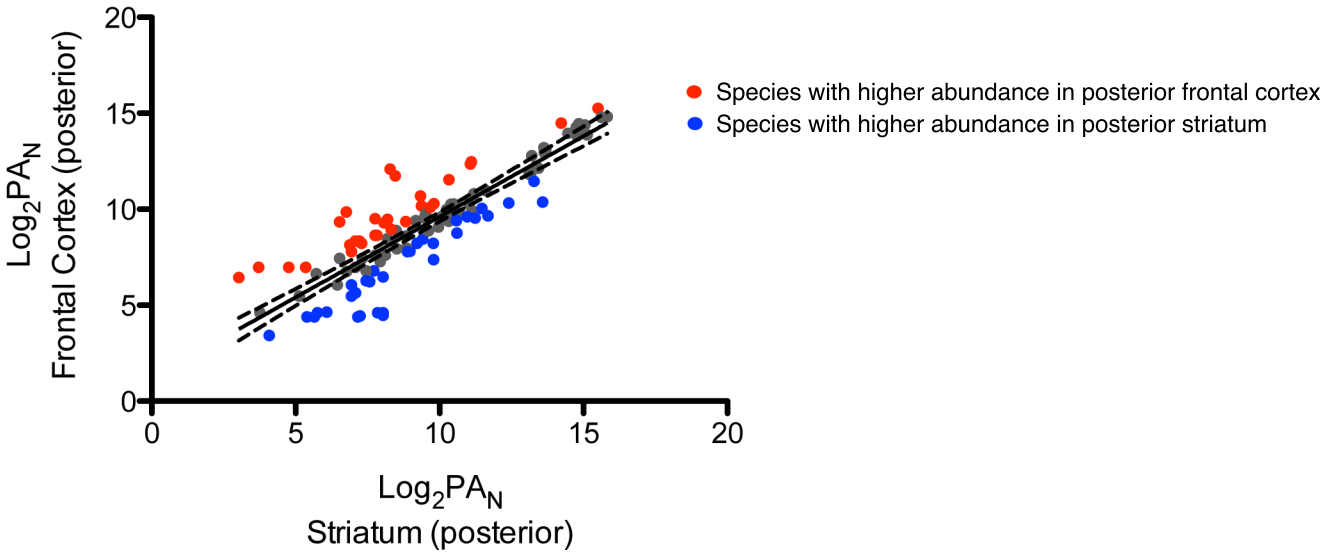
20
15
10
5
0
0
5
10
15
20
Log2PAN
Frontal Cortex (posterior)
Log2PAN
Striatum (posterior)
Species with higher abundance in posterior frontal cortex
Species with higher abundance in posterior striatum

.

Figure 3.1.4b. Heatmap clustering of relative glycerophosphocholine lipid second messenger abundance between posterior regions of uninjured wild-type frontal cortex and striatum. Small molecular weight glycerophosphocholine second messengers were identified by LC-ESI-MS. Data represent the number of standard deviations (Log_2A^*) by which the abundance of a given species in a given animal differs from the mean abundance of the whole population. * denotes species that show at least 1 standard deviation from the mean. These were considered significant and were prioritized for a second level of statistical analysis.

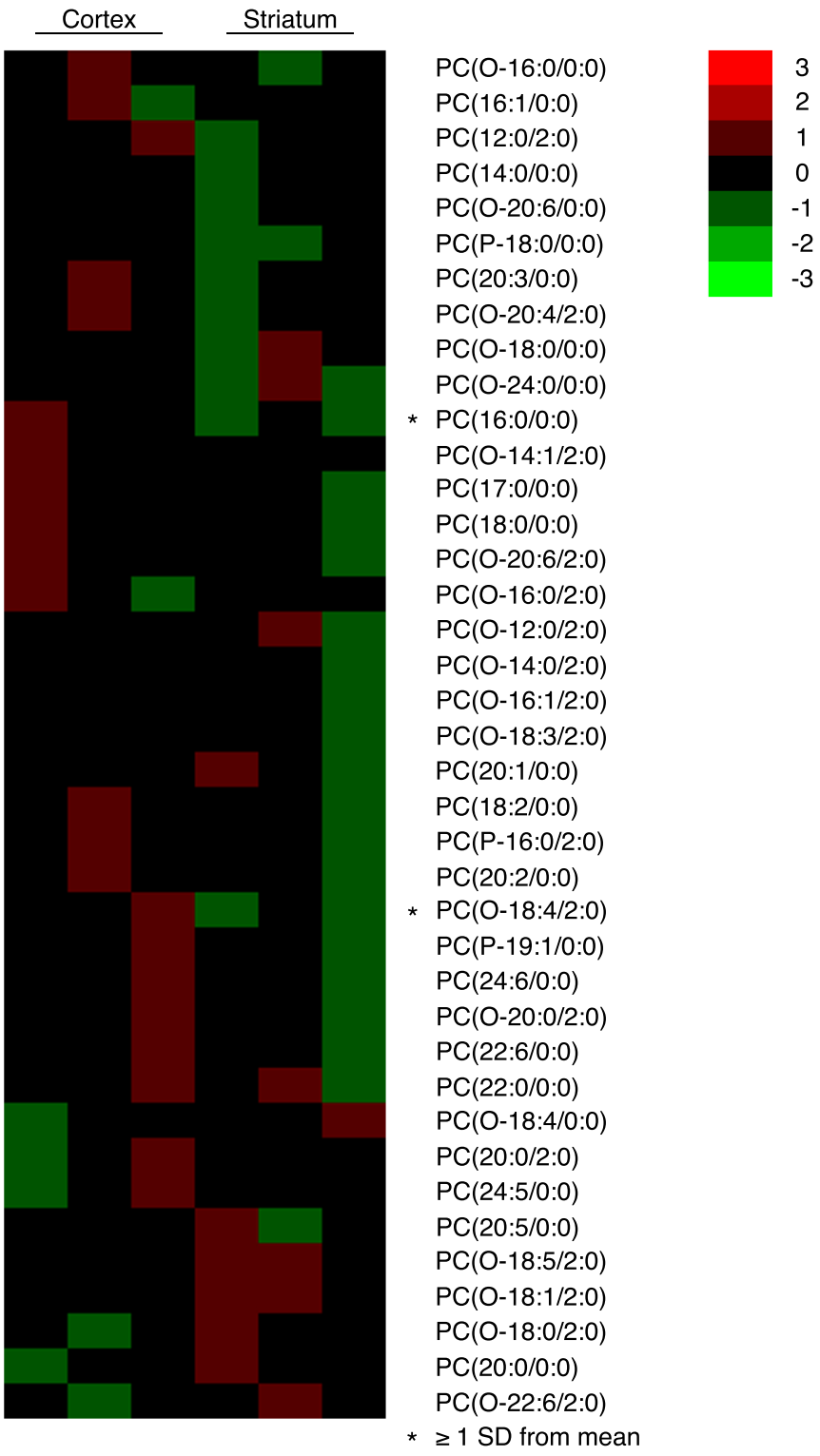
Cortex
Striatum
PC(O-16:0/0:0)
PC(16:1/0:0)
PC(12:0/2:0)
PC(14:0/0:0)
PC(O-20:6/0:0)
PC(P-18:0/0:0)
PC(20:3/0:0)
PC(O-20:4/2:0)
PC(O-18:0/0:0)
PC(O-24:0/0:0)
* PC(16:0/0:0)
PC(O-14:1/2:0)
PC(17:0/0:0)
PC(18:0/0:0)
PC(O-20:6/2:0)
PC(O-16:0/2:0)
PC(O-12:0/2:0)
PC(O-14:0/2:0)
PC(O-16:1/2:0)
PC(O-18:3/2:0)
PC(20:1/0:0)
PC(18:2/0:0)
PC(P-16:0/2:0)
PC(20:2/0:0)
* PC(O-18:4/2:0)
PC(P-19:1/0:0)
PC(24:6/0:0)
PC(O-20:0/2:0)
PC(22:6/0:0)
PC(22:0/0:0)
PC(O-18:4/0:0)
PC(20:0/2:0)
PC(24:5/0:0)
PC(20:5/0:0)
PC(O-18:5/2:0)
PC(O-18:1/2:0)
PC(O-18:0/2:0)
PC(20:0/0:0)
PC(O-22:6/2:0)
* ≥ 1 SD from mean
3
2
1
0
-1
-2
-3

Figure 3.1.4c. Medial-lateral gradients of glycerophosphocholine lipid second messenger abundance between posterior regions of uninjured wild-type frontal cortex and striatum. Small molecular weight glycerophosphocholine second messengers were identified by LC-ESI-MS. Log_2-transformed normalized peak areas (Log_2PA_N) for lipid species exhibiting a regional difference by heatmap analysis were further analyzed in posterior regions of frontal cortex and striatum by paired t-test. *p<0.05. **p<0.01. ***p<0.005.

i. PC(O-14:0/2:0)

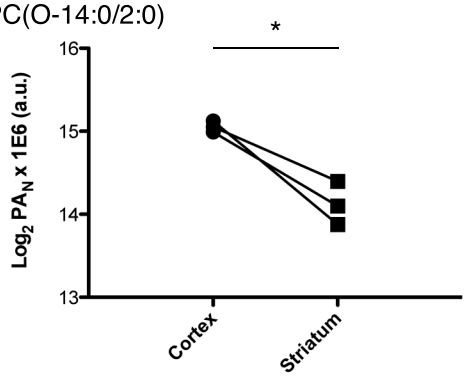

ii.PC(16:0/0:0)

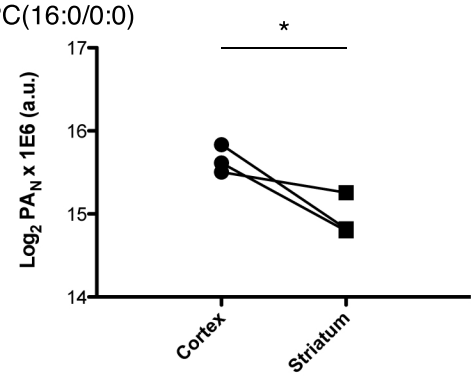

iii. PC(18:2/0:0)

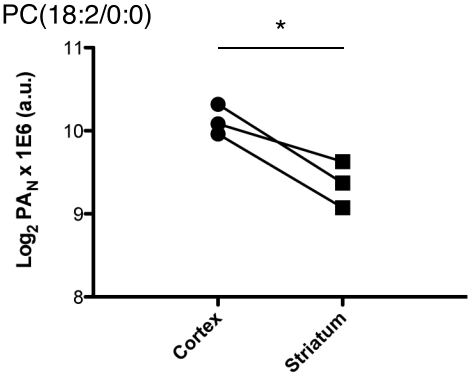

iv. PC(O-16:1/2:0)

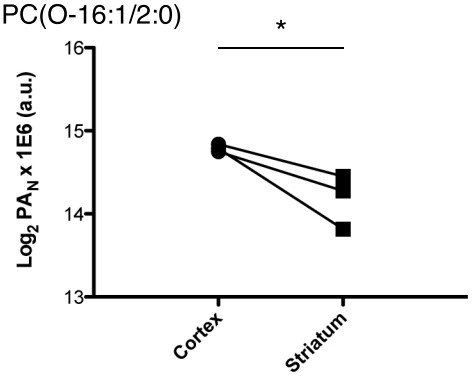

v. PC(P-16:0/2:0)

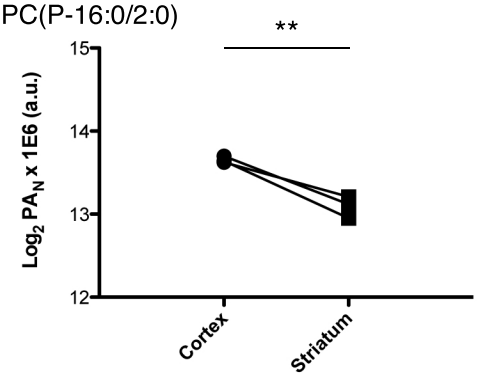

vi. PC(O-18:4/2:0)

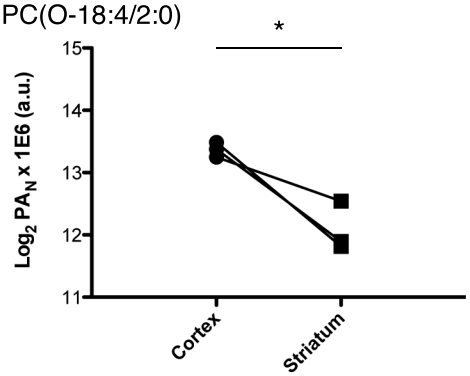

vii. PC(20:3/0:0)

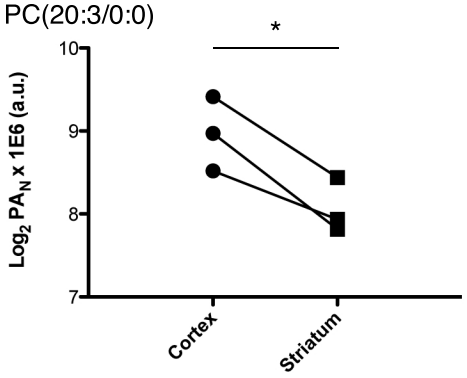

viii.PC(O-18:0/2:0)

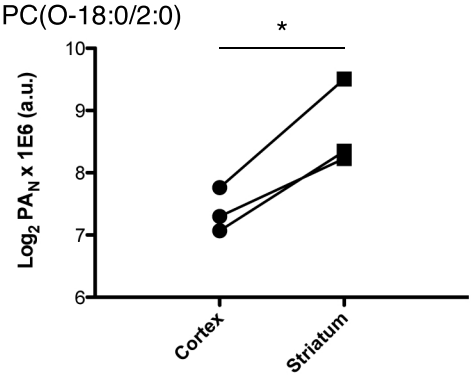

ix. PC(22:6/0:0)

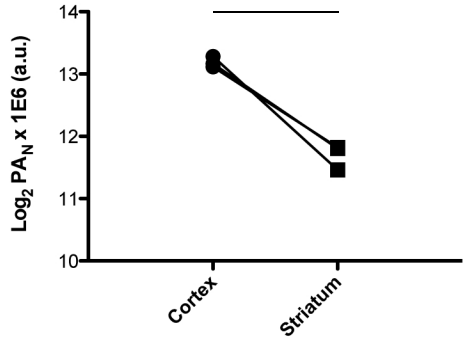

x. PC(O-20:6/2:0)

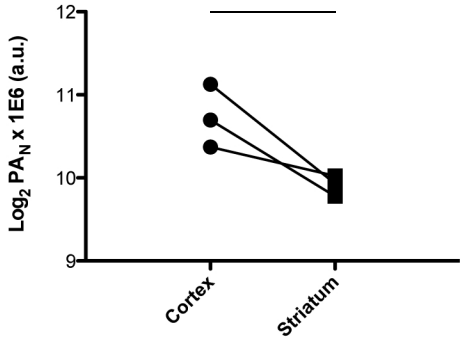

xi. PC(O-20:4/2:0)

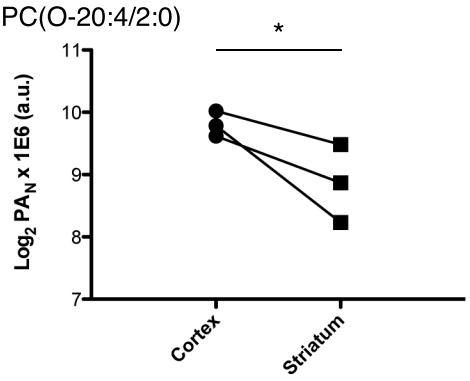

Lipid Species	Mean Log_2PA_N x 10^6		Paired t-test p-value
	Cortex	Striatum	
PC(O-14:0/2:0)	1.51E+01	1.41E+01	0.0162
PC(16:0/0:0)	1.56E+01	1.50E+01	0.0473
PC(18:2/0:0)	1.01E+01	9.36E+00	0.0195
PC(O-16:1/2:0)	1.48E+01	1.42E+01	0.0393
PC(P-16:0/2:0)	1.37E+01	1.31E+01	0.0096
PC(O-18:4/2:0)	1.33E+01	1.24E+01	0.0370
PC(20:3/0:0)	8.97E+00	8.06E+00	0.0164
PC(O-18:0/2:0)	7.38E+00	8.69E+00	0.0152
PC(22:6/0:0)	1.32E+01	1.17E+01	0.0060
PC(O-20:6/2:0)	1.07E+01	9.91E+00	0.0406
PC(O-20:4/2:0)	9.81E+00	8.86E+00	0.0457

Table 3.1.4. Lipid species that show significantly altered abundance between posterior regions of uninjured frontal cortex and striatum by paired t-test.

3.2 MCAO disrupts glycerophosphocholine metabolism with regional specificity in C57Bl/6 striatum and frontal cortex

3.2.1 Lipid differences between anterior and posterior regions of ischemic frontal cortex.

Heatmap analysis using Log_2PA_N x 10^6 $_{Fold\ Change}$ was used to assess the impact of MCAO on the relative abundance of discrete glycerophosphocholine second messenger lipids between anterior and posterior regions of frontal cortex. Five lipid species, PC(O-12:0/2:0), PC(16:0/0:0), PC(20:1/0:0), PC(O-20:6/2:0) and PC(24:5/0:0) fell at least one standard deviation from the species mean and met our first criteria for significant biological change (Fig 3.2.1a). Further, 2-way ANOVA analysis with a Bonferroni *post-hoc* test revealed statistically significant differences in the levels of four of these five lipids between anterior and posterior regions of

Figure 3.2.1a. Heatmap clustering of relative glycerophosphocholine lipid second messenger abundance between anterior and posterior regions of wild-type frontal cortex following MCAO. Small molecular weight glycerophosphocholine second messengers were identified by LC-ESI-MS. Data are expressed as a ratio of abundance of ischemic to uninjured tissue ($Log_2PA_{N\ Fold\ Change}$). The number of standard deviations ($Log_2A^*_{Fold\ Change}$) by which the abundance of a given species in a given animal differs from the mean abundance of the whole population is colour-coded (green (less than expected) to red (greater than expected). * denotes species that show at least 1 standard deviation from the mean. This difference was considered significant and species were prioritized for a second level of statistical analysis.

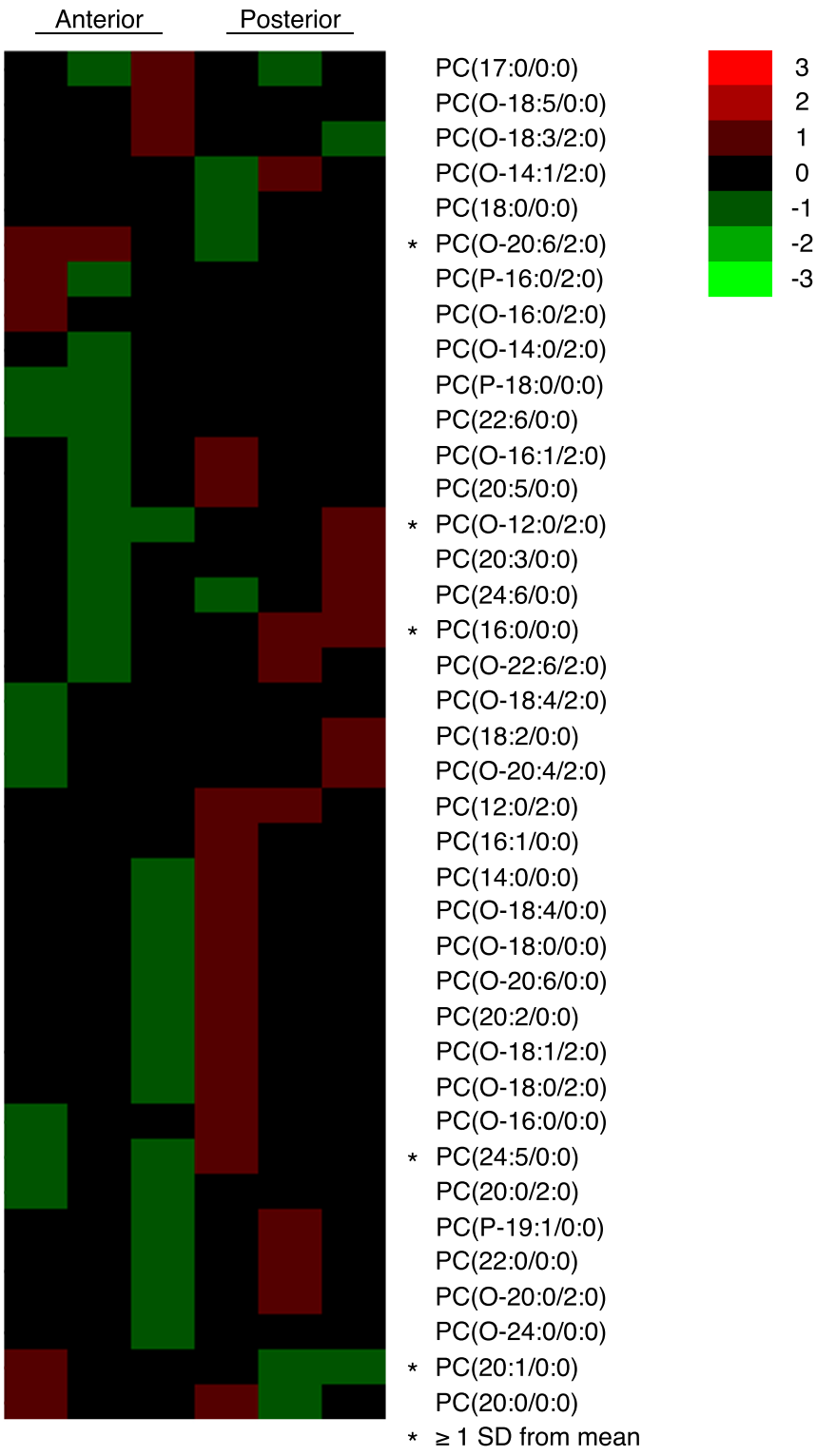
Anterior
Posterior
PC(17:0/0:0)
PC(O-18:5/0:0)
PC(O-18:3/2:0)
PC(O-14:1/2:0)
PC(18:0/0:0)
* PC(O-20:6/2:0)
PC(P-16:0/2:0)
PC(O-16:0/2:0)
PC(O-14:0/2:0)
PC(P-18:0/0:0)
PC(22:6/0:0)
PC(O-16:1/2:0)
PC(20:5/0:0)
* PC(O-12:0/2:0)
PC(20:3/0:0)
PC(24:6/0:0)
* PC(16:0/0:0)
PC(O-22:6/2:0)
PC(O-18:4/2:0)
PC(18:2/0:0)
PC(O-20:4/2:0)
PC(12:0/2:0)
PC(16:1/0:0)
PC(14:0/0:0)
PC(O-18:4/0:0)
PC(O-18:0/0:0)
PC(O-20:6/0:0)
PC(20:2/0:0)
PC(O-18:1/2:0)
PC(O-18:0/2:0)
PC(O-16:0/0:0)
* PC(24:5/0:0)
PC(20:0/2:0)
PC(P-19:1/0:0)
PC(22:0/0:0)
PC(O-20:0/2:0)
PC(O-24:0/0:0)
* PC(20:1/0:0)
PC(20:0/0:0)
* ≥ 1 SD from mean
3
2
1
0
-1
-2
-3

Figure 3.2.1b. Differences in glycerophosphocholine lipid second messenger abundance between anterior and posterior frontal cortex in uninjured wild-type mice and following MCAO. Small molecular weight glycerophosphocholine second messengers were identified by LC-ESI-MS. Data shown represent Log_2-transformed normalized peak area (Log_2PA_N) for species identified as significant by heatmap analysis, compared by paired 2-way ANOVA followed by *post-hoc* Bonferroni. *p<0.05. **p<0.01. ***p<0.005.

i. PC(O-12:0/2:0)

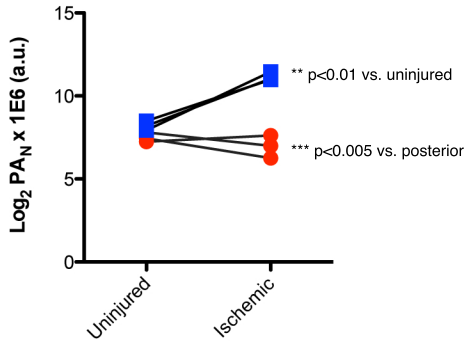

ii.. PC(16:0/0:0)

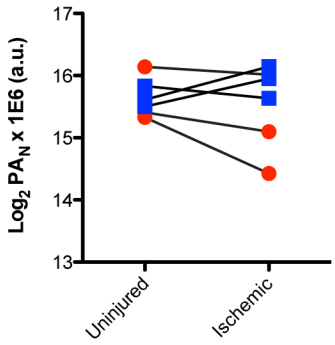

iii. PC(20:1/0:0)

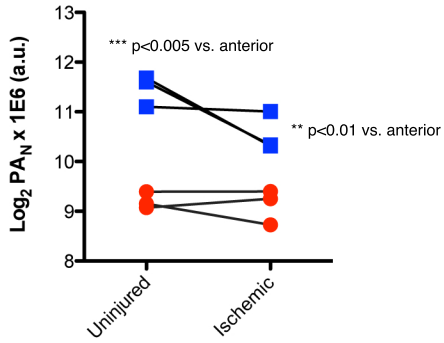

iv. PC(O-20:6/2:0)

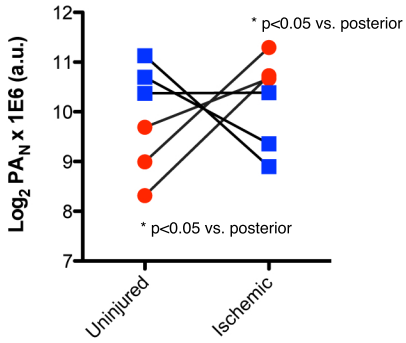

v. PC(24:5/0:0)

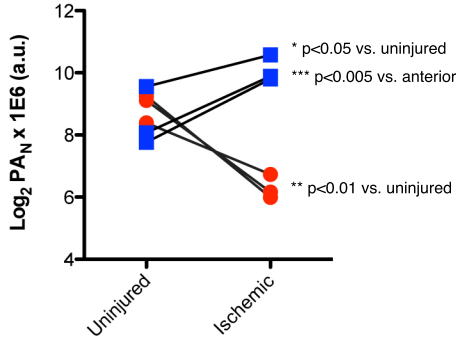



cortex, and injured or uninjured state (Fig 3.2.1b). PC(O-12:0/2:0) was significantly more abundant in the posterior section of cortex following MCAO compared to uninjured (** $p<0.01$) and compared to anterior regions of ischemic cortex (*** $p<0.005$). PC(20:1/0:0) was more abundant in posterior regions of frontal cortex compared to anterior regions, in both uninjured (*** $p<0.005$) and ischemic (** $p<0.01$) tissue. PC(O-20:6/2:0) was more abundant in posterior regions of uninjured cortex (* $p<0.05$), and less abundant in posterior regions of ischemic cortex (* $p<0.05$). PC(24:5/0:0) was significantly more abundant in ischemic tissue in both anterior (** $p<0.01$) and posterior (* $p<0.05$) regions of frontal cortex compared to uninjured. Further, PC(24:5/0:0) was significantly more abundant in posterior regions of ischemic cortex compared to anterior regions of ischemic cortex (** $p<0.01$).

3.2.2 Lipid differences between anterior and posterior regions of ischemic striatum.

Heatmap analysis, as performed in 3.2.1, showed one lipid species, PC(20:0/2:0), that displayed altered abundance between anterior and posterior regions of striatum between the uninjured and ischemic conditions (Fig 3.2.2a). Two-way ANOVA analysis with Bonferroni *post-hoc* test revealed that higher levels of PC(20:0/2:0) were present in ischemic striatum compared to uninjured (* $p<0.05$), and further that PC(20: 0/2:0 was more abundant in anterior than posterior regions of ischemic striatum (** $p<0.01$) (Fig 3.2.2b).

Figure 3.2.2a. Heatmap clustering of relative glycerophosphocholine lipid second messenger abundance between anterior and posterior regions of wild-type striatum following MCAO. Small molecular weight glycerophosphocholine second messengers were identified by LC-ESI-MS. Data are expressed as a ratio of abundance of ischemic to uninjured tissue ($Log_2PA_{N\ Fold\ Change}$). The number of standard deviations ($Log_2A^*_{Fold\ Change}$) by which the abundance of a given species in a given animal differs from the mean abundance of the whole population is colour-coded (green (less than expected) to red (greater than expected). * denotes species that show at least 1 standard deviation from the mean. This difference was considered significant and species were prioritized for a second level of statistical analysis.

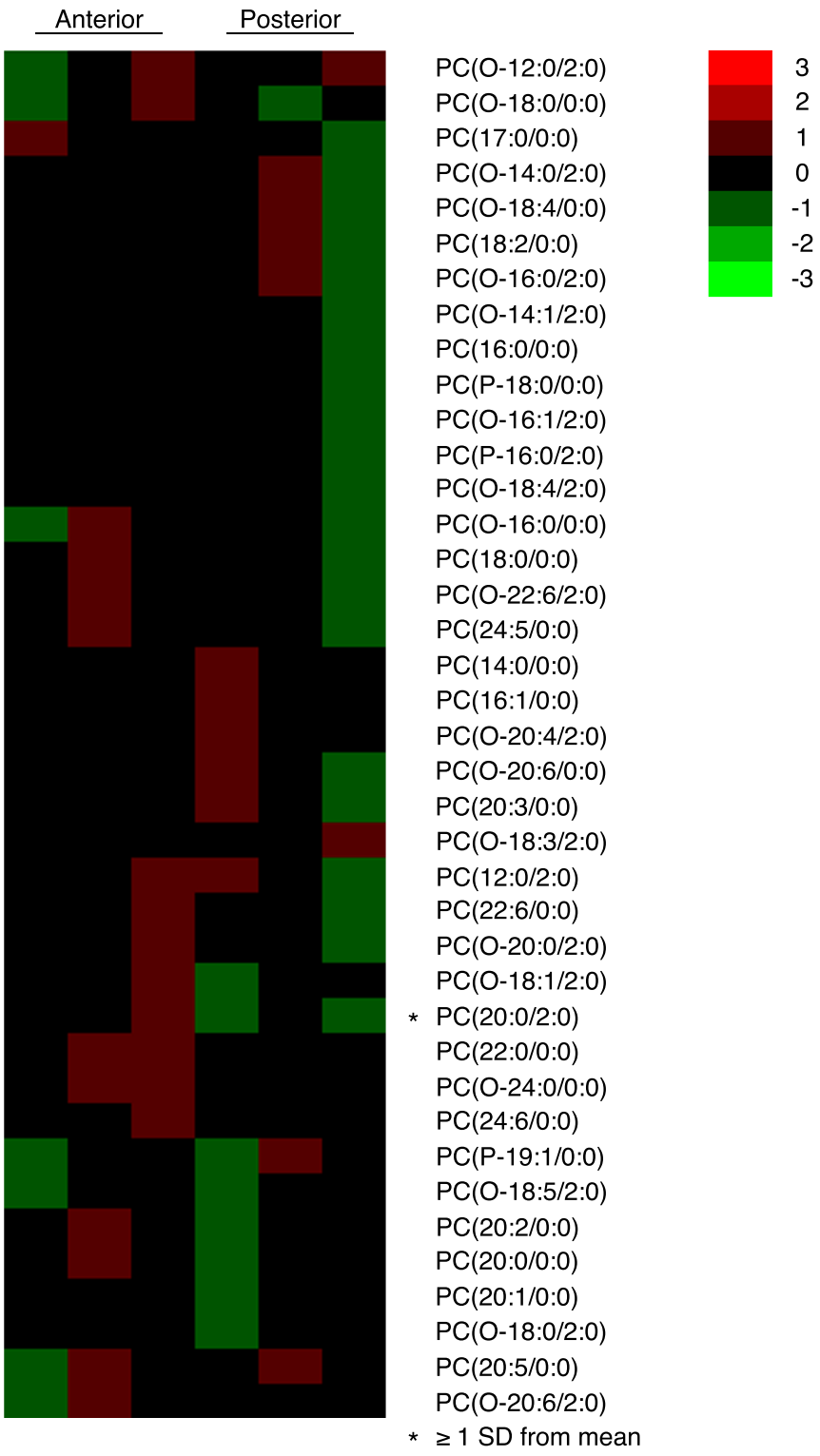
Anterior
Posterior
PC(O-12:0/2:0)
PC(O-18:0/0:0)
PC(17:0/0:0)
PC(O-14:0/2:0)
PC(O-18:4/0:0)
PC(18:2/0:0)
PC(O-16:0/2:0)
PC(O-14:1/2:0)
PC(16:0/0:0)
PC(P-18:0/0:0)
PC(O-16:1/2:0)
PC(P-16:0/2:0)
PC(O-18:4/2:0)
PC(O-16:0/0:0)
PC(18:0/0:0)
PC(O-22:6/2:0)
PC(24:5/0:0)
PC(14:0/0:0)
PC(16:1/0:0)
PC(O-20:4/2:0)
PC(O-20:6/0:0)
PC(20:3/0:0)
PC(O-18:3/2:0)
PC(12:0/2:0)
PC(22:6/0:0)
PC(O-20:0/2:0)
PC(O-18:1/2:0)
* PC(20:0/2:0)
PC(22:0/0:0)
PC(O-24:0/0:0)
PC(24:6/0:0)
PC(P-19:1/0:0)
PC(O-18:5/2:0)
PC(20:2/0:0)
PC(20:0/0:0)
PC(20:1/0:0)
PC(O-18:0/2:0)
PC(20:5/0:0)
PC(O-20:6/2:0)
3
2
1
0
-1
-2
-3
* ≥ 1 SD from mean

Figure 3.2.2b. Differences in glycerophosphocholine lipid second messenger abundance between anterior and posterior striatum in uninjured wild-type mice and following MCAO. Small molecular weight glycerophosphocholine second messengers were identified by LC-ESI-MS. Data shown represent Log_2-transformed normalized peak area (Log_2PA_N) for species identified as significant by heatmap analysis, compared by paired 2-way ANOVA followed by *post-hoc* Bonferroni. *p<0.05. **p<0.01. ***p<0.005.

i. PC(20:0/2:0)

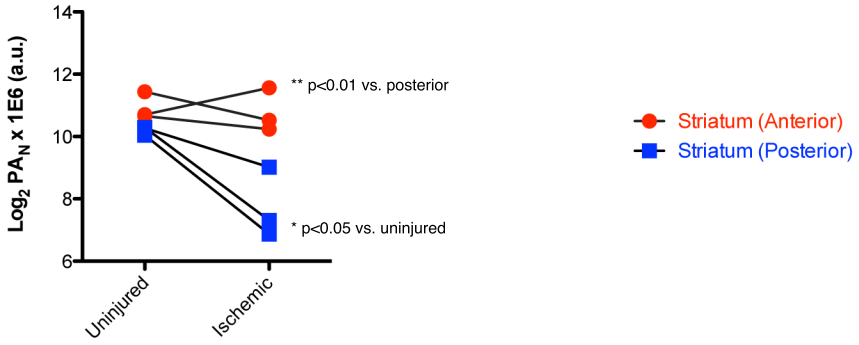
14
12
10
8
6
Log2 PAN x 1E6 (a.u.)
** p<0.01 vs. posterior
* p<0.05 vs. uninjured
Uninjured
Ischemic
Striatum (Anterior)
Striatum (Posterior)

3.2.3 Lipid differences between anterior regions of ischemic striatum and frontal cortex.

Heatmap analysis identified six glycerophosphocholine second messenger lipid species – PC(16:0/0:0), PC(P-18:0/0:0), PC(O-16:1/2:0), PC(O-20:6/0:0), PC(20:1/0:0) an PC(22:0/0:0) – that showed altered abundance between anterior regions of striatum and frontal cortex between the uninjured and ischemic conditions (Fig. 3.2.3a). Of these six species, five showed statistically significant differences in abundance by 2-way ANOVA and *post-hoc* Bonferroni. PC(P-18:0/0:0) was more abundant in anterior ischemic striatum compared to both ischemic anterior cortex (*** $p<0.005$) and uninjured anterior striatum (* $p<0.05$), and less abundant in ischemic anterior frontal cortex compared to uninjured anterior cortex (* $p<0.05$). PC(O-16:1/2:0) was less abundant in anterior ischemic cortex compared to uninjured (* $p<0.05$). PC(O-20:6/0:0) was more abundant in uninjured anterior cortex compared to anterior striatum (*** $p<0.005$), but, conversely, more abundant in ischemic anterior striatum compared to ischemic anterior cortex (* $p<0.05$). In addition, higher levels of PC(O-20:6/0:0) were detected in ischemic anterior striatum relative to uninjured (* $p<0.05$). A reverse relationship was detected in cortex at the same bregma. Levels of PC(O-20:6/0:0) were found to decrease in ischemic compared to uninjured cortex (* $p<0.05$). Further, PC(20:1/0:0) increased in ischemic anterior striatum compared to both uninjured striatum ($p<0.05$), and ischemic anterior cortex (* $p<0.05$). Finally, PC(22:0/0:0) was more abundant in ischemic anterior striatum compared to anterior cortex (* $p<0.05$) (Fig. 3.2.3b).

Figure 3.2.3a. Heatmap clustering of relative glycerophosphocholine lipid second messenger abundance between anterior regions of wild-type frontal cortex and striatum following MCAO. Small molecular weight glycerophosphocholine second messengers were identified by LC-ESI-MS. Data are expressed as a ratio of abundance of ischemic to uninjured tissue ($Log_2PA_{N\ Fold\ Change}$). The number of standard deviations ($Log_2A^*_{Fold\ Change}$) by which the abundance of a given species in a given animal differs from the mean abundance of the whole population is colour-coded (green (less than expected) to red (greater than expected). * denotes species that show at least 1 standard deviation from the mean. This difference was considered significant and species were prioritized for a second level of statistical analysis.

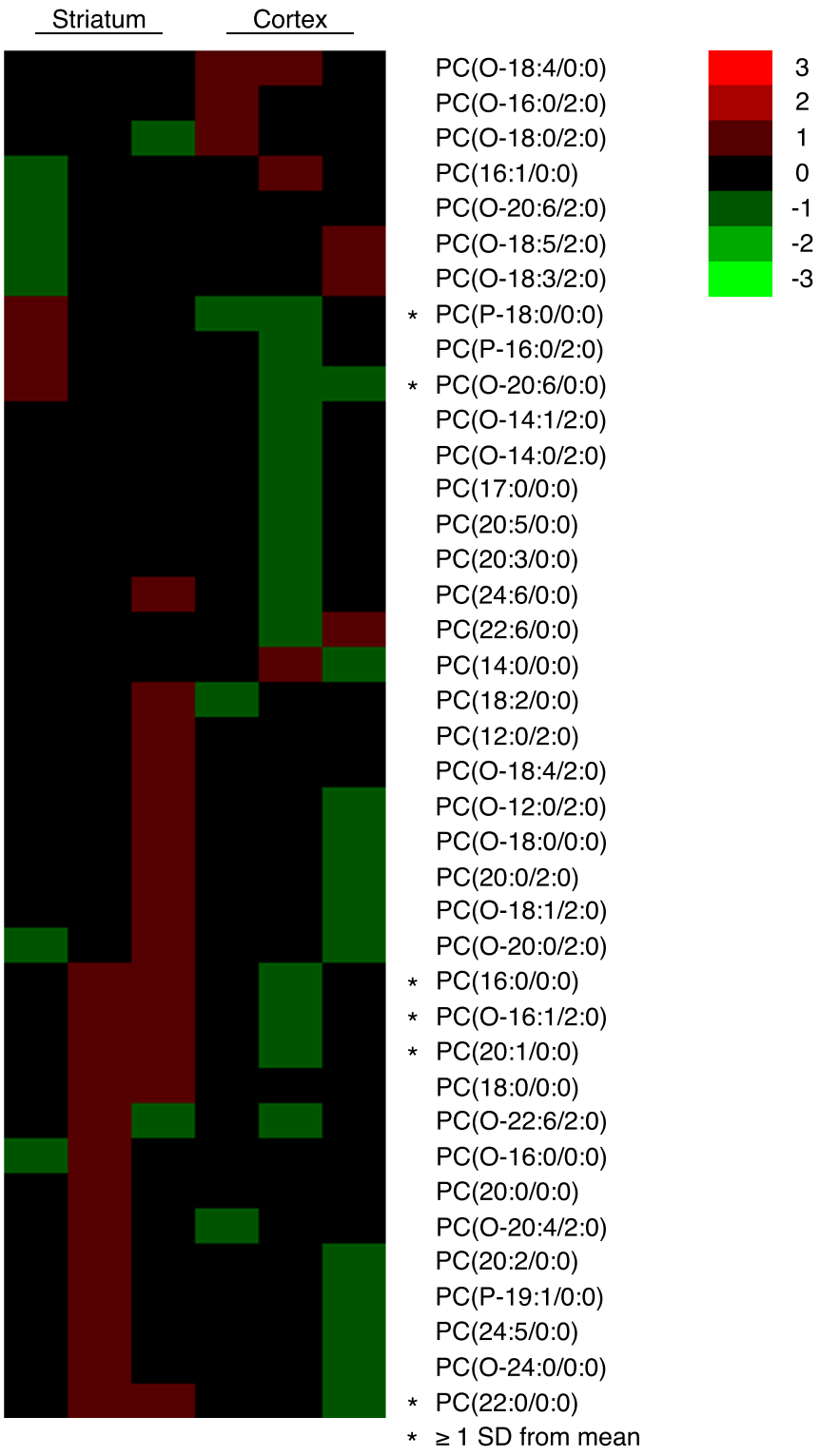
Striatum
Cortex
PC(O-18:4/0:0)
PC(O-16:0/2:0)
PC(O-18:0/2:0)
PC(16:1/0:0)
PC(O-20:6/2:0)
PC(O-18:5/2:0)
PC(O-18:3/2:0)
* PC(P-18:0/0:0)
PC(P-16:0/2:0)
* PC(O-20:6/0:0)
PC(O-14:1/2:0)
PC(O-14:0/2:0)
PC(17:0/0:0)
PC(20:5/0:0)
PC(20:3/0:0)
PC(24:6/0:0)
PC(22:6/0:0)
PC(14:0/0:0)
PC(18:2/0:0)
PC(12:0/2:0)
PC(O-18:4/2:0)
PC(O-12:0/2:0)
PC(O-18:0/0:0)
PC(20:0/2:0)
PC(O-18:1/2:0)
PC(O-20:0/2:0)
* PC(16:0/0:0)
* PC(O-16:1/2:0)
* PC(20:1/0:0)
PC(18:0/0:0)
PC(O-22:6/2:0)
PC(O-16:0/0:0)
PC(20:0/0:0)
PC(O-20:4/2:0)
PC(20:2/0:0)
PC(P-19:1/0:0)
PC(24:5/0:0)
PC(O-24:0/0:0)
* PC(22:0/0:0)
* ≥ 1 SD from mean
3
2
1
0
-1
-2
-3

Figure 3.2.3b. Differences in glycerophosphocholine lipid second messenger abundance between anterior regions of frontal cortex and striatum in uninjured wild-type mice and following MCAO. Small molecular weight glycerophosphocholine second messengers were identified by LC-ESI-MS. Data shown represent Log_2-transformed normalized peak area (Log_2PA_N) for species identified as significant by heatmap analysis, compared by paired 2-way ANOVA followed by *post-hoc* Bonferroni. *p<0.05. **p<0.01. ***p<0.005.

i. PC(16:0/0:0)

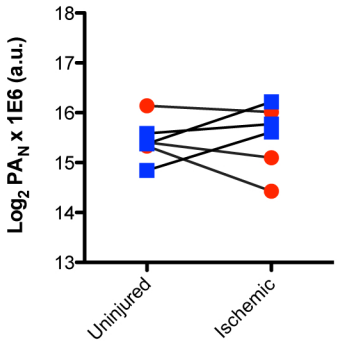

ii. PC(P-18:0/0:0)

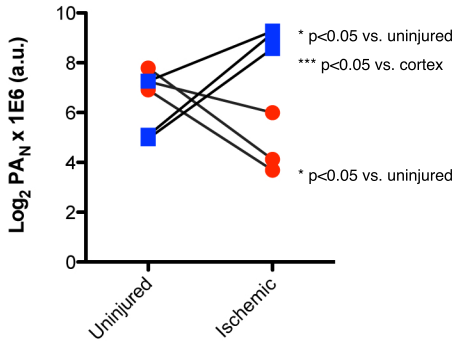

iii. PC(O-16:1/2:0)

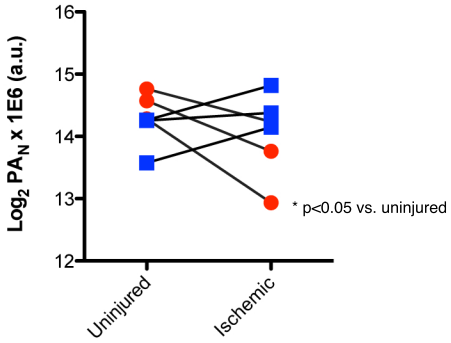

iv. PC(O-20:6/0:0)

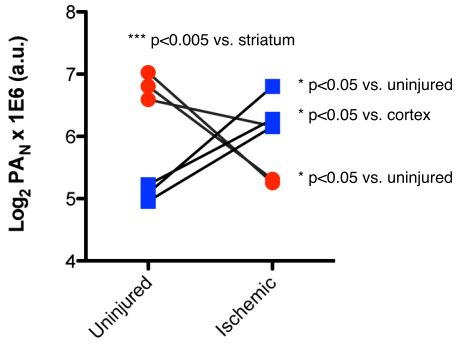

v. PC(20:1/0:0)

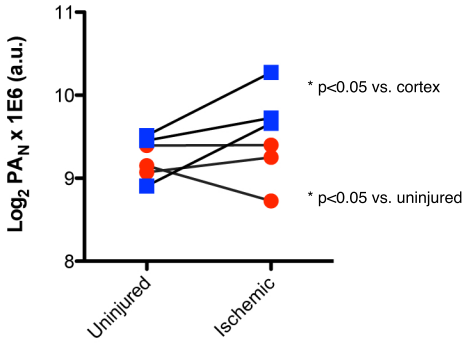

vi. PC(22:0/0:0)

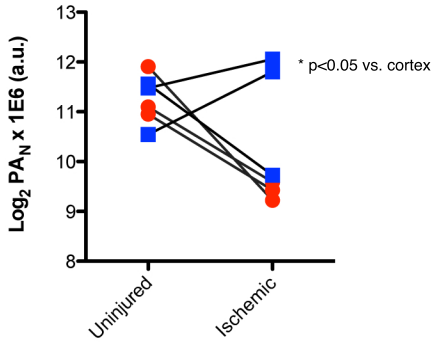

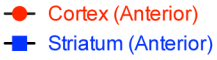

3.2.4 Lipid differences between posterior regions of ischemic striatum and frontal cortex.

Three glycerophosphocholine lipid second messenger species – PC(20:5/0:0), PC(22:6/0:0) and PC(O-20:0/2:0) – showed altered abundance between posterior regions of cortex and striatum between ischemic and uninjured tissue, by heatmap analysis (Fig 3.2.4a). PC(20:5/0:0) was more abundant in posterior regions of ischemic cortex compared to both posterior ischemic striatum (* $p<0.05$, two-way ANOVA with Bonferroni *post-hoc* test) and uninjured posterior cortex (** $p<0.01$). PC(22:6/0:0) was more abundant in posterior cortex compared to posterior striatum in both uninjured (* $p<0.05$) and ischemic (* $p<0.05$) tissue. PC(22:6/0:0) was more abundant in ischemic posterior cortex compared to ischemic posterior striatum (*** $p<0.005$). Finally, PC(O-20:0/2:0) was more abundant in ischemic posterior frontal cortex compared to ischemic posterior striatum (** $p<0.01$) (Fig. 3.2.4b).

3.3. PAFR null-mutation alters glycerophospholipid metabolism in uninjured brain and following MCAO.

We performed the same analyses on $PAFR^{-/-}$ mice identifying a different profile of regional and injury-specific metabolism compared to congenic C57Bl/6 wild-type mice. The analyses presented above on $PAFR^{-/-}$ mice were replicated (Appendix 1) and the changes observed between null-mutant and wild-type mice in uninjured animals and following MCAO are presented in detail below.

Figure 3.2.4a. Heatmap clustering of relative glycerophosphocholine lipid second messenger abundance between posterior regions of wild-type frontal cortex and striatum following MCAO. Small molecular weight glycerophosphocholine second messengers were identified by LC-ESI-MS. Data are expressed as a ratio of abundance of ischemic to uninjured tissue ($Log_2PA_{N\ Fold\ Change}$). The number of standard deviations ($Log_2A^*_{Fold\ Change}$) by which the abundance of a given species in a given animal differs from the mean abundance of the whole population is colour-coded (green (less than expected) to red (greater than expected). * denotes species that show at least 1 standard deviation from the mean. This difference was considered significant and species were prioritized for a second level of statistical analysis.

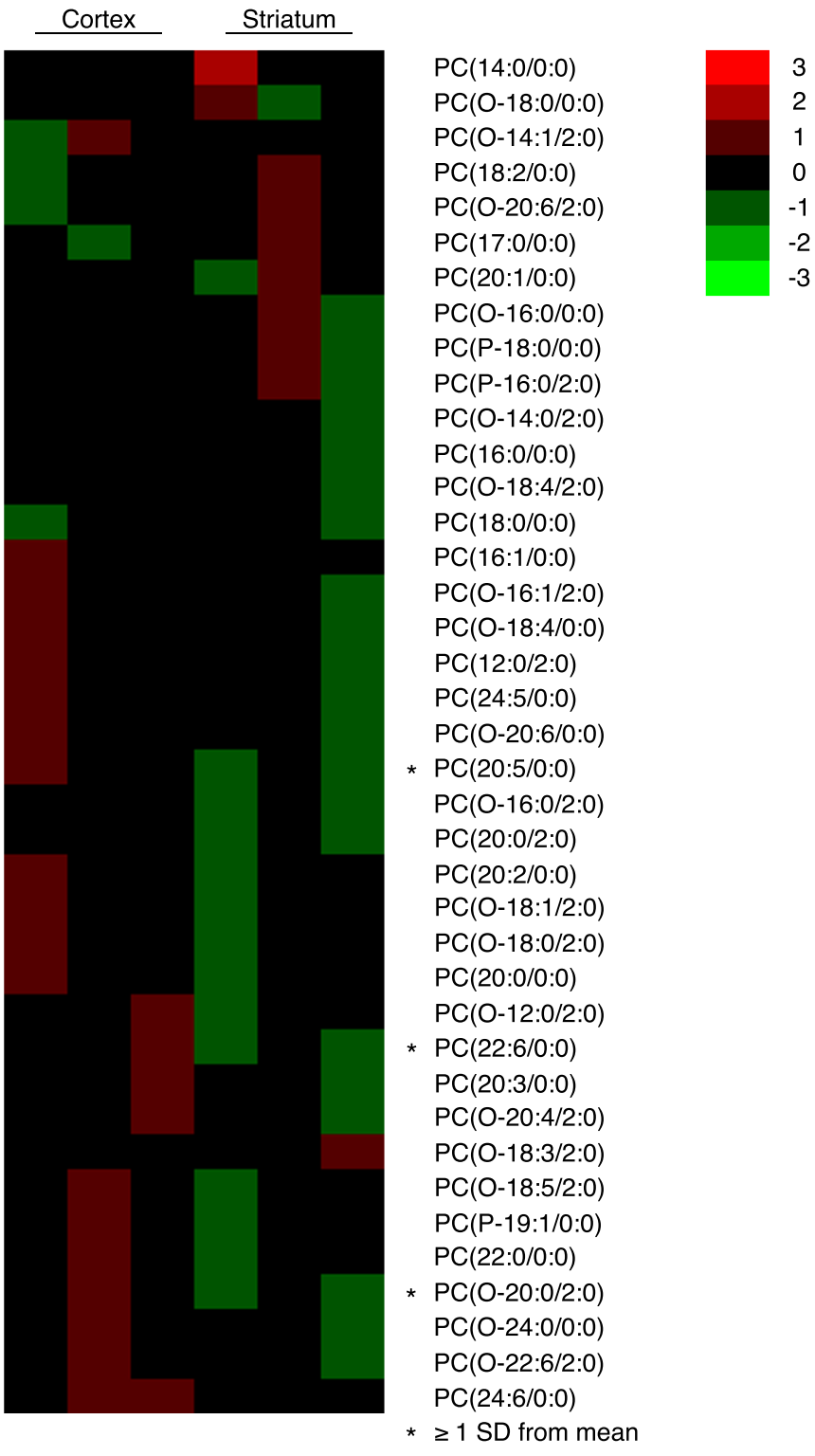
Cortex
Striatum
PC(14:0/0:0)
PC(O-18:0/0:0)
PC(O-14:1/2:0)
PC(18:2/0:0)
PC(O-20:6/2:0)
PC(17:0/0:0)
PC(20:1/0:0)
PC(O-16:0/0:0)
PC(P-18:0/0:0)
PC(P-16:0/2:0)
PC(O-14:0/2:0)
PC(16:0/0:0)
PC(O-18:4/2:0)
PC(18:0/0:0)
PC(16:1/0:0)
PC(O-16:1/2:0)
PC(O-18:4/0:0)
PC(12:0/2:0)
PC(24:5/0:0)
PC(O-20:6/0:0)
* PC(20:5/0:0)
PC(O-16:0/2:0)
PC(20:0/2:0)
PC(20:2/0:0)
PC(O-18:1/2:0)
PC(O-18:0/2:0)
PC(20:0/0:0)
PC(O-12:0/2:0)
* PC(22:6/0:0)
PC(20:3/0:0)
PC(O-20:4/2:0)
PC(O-18:3/2:0)
PC(O-18:5/2:0)
PC(P-19:1/0:0)
PC(22:0/0:0)
* PC(O-20:0/2:0)
PC(O-24:0/0:0)
PC(O-22:6/2:0)
PC(24:6/0:0)
* ≥ 1 SD from mean
3
2
1
0
-1
-2
-3

Figure 3.2.4b. Differences in glycerophosphocholine lipid second messenger abundance between posterior regions of frontal cortex and striatum in uninjured wild-type mice and following MCAO. Small molecular weight glycerophosphocholine second messengers were identified by LC-ESI-MS. Data shown represent Log_2-transformed normalized peak area (Log_2PA_N) for species identified as significant by heatmap analysis, compared by paired 2-way ANOVA followed by *post-hoc* Bonferroni. *p<0.05. **p<0.01. ***p<0.005.

i. PC(20:5/0:0)

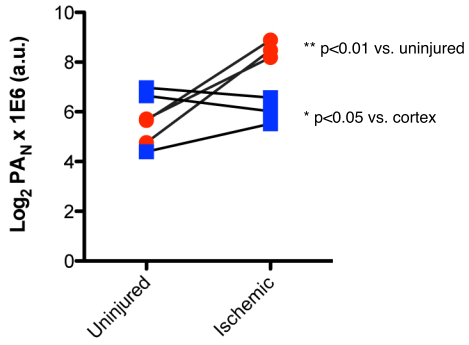

ii. PC(22:6/0:0)

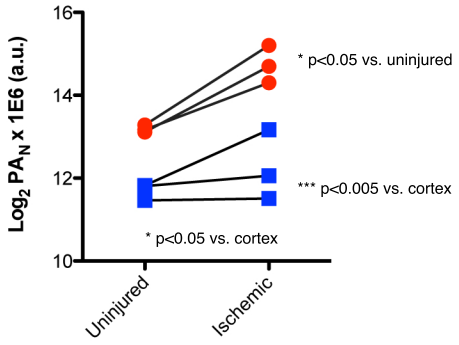

iii. PC(O-20:0/2:0)

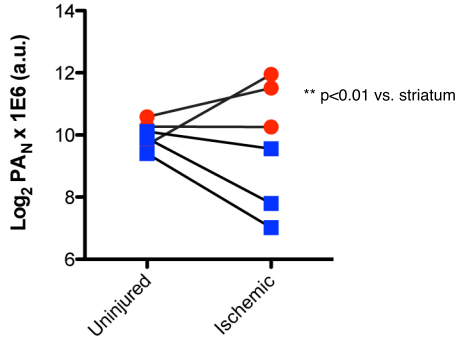

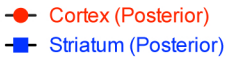

3.3.1 Effect of PAFR null-mutation on anterior-posterior gradients of glycerophosphocholine second messenger lipids in the uninjured frontal cortex.

Thirteen different glycerophosphocholine second messenger lipids displayed differences in abundance between anterior and posterior regions of uninjured frontal cortex in wild-type C57Bl/6 mice, while only four displayed differences over the same regions in PAFR$^{-/-}$ brain. Of these, only two – PC(20:5/0:0) and PC(O-18:0/2:0) – were consistent between wild-type and PAFR$^{-/-}$ frontal cortex, though both showed opposite gradients between the two genotypes (Table 3.3.1). 2-way ANOVA analysis also uncovered differences in glycerophosphocholine second messenger abundance between genotypes, within regions (Table 3.3.1). PC(14:0/0:0) (** $p<0.01$), was more abundant in anterior regions of wild-type frontal cortex compared to PAFR$^{-/-}$, while the opposite was true for PC(O-18:4/0:0) (* $p<0.05$). PC(P-18:0/0:0), PC(20:5/0:0) and PC(20:1/0:0) were all more abundant in posterior regions of cortex in wild-type brain compared to PAFR$^{-/-}$ (all * $p<0.05$).

3.3.2 Effect of PAFR null-mutation on anterior-posterior gradients of glycerophosphocholine second messenger lipids in the uninjured striatum.

A total of ten lipid species displayed anterior-posterior gradients in uninjured striatum between wild-type and PAFR$^{-/-}$ animals, only two of which, PC(20:3/0:0) and PC(24:5/0:0), were common to both genotypes. PC(24:5/0:0) was more abundant in anterior regions of striatum in both genotypes, while PC(20:3/0:0) was

Table 3.3.1. Relative abundance of glycerophosphocholine lipid second messenger species between anterior and posterior regions of uninjured cortex in wild-type and PAFR$^{-/-}$ animals. Data shown represent the ratio of log_2-transformed normalized peak area (Log_2PA_N) of all conditions compared to respective wild-type anterior cortex. Statistics are paired 2-way ANOVA followed by *post-hoc* Bonferroni. *p<0.05. **p<0.01. ***p<0.005.

Lipid Species	Mean Fold Change				2-way ANOVA
	Anterior Cortex		Posterior Cortex		
	wild-type (A)	PAFR$^{-/-}$ (B)	wild-type (C)	PAFR$^{-/-}$ (D)	p-value
PC(O-12:0/2:0)	1.0000	1.0744	1.0945	1.0350	* p<0.05 A vs. C [1]
PC(14:0/0:0)	1.0000	0.7194	1.0073	0.9359	** p<0.01 A vs. B [2] ** p<0.01 B vs. D [2]
PC(O-18:4/0:0)	1.0000	1.4994	1.2742	1.0354	* p<0.05 A vs. B [1] * p<0.05 B vs. D [1]
PC(P-18:0/0:0)	1.0000	0.9232	1.0231	0.7105	* p<0.05 C vs. D [3]
PC(17:0/0:0)	1.0000	0.8543	1.1442	1.0595	
PC(20:5/0:0)	1.0000	1.0668	1.2174	0.8758	* p<0.05 C vs. D [1]
PC(O-18:3/2:0)	1.0000	1.2791	1.3980	1.1780	* p<0.05 A vs. C [1]
PC(O-18:1/2:0)	1.0000	0.9842	0.7535	0.7820	** p<0.01 A vs. C [4] * p<0.05 B vs. D [5]
PC(20:1/0:0)	1.0000	0.9897	1.2452	1.0710	* p<0.05 C vs. D [6] ** p<0.01 A vs. C [7]
PC(O-18:0/2:0)	1.0000	1.0793	1.0933	0.9003	
PC(20:0/0:0)	1.0000	1.0019	1.1407	1.0708	
PC(O-20:6/2:0)	1.0000	1.0717	1.1926	1.0699	
PC(O-20:0/2:0)	1.0000	1.1163	1.0962	1.0850	
PC(O-24:0/0:0)	1.0000	0.9046	1.2035	1.0993	
PC (O-22:6/2:0)	1.0000	0.8778	0.8434	0.8488	

1. 2 way ANOVA, Genotype X Region interaction, p<0.05; *post-hoc* Bonferroni, p<0.05.
2. 2 way ANOVA, Main effect of genotype, p<0.01; Main effect of region, p<0.05; Genotype X Region interaction, p<0.05; *post-hoc* Bonferroni, p<0.01.
3. 2 way ANOVA, Main effect of genotype, p<0.05; *post-hoc* Bonferroni, p<0.05.
4. 2 way ANOVA, Main effect of region, p<0.005; *post-hoc* Bonferroni, p<0.01.
5. 2 way ANOVA, Main effect of region, p<0.005; *post-hoc* Bonferroni, p<0.05.
6. 2 way ANOVA, Main effect of region, p<0.01; *post-hoc* Bonferroni, p<0.05.
7. 2 way ANOVA, Main effect of region, p<0.01; *post-hoc* Bonferroni, p<0.01.

higher in anterior striatum in wild-type animals, and higher in posterior striatum in null-mutant animals. Next, 2-way ANOVA analysis revealed four lipids – PC(18:0/0:0) (** $p<0.01$), PC(20:3/0:0) (** $p<0.01$), PC(O-20:6/2:0) (* $p<0.05$) and PC(20:0/2:0) (* $p<0.05$) – that were more abundant in wild-type anterior striatum compared to $PAFR^{-/-}$ (Table 3.3.2). No species displayed statistically significant differences in abundance between genotypes in uninjured posterior striatum.

3.3.3 Effect of PAFR null-mutation on medial-lateral gradients of glycerophosphocholine second messenger lipids between anterior regions the uninjured striatum and frontal cortex.

Ten different glycerophosphocholine lipid second messenger species displayed medial-lateral gradients in anterior regions of uninjured frontal cortex and striatum, between wild-type and PAFR null-mutant animals. Of these, only two species – PC(O-18:0/0:0) and PC(O-18:1/2:0) – were found in both genotypes, and both were higher in uninjured cortex compared to striatum, regardless of genotype. 2-way ANOVA analysis identified only one species that displayed a regional difference between genotypes. PC(O-18:4/0:0) was more highly abundant in the uninjured anterior frontal cortex of $PAFR^{-/-}$ animals relative to wild-type (** $p<0.01$, Table 3.3.3).

Table 3.3.2. Relative abundance of glycerophosphocholine lipid second messenger species between anterior and posterior regions of uninjured striatum in wild-type and PAFR$^{-/-}$ animals. Data shown represent the ratio of log_2-transformed normalized peak area (Log_2PA_N) of all conditions compared to wild-type anterior striatum. Statistics are paired 2-way ANOVA followed by *post-hoc* Bonferroni. *p<0.05. **p<0.01. ***p<0.005.

Lipid Species	Mean Fold Change				2-way ANOVA
	Anterior Striatum		Posterior Striatum		
	wild-type (A)	PAFR$^{-/-}$ (B)	wild-type (C)	PAFR$^{-/-}$ (D)	p-value
PC(O-16:1/2:0)	1.0000	0.9545	1.0108	1.0049	* p<0.05 B vs. D[1]
PC(18:0/0:0)	1.0000	0.9431	1.0001	0.9929	** p<0.01 A vs. B [2] * p<0.05 B vs. D [3]
PC(O-18:5/2:0)	1.0000	1.3184	1.1027	0.7609	* p<0.05 B vs. D [4]
PC(O-18:4/2:0)	1.0000	1.0247	0.9983	1.0755	
PC(20:3/0:0)	1.0000	0.8091	0.9094	0.9139	** p<0.01 A vs. B [5]
PC(O-18:1/2:0)	1.0000	0.8601	1.1801	0.9999	
PC(20:1/0:0)	1.0000	0.9211	1.1880	1.0788	
PC(O-20:6/2:0)	1.0000	0.8215	0.9727	0.9983	* p<0.05 A vs. B [4] * p<0.05 B vs. D [4]
PC(20:0/2:0)	1.0000	0.9128	0.9333	0.9053	* p<0.05 A vs. B [6] * p<0.05 A vs. C [6]
PC(24:5/0:0)	1.0000	0.9027	1.0982	1.0047	

1. 2 way ANOVA, Main effect of region, p<0.05; *post-hoc* Bonferroni, p<0.05.
2. 2 way ANOVA, Main effect of genotype, p<0.05; Main effect of region, p<0.05; Genotype X Region interaction, p<0.05; *post-hoc* Bonferroni, p<0.01.
3. 2 way ANOVA, Main effect of genotype, p<0.05; Main effect of region, p<0.05; Genotype X Region interaction, p<0.05; *post-hoc* Bonferroni, p<0.05.
4. 2 way ANOVA, Genotype X Region interaction, p<0.05; *post-hoc* Bonferroni, p<0.05.
5. 2 way ANOVA, Main effect of genotype, p<0.05; Genotype X Region interaction, p<0.05; *post-hoc* Bonferroni, p<0.01.
6. 2 way ANOVA, Main effect of genotype, p<0.01; *post-hoc* Bonferroni, p<0.05.

Table 3.3.3. Relative abundance of glycerophosphocholine lipid second messenger species between anterior regions of uninjured frontal cortex and striatum in wild-type and PAFR$^{-/-}$ animals. Data shown represent the ratio of log_2-transformed normalized peak area (Log_2PA_N) of all conditions compared to wild-type anterior cortex. Statistics are paired 2-way ANOVA followed by *post-hoc* Bonferroni. *p<0.05. **p<0.01. ***p<0.005.

Lipid Species	Mean Fold Change				2-way ANOVA
	Anterior Cortex		Anterior Striatum		
	wild-type (A)	PAFR$^{-/-}$ (B)	wild-type (C)	PAFR$^{-/-}$ (D)	p-value
PC(O-14:1/2:0)	1.0000	0.9531	0.9430	0.9271	
PC(O-18:4/0:0)	1.0000	1.4994	1.3628	1.4731	** p<0.01 A vs. B[1] * p<0.05 A vs. C [2]
PC(O-18:0/0:0)	1.0000	0.9535	0.7536	0.6832	*** p<0.005 A vs. C [3] *** p<0.005 B vs. D [3]
PC(O-20:6/0:0)	1.0000	0.9695	0.7477	0.8285	
PC(O-18:4/2:0)	1.0000	0.9909	0.9179	0.9405	
PC(O-18:3/2:0)	1.0000	1.2791	1.4324	1.3131	
PC(O-18:1/2:0)	1.0000	0.9842	0.8289	0.7129	* p<0.05 A vs. C [4] ** p<0.01 B vs. D [5]
PC(O-18:0/2:0)	1.0000	1.0793	1.2223	1.1589	** p<0.01 A vs. C [6]
PC(20:0/2:0)	1.0000	1.0688	0.9820	0.8964	
PC (O-22:6/2:0)	1.0000	0.8778	1.0607	0.9997	

1. 2 way ANOVA, Main effect of genotype, p<0.01; *post-hoc* Bonferroni, p<0.05.
2. 2 way ANOVA, Main effect of genotype, p<0.01; *post-hoc* Bonferroni, p<0.01.
3. 2 way ANOVA, Main effect of genotype, p<0.05; Main effect of region, p<0.005; *post-hoc* Bonferroni, p<0.005.
4. 2 way ANOVA, Main effect of region, p<0.005; *post-hoc* Bonferroni, p<0.05.
5. 2 way ANOVA, Main effect of region, p<0.005; *post-hoc* Bonferroni, p<0.01.
6. 2 way ANOVA, Main effect of region, p<0.01; *post-hoc* Bonferroni, p<0.01.

3.3.4 Effect of PAFR null-mutation on medial-lateral gradients of glycerophosphocholine second messenger lipids between posterior regions of the uninjured striatum and frontal cortex.

Of the eighteen glycerophosphocholine lipid second messenger species identified between wild-type and PAFR null-mutant uninjured posterior frontal cortex and striatum, only one – PC(O-18:0/2:0) – was common to both genotypes. In both cases, PC(O-18:0/2:0) was more abundant in posterior striatum compared to cortex. Further, seven species displayed different levels of abundant within the same region, between wild-type and $PAFR^{-/-}$ brain. PC(O-14:0/2:0) (** $p<0.01$), PC(16:0/0:0) (* $p<0.05$), PC(P-18:0/0:0) (* $p<0.05$), PC(18:2/0:0) (** $p<0.01$), PC(O-16:1/2:0) (** $p<0.01$) and PC(P-16:0/2:0) (** $p<0.01$) were all more abundant in the uninjured posterior cortex of wild-type animals compared to $PAFR^{-/-}$. Only PC(O-18:5/2:0) (* $p<0.05$) was more abundant in the uninjured posterior cortex of $PAFR^{-/-}$ animals. Further, PC(O-18:4/2:0) was more abundant in the uninjured posterior striatum of $PAFR^{-/-}$ animals compared to wild-type, but displayed no such gradient in cortical tissue (Table 3.3.4).

Table 3.3.4. Relative abundance of glycerophosphocholine lipid second messenger species between posterior regions of uninjured frontal cortex and striatum in wild-type and PAFR$^{-/-}$ animals. Data shown represent the ratio of log_2-transformed normalized peak area (Log_2PA_N) of all conditions compared to wild-type posterior cortex. Statistics are paired 2-way ANOVA followed by *post-hoc* Bonferroni. *p<0.05. **p<0.01. ***p<0.005.

Lipid Species	Mean Fold Change				2-way ANOVA
	Posterior Cortex		Posterior Striatum		
	wild-type (A)	PAFR$^{-/-}$ (B)	wild-type (C)	PAFR$^{-/-}$ (D)	p-value
PC(O-16:0/0:0)	1.0000	0.8740	0.9176	0.9631	
PC(O-14:1/2:0)	1.0000	0.8294	0.8529	0.8797	
PC(16:1/0:0)	1.0000	1.0654	1.0098	1.0257	
PC(O-14:0/2:0)	1.0000	0.9574	0.9381	0.9526	** p<0.01 A vs. B [1] *** p<0.005 A vs. C [2]
PC(16:0/0:0)	1.0000	0.9674	0.9558	0.9535	* p<0.05 A vs. B [3] ** p<0.01 A vs. C [4]
PC(P-18:0/0:0)	1.0000	0.6944	0.7035	0.9403	* p<0.05 A vs. B [5] * p<0.05 A vs. C [5]
PC(P-19:1/0:0)	1.0000	0.9459	0.9379	0.9611	
PC(18:2/0:0)	1.0000	0.8736	0.9246	0.9122	** p<0.01 A vs. B [6]
PC(O-16:1/2:0)	1.0000	0.9486	0.9588	0.9533	** p<0.01 A vs. B [6] * p<0.05 A vs. C [7]
PC(P-16:0/2:0)	1.0000	0.9496	0.9589	0.9640	** p<0.01 A vs. B [8] ** p<0.01 A vs. C [8]

1. 2 way ANOVA, Main effect of genotype, p<0.05; Main effect of region, p<0.005; Genotype X Region interaction, p<0.005; *post-hoc* Bonferroni, p<0.01.
2. 2 way ANOVA, Main effect of genotype, p<0.05; Main effect of region, p<0.005; Genotype X Region interaction, p<0.005; *post-hoc* Bonferroni, p<0.005.
3. 2 way ANOVA, Main effect of region, p<0.01; *post-hoc* Bonferroni, p<0.05.
4. 2 way ANOVA, Main effect of region, p<0.01; *post-hoc* Bonferroni, p<0.01.
5. 2 way ANOVA, Genotype X Region interaction, p<0.01; *post-hoc* Bonferroni, p<0.05.
6. 2 way ANOVA, Main effect of genotype, p<0.05; Genotype X Region interaction, p<0.05; *post-hoc* Bonferroni, p<0.01.
7. 2 way ANOVA, Main effect of genotype, p<0.05; Genotype X Region interaction, p<0.05; *post-hoc* Bonferroni, p<0.05.
8. 2 way ANOVA, Main effect of genotype, p<0.01; Genotype X Region interaction, p<0.01; *post-hoc* Bonferroni, p<0.01.

Lipid Species	Mean Fold Change				2-way ANOVA
	Posterior Cortex		Posterior Striatum		
	wild-type (A)	PAFR$^{-/-}$ (B)	wild-type (C)	PAFR$^{-/-}$ (D)	p-value
PC(O-18:5/2:0)	1.0000	1.8874	1.5547	1.0729	* p<0.05 A vs. B [1]
					* p<0.05 B vs. D [1]
PC(O-18:4/2:0)	1.0000	0.9713	0.9293	0.9769	* p<0.05 C vs. D [2]
					** p<0.01 A vs. C [3]
PC(20:3/0:0)	1.0000	0.9066	0.8990	0.9035	
PC(O-18:0/2:0)	1.0000	0.8234	1.1786	1.1727	** p<0.01 B vs. D [4]
PC(20:0/0:0)	1.0000	0.9387	1.2280	1.1669	** p<0.01 A vs. C [5]
					** p<0.01 B vs. D [5]
PC(22:6/0:0)	1.0000	0.9590	0.8870	0.9415	*** p<0.005 A vs. C [6]
PC(O-20:6/2:0)	1.0000	0.8971	0.9235	0.9478	
PC(O-20:4/2:0)	1.0000	0.9366	0.9033	0.9318	

1. 2 way ANOVA, Genotype X Region interaction, p<0.01; *post-hoc* Bonferroni, p<0.05.
2. 2 way ANOVA, Main effect of genotype, p<0.05; Genotype X Region interaction, p<0.01; *post-hoc* Bonferroni, p<0.05.
3. 2 way ANOVA, Main effect of genotype, p<0.05; Genotype X Region interaction, p<0.01; *post-hoc* Bonferroni, p<0.05.
4. 2 way ANOVA, Main effect of region, p<0.01; *post-hoc* Bonferroni, p<0.01.
5. 2 way ANOVA, Main effect of region, p<0.005; *post-hoc* Bonferroni, p<0.01.
6. 2 way ANOVA, Main effect of region, p<0.001; Genotype X Region interaction, p<0.01; *post-hoc* Bonferroni, p<0.005.

3.4 MCAO altered glycerophospholipid metabolism in PAFR$^{-/-}$ mice

3.4.1 Lipid differences between anterior and posterior regions of ischemic frontal cortex in PAFR$^{-/-}$ mice.

In wild-type mice, we found five lipid species, PC(O-12:0/2:0), PC(16:0/0:0), PC(20:1/0:0), PC(O-20:6/2:0) and PC(24:5/0:0) whose abundance was altered significantly following ischemic injury in the frontal cortex. Heatmap analysis, using $Log_2PA_N \times 10^6_{Fold\ Change}$ data, was also used to assess regional differences in glycerophosphocholine second messenger lipid abundance in PAFR$^{-/-}$ brain. No changes in the species identified in wild-type mice were detected. Rather, four different lipid species, PC(O-14:1/2:0), PC(18:2/0:0), PC(O-20:4/2:0) and PC(O-20:0/2:0), displayed greater than one standard deviation from the mean of the array (Fig. 3.4.1a). Of these, three species showed significant alterations in abundance by 2-way ANOVA and *post-hoc* Bonferroni. PC(O-14:1/2:0) was more abundant in posterior regions of ischemic cortex compared to uninjured (** $p<0.01$), and was more abundant in posterior regions compared to anterior in ischemic tissue (** $p<0.01$). PC(18:2/0:0) was more abundant in ischemic tissue compared to uninjured, in posterior regions of cortex (* $p<0.05$). PC(O-20:4/2:0) was more abundant in ischemic tissue compared to uninjured in posterior regions of cortex (** $p<0.01$) and in posterior regions compared to anterior in ischemic tissue (* $p<0.05$) (Fig 3.4.1b).

Figure 3.4.1a. Heatmap clustering of relative glycerophosphocholine lipid second messenger abundance between anterior and posterior regions of PAFR$^{-/-}$ frontal cortex following MCAO. Small molecular weight glycerophosphocholine second messengers were identified by LC-ESI-MS. Data are expressed as a ratio of abundance of ischemic to uninjured tissue ($Log_2PA_{N\ Fold\ Change}$). The number of standard deviations ($Log_2A^*_{Fold\ Change}$) by which the abundance of a given species in a given animal differs from the mean abundance of the whole population is colour-coded (green (less than expected) to red (greater than expected). * denotes species that show at least 1 standard deviation from the mean. This difference was considered significant and species were prioritized for a second level of statistical analysis.

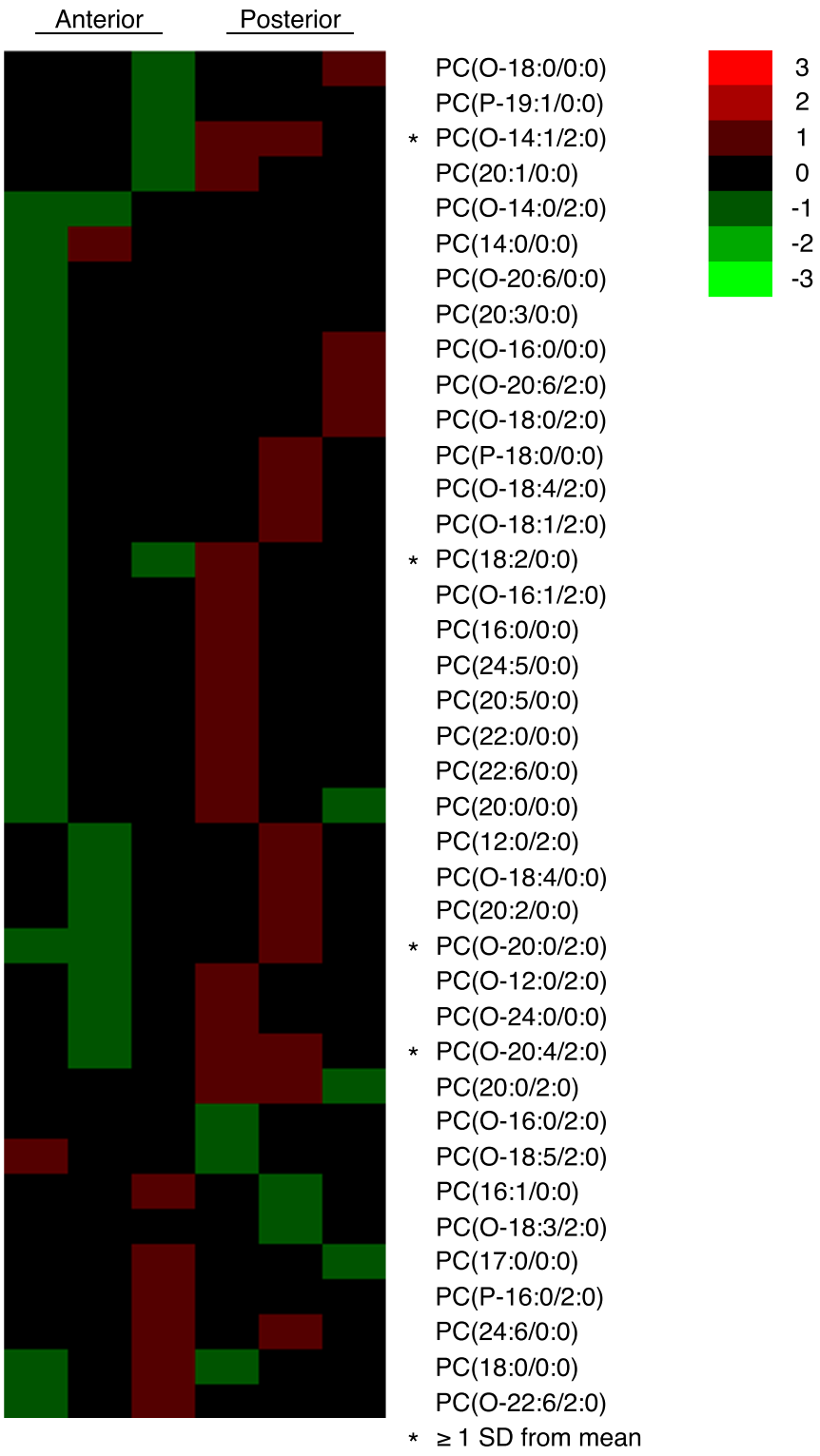
Anterior
Posterior
PC(O-18:0/0:0)
PC(P-19:1/0:0)
* PC(O-14:1/2:0)
PC(20:1/0:0)
PC(O-14:0/2:0)
PC(14:0/0:0)
PC(O-20:6/0:0)
PC(20:3/0:0)
PC(O-16:0/0:0)
PC(O-20:6/2:0)
PC(O-18:0/2:0)
PC(P-18:0/0:0)
PC(O-18:4/2:0)
PC(O-18:1/2:0)
* PC(18:2/0:0)
PC(O-16:1/2:0)
PC(16:0/0:0)
PC(24:5/0:0)
PC(20:5/0:0)
PC(22:0/0:0)
PC(22:6/0:0)
PC(20:0/0:0)
PC(12:0/2:0)
PC(O-18:4/0:0)
PC(20:2/0:0)
* PC(O-20:0/2:0)
PC(O-12:0/2:0)
PC(O-24:0/0:0)
* PC(O-20:4/2:0)
PC(20:0/2:0)
PC(O-16:0/2:0)
PC(O-18:5/2:0)
PC(16:1/0:0)
PC(O-18:3/2:0)
PC(17:0/0:0)
PC(P-16:0/2:0)
PC(24:6/0:0)
PC(18:0/0:0)
PC(O-22:6/2:0)
* ≥ 1 SD from mean
3
2
1
0
-1
-2
-3

Figure 3.4.1b. Differences in glycerophosphocholine lipid second messenger abundance between anterior and posterior frontal cortex in uninjured PAFR$^{-/-}$ mice and following MCAO. Small molecular weight glycerophosphocholine second messengers were identified by LC-ESI-MS. Data shown represent Log_2-transformed normalized peak area (Log_2PA_N) for species identified as significant by heatmap analysis, compared by paired 2-way ANOVA followed by *post-hoc* Bonferroni. *p<0.05. **p<0.01. ***p<0.005.

i. PC(O-14:1/2:0)

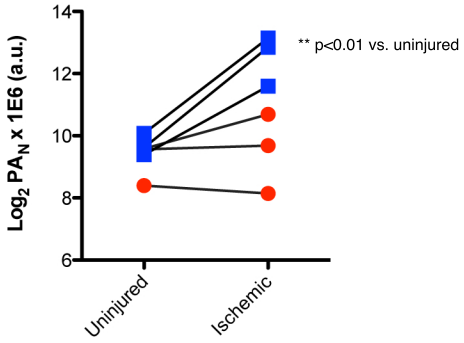

ii.. PC(18:2/0:0)

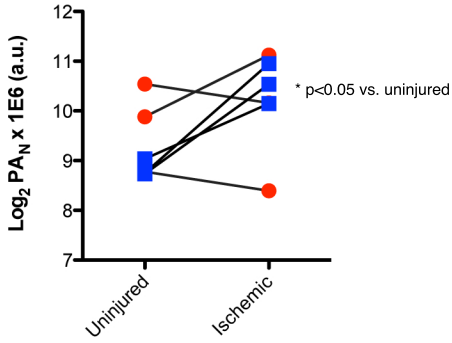

iii. PC(O-20:4/2:0)

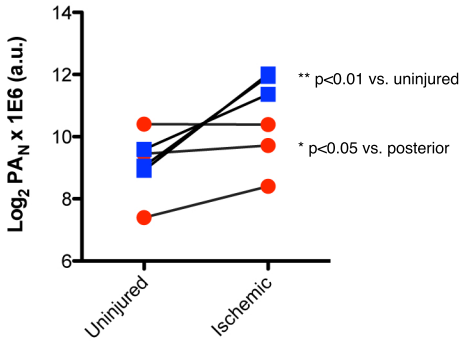

iv. PC(O-20:0/2:0)

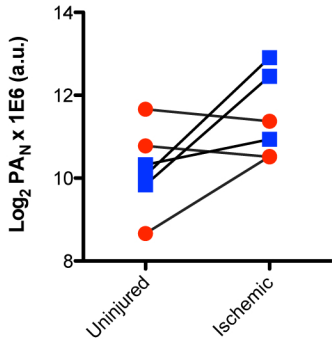



3.4.2 Lipid differences between anterior and posterior regions of ischemic frontal striatum in PAFR$^{-/-}$ mice.

In wild-type mice, only PC(20:0.2:0) exhibited an anterior/posterior gradient in injured striatum. In PAFR$^{-/-}$ mice, PC(20:0.2:0) did not appreciably change. Four glycerophosphocholine second messenger lipid species – PC(O-14:0/2:0), PC(P-18:0/0:0), PC(O-16:1/2:0) and PC(24:6/0:0) – showed different abundances between anterior and posterior regions of striatum in PAFR$^{-/-}$ brain by heatmap analysis (Fig 3.4.2a). PC(O-14:0/2:0) was more abundant in ischemic tissue compared to uninjured, in anterior regions of striatum (* $p<0.05$, 2-way ANOVA and *post-hoc* Bonferroni), and was more abundant in anterior regions of striatum compared to posterior, in ischemic tissue (* $p<0.05$). PC(P-18:0/0:0) was more abundant in anterior regions of ischemic striatum compared to posterior (* $p<0.05$). PC(O-16:1/2:0) was more abundant in anterior striatum relative to posterior in ischemic tissue (* $p<0.05$), but was more abundant in posterior region in uninjured tissue (** $p<0.01$). Finally, PC(24:6/0:0) was more abundant in uninjured tissue compared to injured in posterior regions of striatum (* $p<0.05$), and was more abundant is anterior regions compared to posterior in ischemic striatum (*** $p<0.005$) (Fig. 3.4.2b).

Figure 3.4.2a. Heatmap clustering of relative glycerophosphocholine lipid second messenger abundance between anterior and posterior regions of PAFR$^{-/-}$ striatum following MCAO. Small molecular weight glycerophosphocholine second messengers were identified by LC-ESI-MS. Data are expressed as a ratio of abundance of ischemic to uninjured tissue ($Log_2PA_{N\ Fold\ Change}$). The number of standard deviations ($Log_2A^*_{Fold\ Change}$) by which the abundance of a given species in a given animal differs from the mean abundance of the whole population is colour-coded (green (less than expected) to red (greater than expected). * denotes species that show at least 1 standard deviation from the mean. This difference was considered significant and species were prioritized for a second level of statistical analysis.

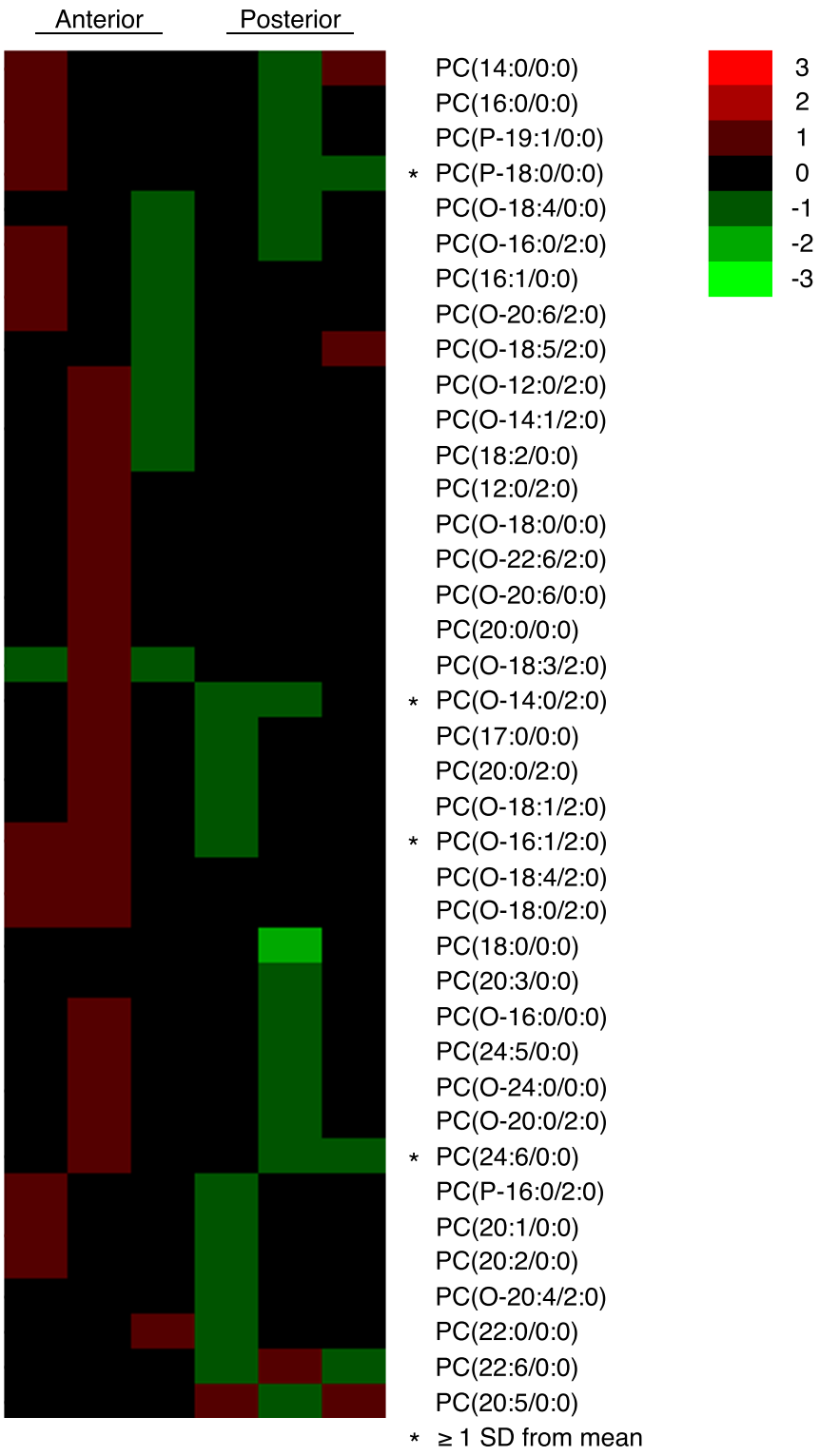
Anterior
Posterior
PC(14:0/0:0)
PC(16:0/0:0)
PC(P-19:1/0:0)
* PC(P-18:0/0:0)
PC(O-18:4/0:0)
PC(O-16:0/2:0)
PC(16:1/0:0)
PC(O-20:6/2:0)
PC(O-18:5/2:0)
PC(O-12:0/2:0)
PC(O-14:1/2:0)
PC(18:2/0:0)
PC(12:0/2:0)
PC(O-18:0/0:0)
PC(O-22:6/2:0)
PC(O-20:6/0:0)
PC(20:0/0:0)
PC(O-18:3/2:0)
* PC(O-14:0/2:0)
PC(17:0/0:0)
PC(20:0/2:0)
PC(O-18:1/2:0)
* PC(O-16:1/2:0)
PC(O-18:4/2:0)
PC(O-18:0/2:0)
PC(18:0/0:0)
PC(20:3/0:0)
PC(O-16:0/0:0)
PC(24:5/0:0)
PC(O-24:0/0:0)
PC(O-20:0/2:0)
* PC(24:6/0:0)
PC(P-16:0/2:0)
PC(20:1/0:0)
PC(20:2/0:0)
PC(O-20:4/2:0)
PC(22:0/0:0)
PC(22:6/0:0)
PC(20:5/0:0)
* ≥ 1 SD from mean
3
2
1
0
-1
-2
-3

Figure 3.4.2b. Differences in glycerophosphocholine lipid second messenger abundance between anterior and posterior striatum in uninjured PAFR$^{-/-}$ mice and following MCAO. Small molecular weight glycerophosphocholine second messengers were identified by LC-ESI-MS. Data shown represent Log_2-transformed normalized peak area (Log_2PA_N) for species identified as significant by heatmap analysis, compared by paired 2-way ANOVA followed by *post-hoc* Bonferroni. *p<0.05. **p<0.01. ***p<0.005.

i. PC(O-14:0/2:0)

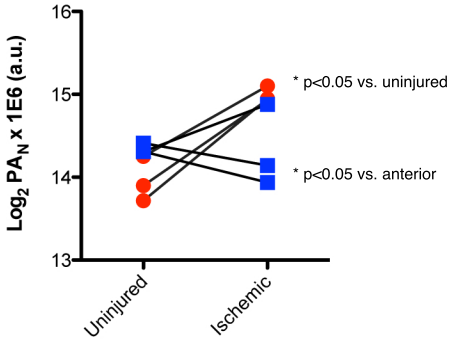

ii. PC(P-18:0/0:0)

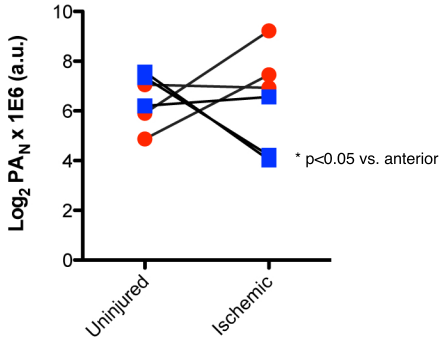

iii. PC(O-16:1/2:0)

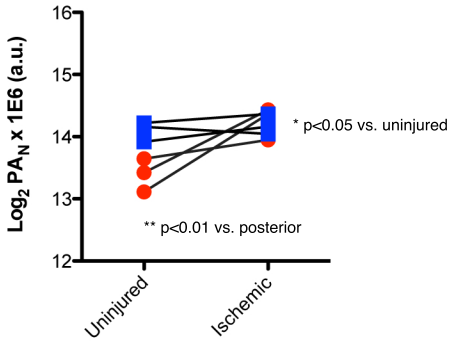

iv. PC(24:6/0:0)

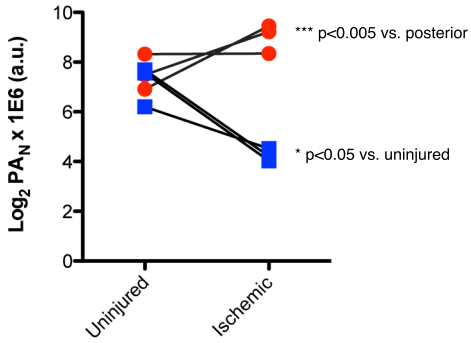

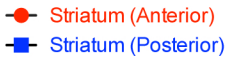

3.4.3 Lipid differences between anterior regions of ischemic frontal striatum and cortex in PAFR$^{-/-}$ mice.

Whereas six species varied between ischemic regions in anterior sections in wild-type mice, heatmap analysis identified four lipid species – PC(O-16:0/0:0), PC(16:1/0:0), PC(O-20:0/2:0) and PC(24:6/0:0) that showed differences of abundance of greater than one standard deviation from the mean of the population (Fig. 3.4.3a), however none of these showed statistically significant changes by two-way ANOVA analysis (Fig. 3.4.3b). No overlap with wild-type metabolism was observed.

3.4.4 Lipid differences between posterior regions of ischemic frontal striatum and cortex in PAFR$^{-/-}$ mice.

Heatmap analysis revealed eight lipid species with altered abundance between posterior regions of striatum and frontal cortex in PAFR$^{-/-}$ mice. Of these, five showed similar patterns of change based on two-way ANOVA analysis. PC(O-14:1/2:0), PC(O-14:0:2:0), PC(P-19:1/0:0), PC(22:6/0:0) and PC(O-24:0/0:0) are all significantly more abundant in ischemic regions of posterior frontal cortex compared to uninjured, and are more abundant in posterior regions of ischemic cortex compared ischemic striatum. Interestingly, PC(22:6/0:0) was also found to change in wild-type mice. PC(P-18:0/0:0) was more abundant in posterior regions of ischemic cortex compared to striatum (* $p<0.05$). PC(18:2/0:0) was more abundant in ischemic regions of posterior cortex compared to uninjured (** $p<0.01$), and PC(O-20:0/2:0) was more abundant in posterior regions of cortex than striatum in

Figure 3.4.3a. Heatmap clustering of relative glycerophosphocholine lipid second messenger abundance between anterior regions of PAFR$^{-/-}$ frontal cortex and striatum following MCAO. Small molecular weight glycerophosphocholine second messengers were identified by LC-ESI-MS. Data are expressed as a ratio of abundance of ischemic to uninjured tissue ($Log_2PA_{N\ Fold\ Change}$). The number of standard deviations ($Log_2A^*_{Fold\ Change}$) by which the abundance of a given species in a given animal differs from the mean abundance of the whole population is colour-coded (green (less than expected) to red (greater than expected). * denotes species that show at least 1 standard deviation from the mean. This difference was considered significant and species were prioritized for a second level of statistical analysis.

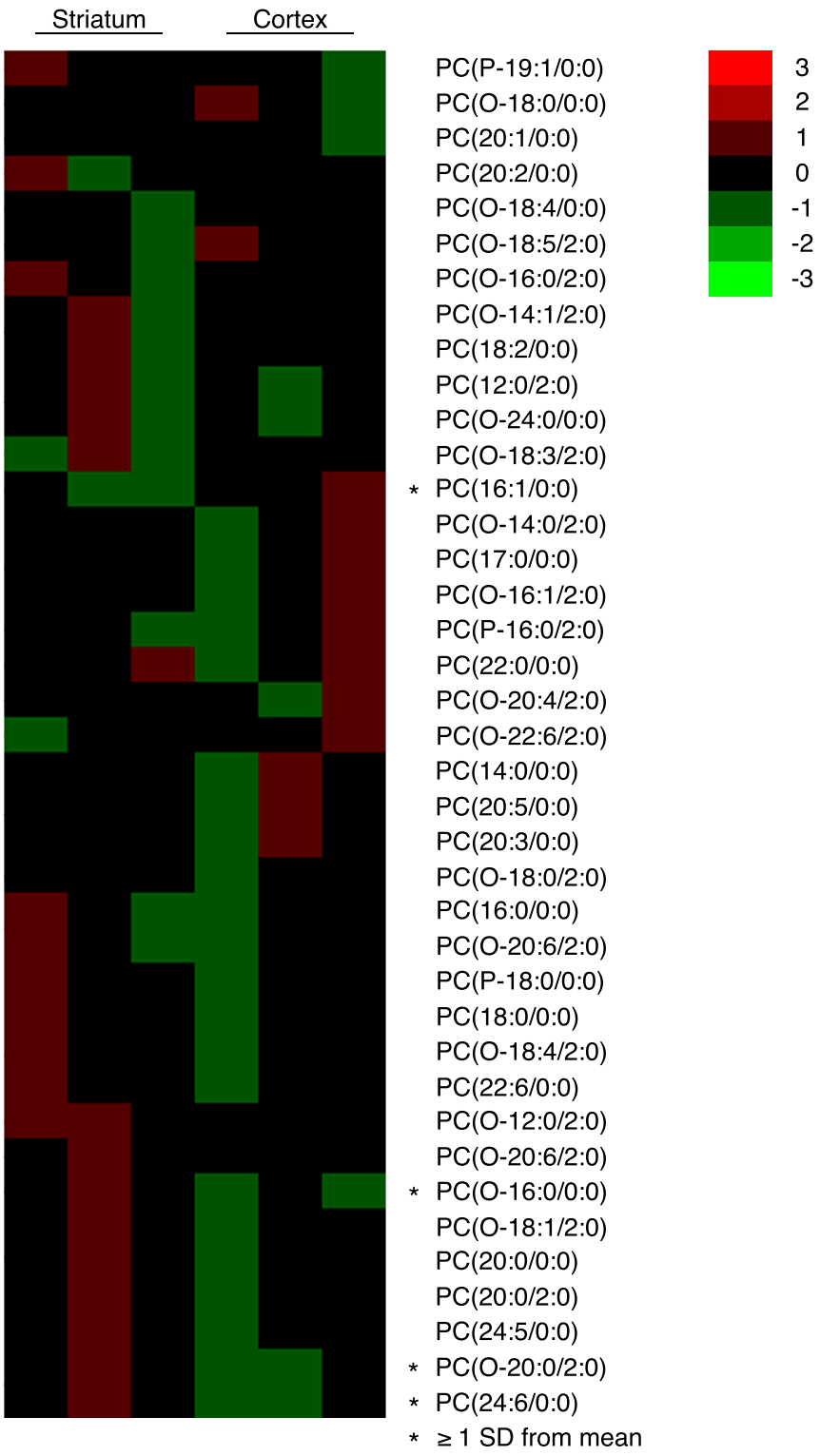
Striatum
Cortex
PC(P-19:1/0:0)
PC(O-18:0/0:0)
PC(20:1/0:0)
PC(20:2/0:0)
PC(O-18:4/0:0)
PC(O-18:5/2:0)
PC(O-16:0/2:0)
PC(O-14:1/2:0)
PC(18:2/0:0)
PC(12:0/2:0)
PC(O-24:0/0:0)
PC(O-18:3/2:0)
* PC(16:1/0:0)
PC(O-14:0/2:0)
PC(17:0/0:0)
PC(O-16:1/2:0)
PC(P-16:0/2:0)
PC(22:0/0:0)
PC(O-20:4/2:0)
PC(O-22:6/2:0)
PC(14:0/0:0)
PC(20:5/0:0)
PC(20:3/0:0)
PC(O-18:0/2:0)
PC(16:0/0:0)
PC(O-20:6/2:0)
PC(P-18:0/0:0)
PC(18:0/0:0)
PC(O-18:4/2:0)
PC(22:6/0:0)
PC(O-12:0/2:0)
PC(O-20:6/2:0)
* PC(O-16:0/0:0)
PC(O-18:1/2:0)
PC(20:0/0:0)
PC(20:0/2:0)
PC(24:5/0:0)
* PC(O-20:0/2:0)
* PC(24:6/0:0)
* ≥ 1 SD from mean
3
2
1
0
-1
-2
-3

Figure 3.4.3b. Differences in glycerophosphocholine lipid second messenger abundance between anterior regions of frontal cortex and striatum in uninjured PAFR$^{-/-}$ mice and following MCAO. Small molecular weight glycerophosphocholine second messengers were identified by LC-ESI-MS. Data shown represent Log_2-transformed normalized peak area (Log_2PA_N) for species identified as significant by heatmap analysis, compared by paired 2-way ANOVA followed by *post-hoc* Bonferroni. *p<0.05. **p<0.01. ***p<0.005.

i. PC(16:0/0:0)

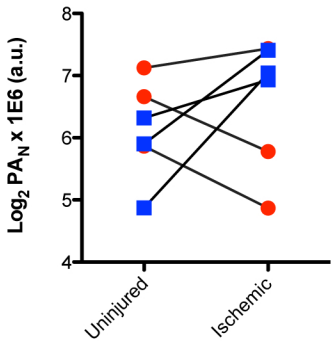

ii. PC(16:1/0:0)

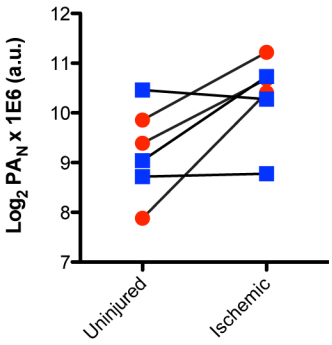

iii. PC(O-20:0/2:0)

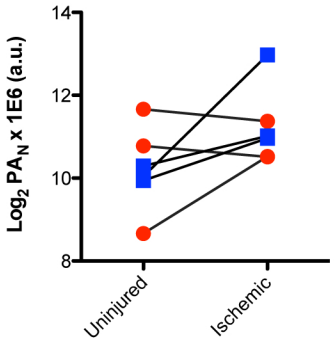

iv. PC(24:6/0:0)

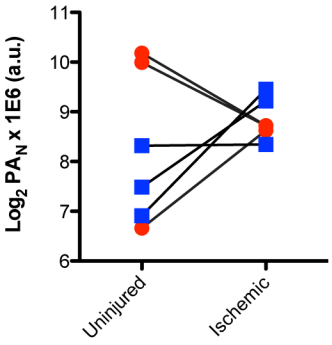

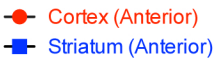

ischemic brain (*** p<0.005) (Fig. 3.4.4b). This latter comparison was the only change common to both PAFR$^{-/-}$ and PAFR$^{+/+}$ mice.

3.5 Region-specific differences in discrete glycerophosphocholine second messenger lipid abundance in frontal cortex and striatum between C57Bl/6 and PAFR null-mutant mice following MCAO.

Because the analyses above suggested a difference in glycerophosphocholine second messenger metabolism following MCAO as a result of the loss of PAFR , the levels of each species was compared directly between genotypes

3.5.1 Lipid differences in anterior frontal cortex between wild-type C57Bl/6 and PAFR$^{-/-}$ following MCAO.

Two glycerophosphocholine second messenger species – PC(P-18:0/0:0) and PC(20:2/0:0) – showed greater than one standard deviation difference from the mean of the sample population by heatmap analysis (Fig 3.5.1a). A closer analysis indicated that PC(P-18:0/0:0) was not significantly different between ischemic and uninjured anterior frontal cortex in wild-type and PAFR$^{-/-}$ brain, but that PC(20:0/0:0) was more abundant in ischemic tissue compared to uninjured in PAFR$^{-/-}$ brain (* p<0.05, 2-way ANOVA with *post-hoc* Bonferroni) (Fig 3.5.1b).

Figure 3.4.4a. Heatmap clustering of relative glycerophosphocholine lipid second messenger abundance between posterior regions of PAFR$^{-/-}$ frontal cortex and striatum following MCAO. Small molecular weight glycerophosphocholine second messengers were identified by LC-ESI-MS. Data are expressed as a ratio of abundance of ischemic to uninjured tissue ($Log_2PA_{N\ Fold\ Change}$). The number of standard deviations ($Log_2A^*_{Fold\ Change}$) by which the abundance of a given species in a given animal differs from the mean abundance of the whole population is colour-coded (green (less than expected) to red (greater than expected). * denotes species that show at least 1 standard deviation from the mean. This difference was considered significant and species were prioritized for a second level of statistical analysis.

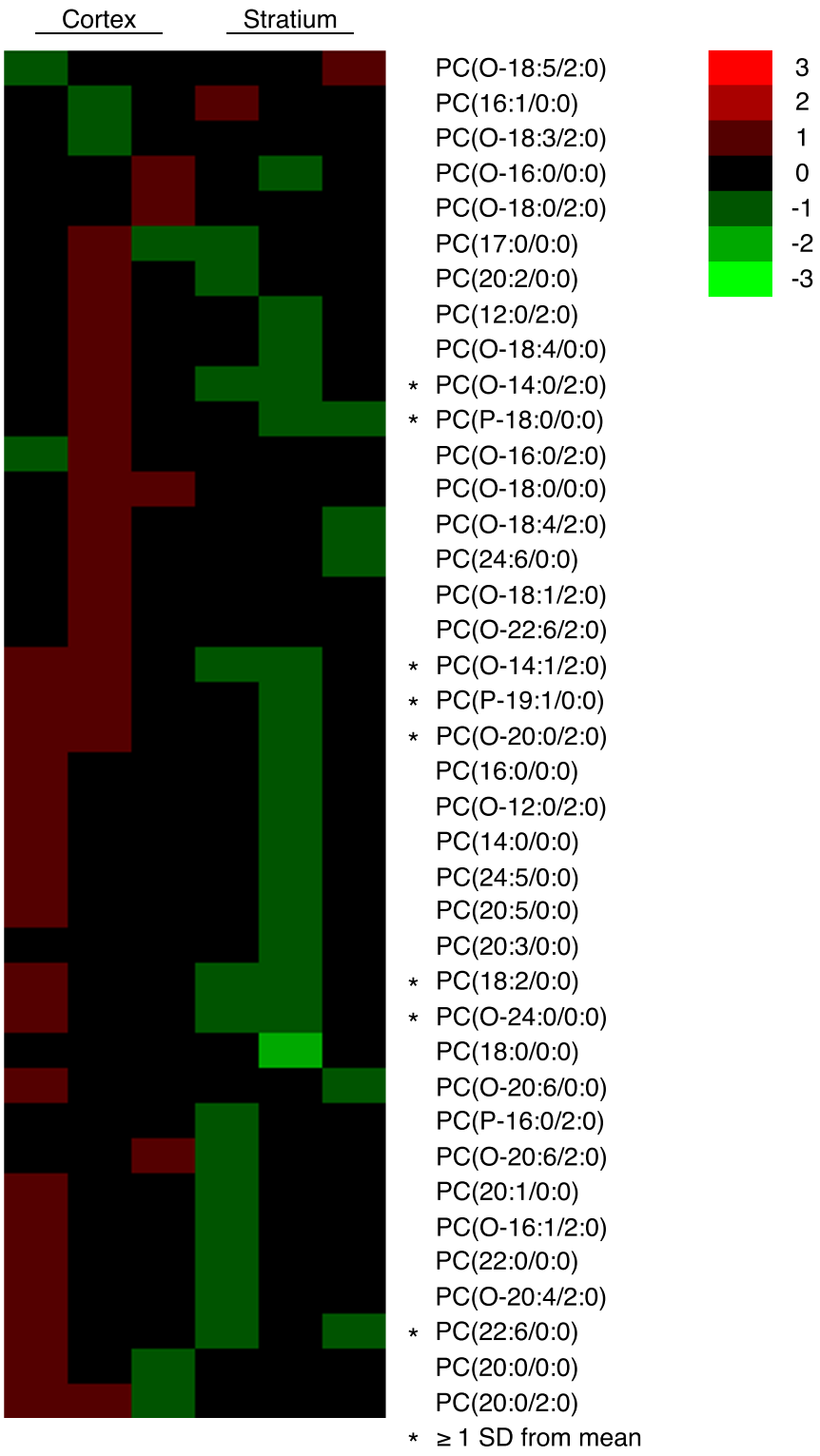
Cortex
Stratium
PC(O-18:5/2:0)
PC(16:1/0:0)
PC(O-18:3/2:0)
PC(O-16:0/0:0)
PC(O-18:0/2:0)
PC(17:0/0:0)
PC(20:2/0:0)
PC(12:0/2:0)
PC(O-18:4/0:0)
* PC(O-14:0/2:0)
* PC(P-18:0/0:0)
PC(O-16:0/2:0)
PC(O-18:0/0:0)
PC(O-18:4/2:0)
PC(24:6/0:0)
PC(O-18:1/2:0)
PC(O-22:6/2:0)
* PC(O-14:1/2:0)
* PC(P-19:1/0:0)
* PC(O-20:0/2:0)
PC(16:0/0:0)
PC(O-12:0/2:0)
PC(14:0/0:0)
PC(24:5/0:0)
PC(20:5/0:0)
PC(20:3/0:0)
* PC(18:2/0:0)
* PC(O-24:0/0:0)
PC(18:0/0:0)
PC(O-20:6/0:0)
PC(P-16:0/2:0)
PC(O-20:6/2:0)
PC(20:1/0:0)
PC(O-16:1/2:0)
PC(22:0/0:0)
PC(O-20:4/2:0)
* PC(22:6/0:0)
PC(20:0/0:0)
PC(20:0/2:0)
* ≥ 1 SD from mean
3
2
1
0
-1
-2
-3

Figure 3.4.4b. Differences in glycerophosphocholine lipid second messenger abundance between posterior regions of frontal cortex and striatum in uninjured PAFR$^{-/-}$ mice and following MCAO. Small molecular weight glycerophosphocholine second messengers were identified by LC-ESI-MS. Data shown represent Log_2-transformed normalized peak area (Log_2PA_N) for species identified as significant by heatmap analysis, compared by paired 2-way ANOVA followed by *post-hoc* Bonferroni. *p<0.05. **p<0.01. ***p<0.005.

i. PC(O-14:1/2:0)

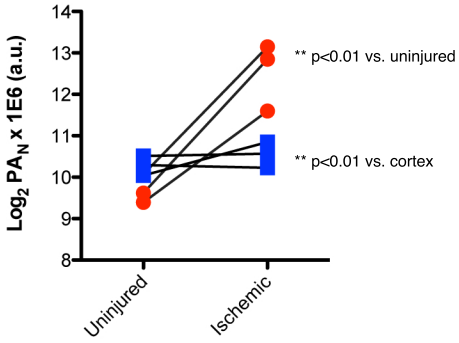

ii. PC(O-14:0/2:0)

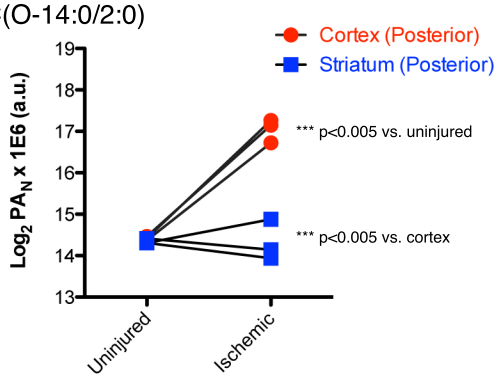

iii. PC(P-18:0/0:0)

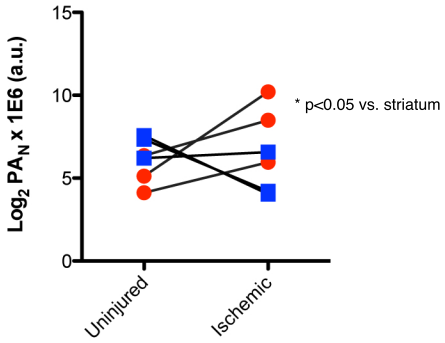

iv. PC(P-19:1/0:0)

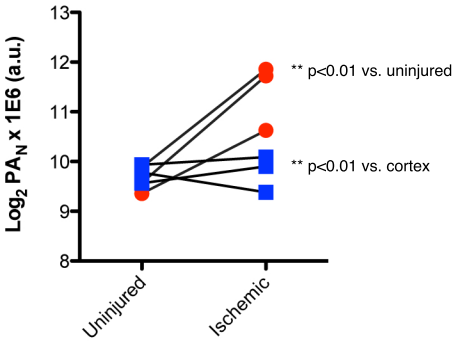

v. PC(18:2/0:0)

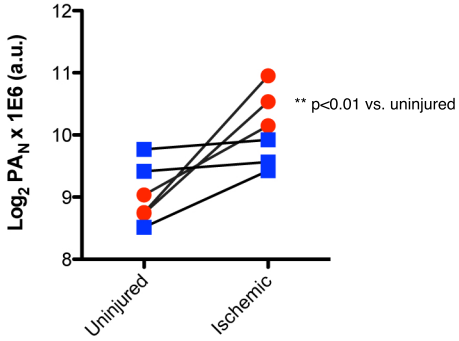

vi. PC(22:6/0:0)

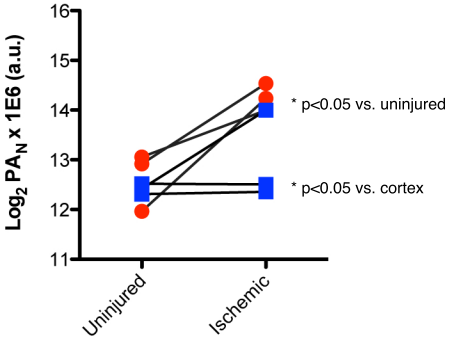

vii. PC(O-20:0/2:0)

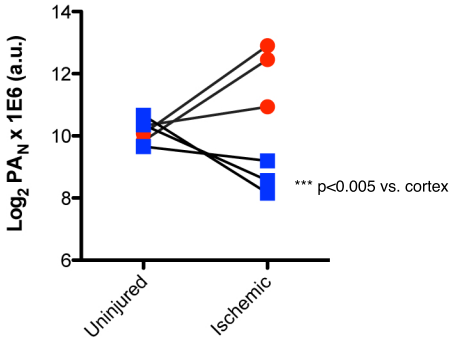

viii. PC(O-24/0:0)

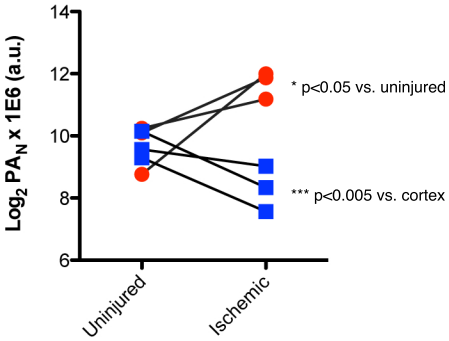

Figure 3.5.1a. Heatmap clustering of relative glycerophosphocholine lipid second messenger abundance in anterior regions of frontal cortex between wild-type and PAFR$^{-/-}$ mice following MCAO. Small molecular weight glycerophosphocholine second messengers were identified by LC-ESI-MS. Data are expressed as a ratio of abundance of ischemic to uninjured tissue ($Log_2PA_{N\ Fold\ Change}$). The number of standard deviations ($Log_2A^*_{Fold\ Change}$) by which the abundance of a given species in a given animal differs from the mean abundance of the whole population is colour-coded (green (less than expected) to red (greater than expected). * denotes species that show at least 1 standard deviation from the mean. This difference was considered significant and species were prioritized for a second level of statistical analysis.

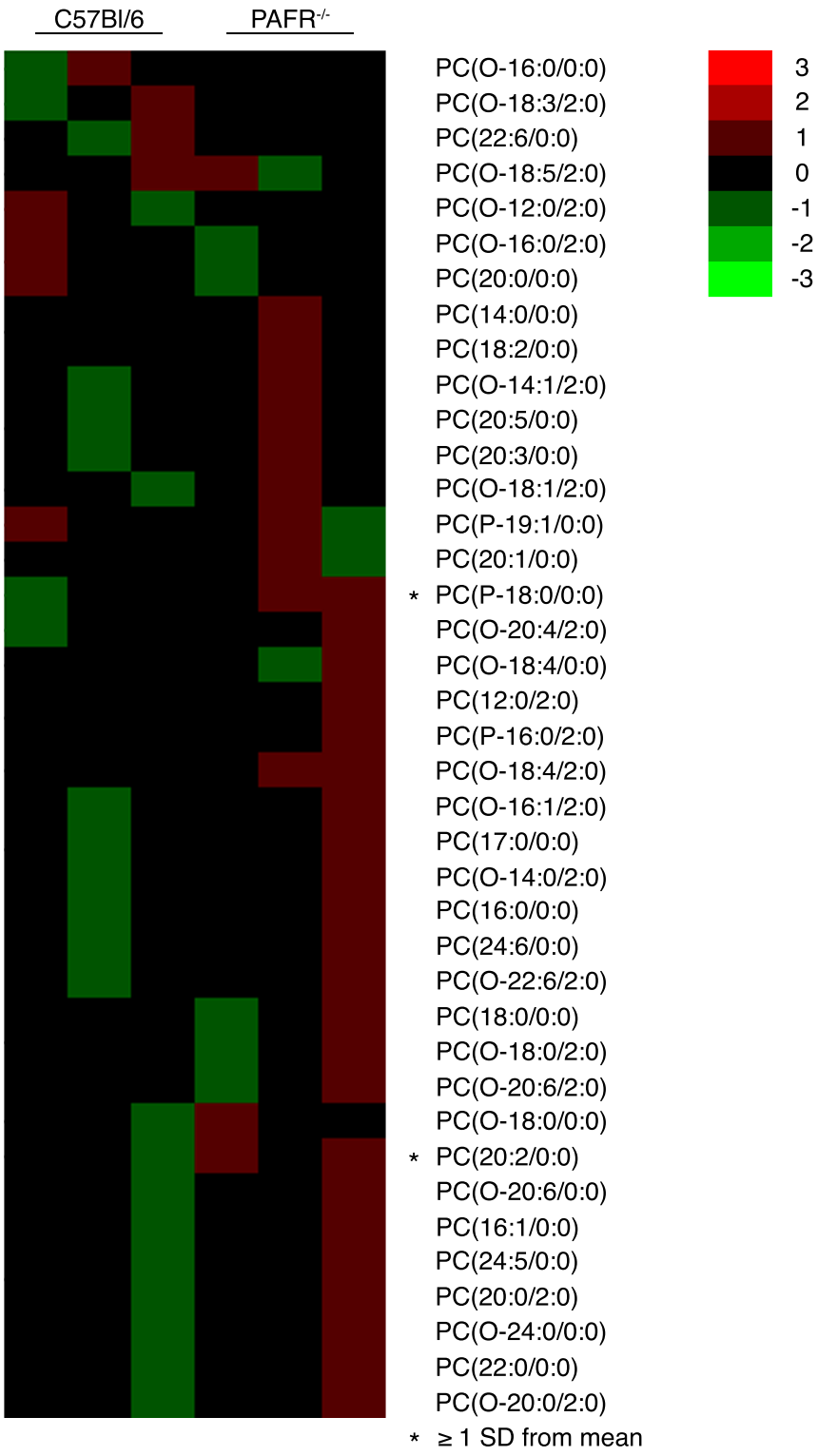
C57Bl/6
PAFR-/-
PC(O-16:0/0:0)
PC(O-18:3/2:0)
PC(22:6/0:0)
PC(O-18:5/2:0)
PC(O-12:0/2:0)
PC(O-16:0/2:0)
PC(20:0/0:0)
PC(14:0/0:0)
PC(18:2/0:0)
PC(O-14:1/2:0)
PC(20:5/0:0)
PC(20:3/0:0)
PC(O-18:1/2:0)
PC(P-19:1/0:0)
PC(20:1/0:0)
* PC(P-18:0/0:0)
PC(O-20:4/2:0)
PC(O-18:4/0:0)
PC(12:0/2:0)
PC(P-16:0/2:0)
PC(O-18:4/2:0)
PC(O-16:1/2:0)
PC(17:0/0:0)
PC(O-14:0/2:0)
PC(16:0/0:0)
PC(24:6/0:0)
PC(O-22:6/2:0)
PC(18:0/0:0)
PC(O-18:0/2:0)
PC(O-20:6/2:0)
PC(O-18:0/0:0)
* PC(20:2/0:0)
PC(O-20:6/0:0)
PC(16:1/0:0)
PC(24:5/0:0)
PC(20:0/2:0)
PC(O-24:0/0:0)
PC(22:0/0:0)
PC(O-20:0/2:0)
3
2
1
0
-1
-2
-3
* ≥ 1 SD from mean

Figure 3.5.1b. Differences in glycerophosphocholine lipid second messenger abundance in anterior frontal cortex between uninjured wild-type and PAFR$^{-/-}$ mice and following MCAO. Small molecular weight glycerophosphocholine second messengers were identified by LC-ESI-MS. Data shown represent Log_2-transformed normalized peak area (Log_2PA_N) for species identified as significant by heatmap analysis, compared by paired 2-way ANOVA followed by *post-hoc* Bonferroni. *p<0.05. **p<0.01. ***p<0.005.

i. PC(P-18:0/0:0)

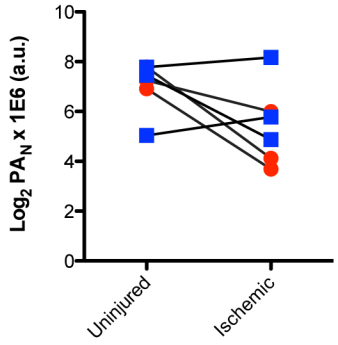

ii. PC(20:2/0:0)

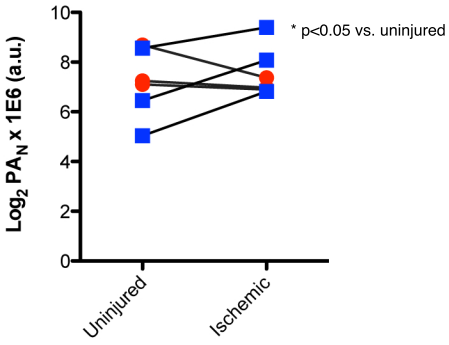



3.5.2 Lipid differences in posterior frontal cortex between wild-type C57Bl/6 and PAFR$^{-/-}$ following MCAO.

One lipid species, PC(20:1/0:0), showed greater than one standard deviation from the population mean by heatmap analysis (Fig 3.5.2a), and was significantly more abundant in wild-type posterior frontal cortex compared to PAFR$^{-/-}$ (** $p<0.01$) in uninjured tissue, yet was more abundant in PAFR$^{-/-}$ posterior frontal cortex compared to wild-type in ischemic tissue (** $p<0.01$). Further, in PAFR$^{-/-}$ tissue, PC(20:1/0:0) levels were higher in ischemic tissue relative to uninjured (* $p<0.05$) (Fig. 3.5.2b).

3.5.3 Lipid differences in anterior striatum between wild-type C57Bl/6 and PAFR$^{-/-}$ following MCAO.

There were no lipid species that displayed significant differences in abundance between wild-type and PAFR$^{-/-}$ anterior striatum in uninjured and ischemic tissue by heatmap analysis (Fig 3.5.3).

3.5.4 Lipid differences in posterior striatum between wild-type C57Bl/6 and PAFR$^{-/-}$ following MCAO.

Finally, heatmap analysis identified the same two lipid species, PC(P-18:0/0:0) and PC(20:0/2:0), that showed differences in abundance between wild-type and PAFR$^{-/-}$ in posterior cortex were also altered in posterior striatum in

Figure 3.5.2a. Heatmap clustering of relative glycerophosphocholine lipid second messenger abundance in posterior regions of frontal cortex between wild-type and PAFR$^{-/-}$ mice following MCAO. Small molecular weight glycerophosphocholine second messengers were identified by LC-ESI-MS. Data are expressed as a ratio of abundance of ischemic to uninjured tissue ($Log_2PA_{N\ Fold\ Change}$). The number of standard deviations ($Log_2A^*_{Fold\ Change}$) by which the abundance of a given species in a given animal differs from the mean abundance of the whole population is colour-coded (green (less than expected) to red (greater than expected). * denotes species that show at least 1 standard deviation from the mean. This difference was considered significant and species were prioritized for a second level of statistical analysis.

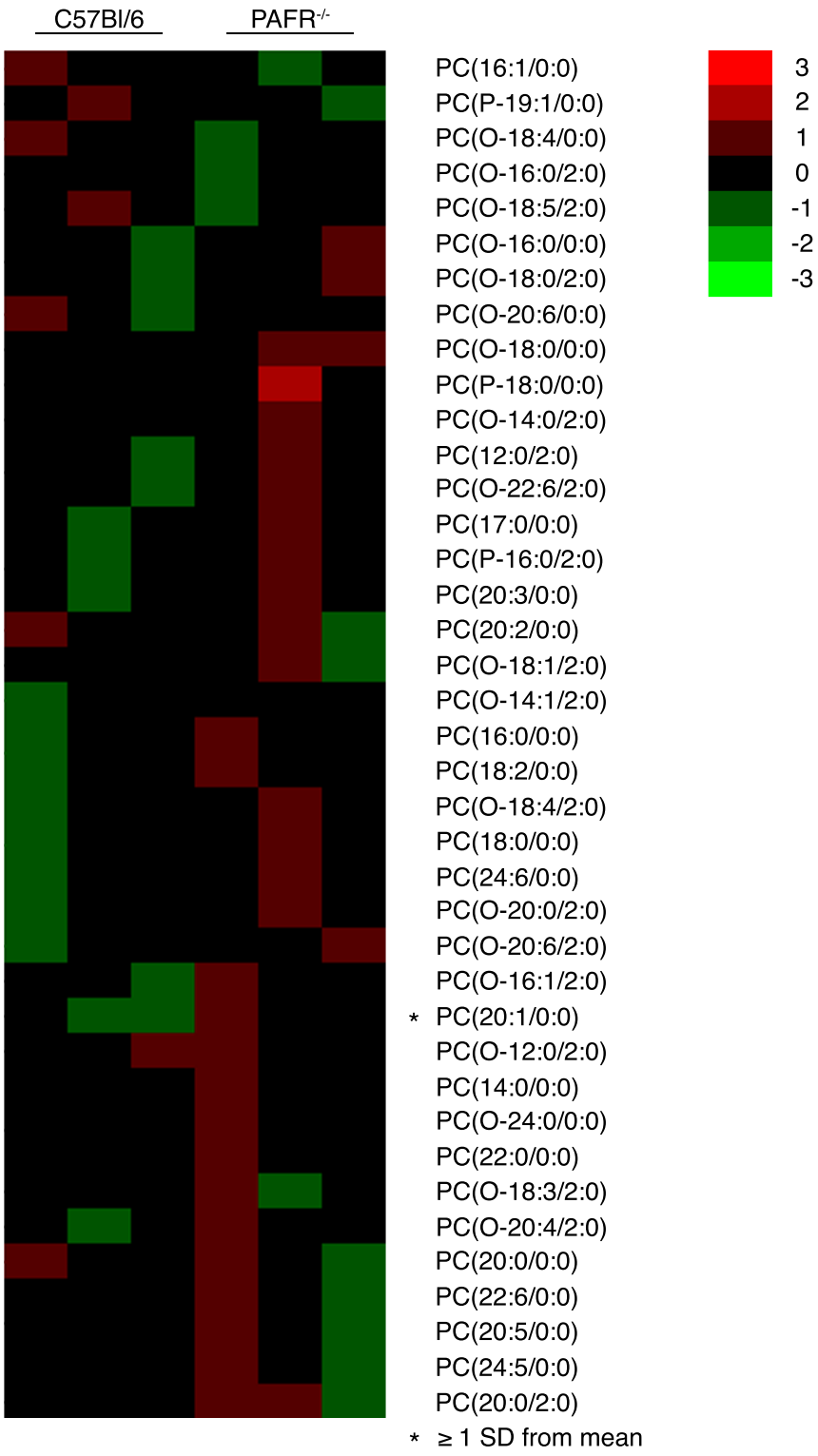
C57Bl/6
PAFR-/-
PC(16:1/0:0)
PC(P-19:1/0:0)
PC(O-18:4/0:0)
PC(O-16:0/2:0)
PC(O-18:5/2:0)
PC(O-16:0/0:0)
PC(O-18:0/2:0)
PC(O-20:6/0:0)
PC(O-18:0/0:0)
PC(P-18:0/0:0)
PC(O-14:0/2:0)
PC(12:0/2:0)
PC(O-22:6/2:0)
PC(17:0/0:0)
PC(P-16:0/2:0)
PC(20:3/0:0)
PC(20:2/0:0)
PC(O-18:1/2:0)
PC(O-14:1/2:0)
PC(16:0/0:0)
PC(18:2/0:0)
PC(O-18:4/2:0)
PC(18:0/0:0)
PC(24:6/0:0)
PC(O-20:0/2:0)
PC(O-20:6/2:0)
PC(O-16:1/2:0)
* PC(20:1/0:0)
PC(O-12:0/2:0)
PC(14:0/0:0)
PC(O-24:0/0:0)
PC(22:0/0:0)
PC(O-18:3/2:0)
PC(O-20:4/2:0)
PC(20:0/0:0)
PC(22:6/0:0)
PC(20:5/0:0)
PC(24:5/0:0)
PC(20:0/2:0)
* ≥ 1 SD from mean
3
2
1
0
-1
-2
-3

Figure 3.5.2b. Differences in glycerophosphocholine lipid second messenger abundance in posterior frontal cortex between uninjured wild-type and PAFR$^{-/-}$ mice and following MCAO. Small molecular weight glycerophosphocholine second messengers were identified by LC-ESI-MS. Data shown represent Log_2-transformed normalized peak area (Log_2PA_N) for species identified as significant by heatmap analysis, compared by paired 2-way ANOVA followed by *post-hoc* Bonferroni. *p<0.05. **p<0.01. ***p<0.005.

i. PC(20:1/0:0)

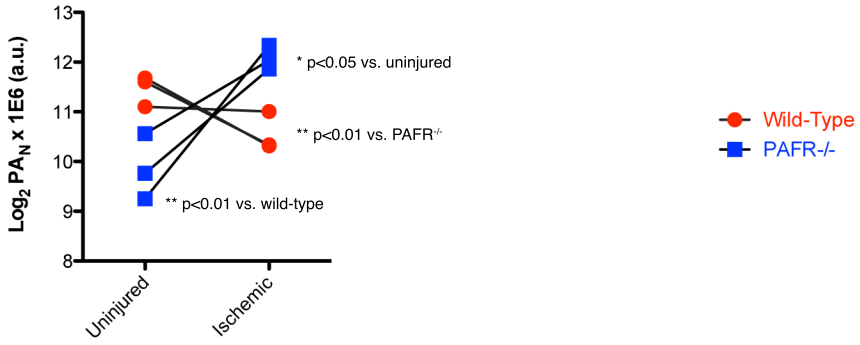
13
12
11
10
9
8
Log2 PAN x 1E6 (a.u.)
* p<0.05 vs. uninjured
** p<0.01 vs. PAFR-/-
** p<0.01 vs. wild-type
Uninjured
Ischemic
Wild-Type
PAFR-/-

Figure 3.5.3a. Heatmap clustering of relative glycerophosphocholine lipid second messenger abundance in anterior regions of striatum between wild-type and PAFR$^{-/-}$ mice following MCAO. Small molecular weight glycerophosphocholine second messengers were identified by LC-ESI-MS. Data are expressed as a ratio of abundance of ischemic to uninjured tissue ($Log_2PA_{N\ Fold\ Change}$). The number of standard deviations ($Log_2A^*_{Fold\ Change}$) by which the abundance of a given species in a given animal differs from the mean abundance of the whole population is colour-coded (green (less than expected) to red (greater than expected). * denotes species that show at least 1 standard deviation from the mean. This difference was considered significant and species were prioritized for a second level of statistical analysis.

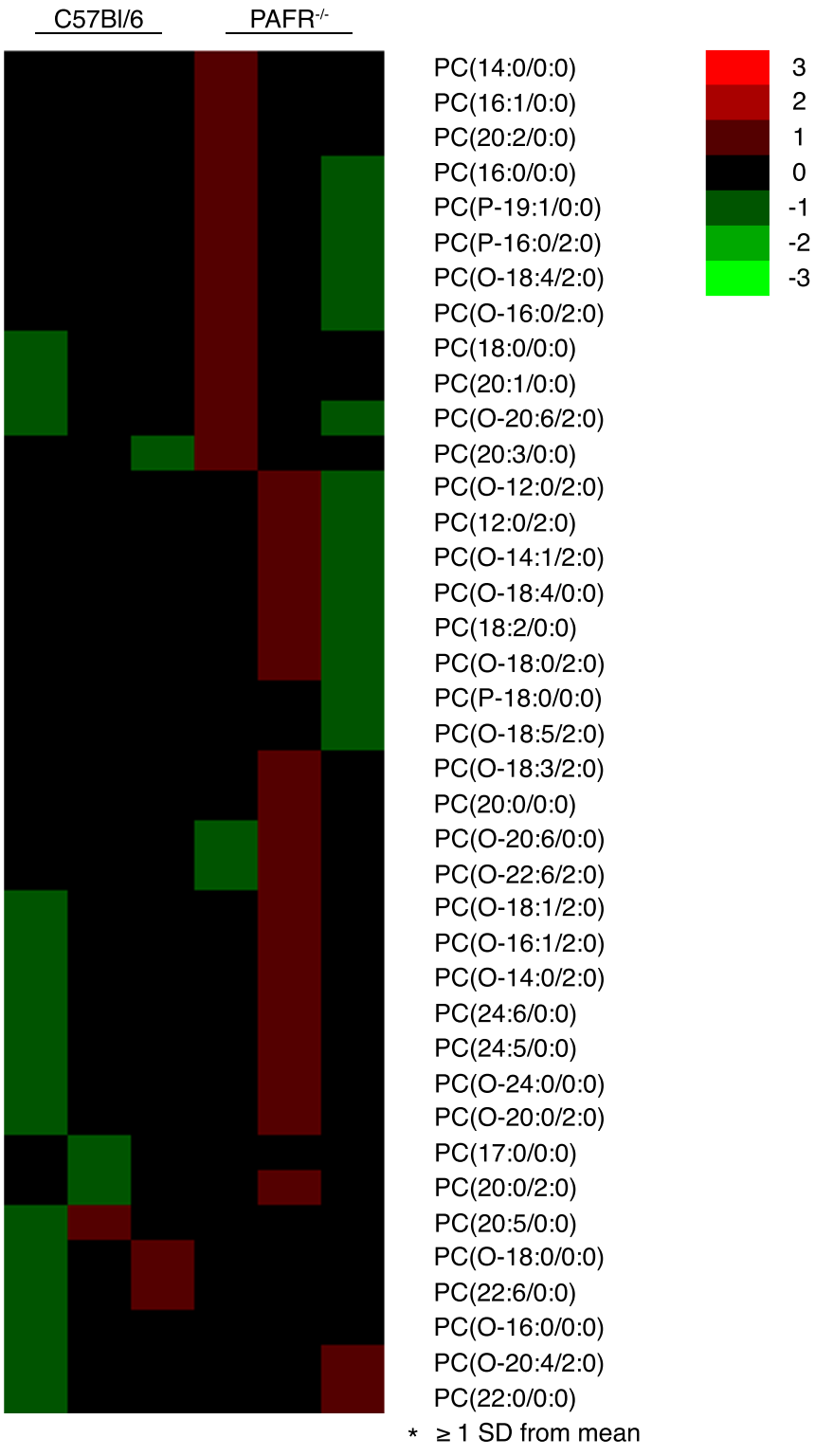
C57Bl/6
PAFR-/-
PC(14:0/0:0)
PC(16:1/0:0)
PC(20:2/0:0)
PC(16:0/0:0)
PC(P-19:1/0:0)
PC(P-16:0/2:0)
PC(O-18:4/2:0)
PC(O-16:0/2:0)
PC(18:0/0:0)
PC(20:1/0:0)
PC(O-20:6/2:0)
PC(20:3/0:0)
PC(O-12:0/2:0)
PC(12:0/2:0)
PC(O-14:1/2:0)
PC(O-18:4/0:0)
PC(18:2/0:0)
PC(O-18:0/2:0)
PC(P-18:0/0:0)
PC(O-18:5/2:0)
PC(O-18:3/2:0)
PC(20:0/0:0)
PC(O-20:6/0:0)
PC(O-22:6/2:0)
PC(O-18:1/2:0)
PC(O-16:1/2:0)
PC(O-14:0/2:0)
PC(24:6/0:0)
PC(24:5/0:0)
PC(O-24:0/0:0)
PC(O-20:0/2:0)
PC(17:0/0:0)
PC(20:0/2:0)
PC(20:5/0:0)
PC(O-18:0/0:0)
PC(22:6/0:0)
PC(O-16:0/0:0)
PC(O-20:4/2:0)
PC(22:0/0:0)
3
2
1
0
-1
-2
-3
* ≥ 1 SD from mean

uninjured and ischemic tissue (Fig 3.5.4a). Closer analysis confirmed, that as in cortex, PC(P-18:0/0:0) was not significantly different, as determined by 2-way ANOVA. PC(20:0/2:0) was, however, more abundant in uninjured tissue compared to ischemic in wild-type posterior striatum (* $p<0.05$), and was more abundant in ischemic $PAFR^{-/-}$ posterior striatum compared to ischemic wild-type tissue as observed in cortex (* $p<0.05$) (Fig. 3.5.4b).

Figure 3.5.4a. Heatmap clustering of relative glycerophosphocholine lipid second messenger abundance in posterior regions of striatum between wild-type and PAFR$^{-/-}$ mice following MCAO. Small molecular weight glycerophosphocholine second messengers were identified by LC-ESI-MS. Data are expressed as a ratio of abundance of ischemic to uninjured tissue ($Log_2PA_{N\ Fold\ Change}$). The number of standard deviations ($Log_2A^*_{Fold\ Change}$) by which the abundance of a given species in a given animal differs from the mean abundance of the whole population is colour-coded (green (less than expected) to red (greater than expected). * denotes species that show at least 1 standard deviation from the mean. This difference was considered significant and species were prioritized for a second level of statistical analysis.

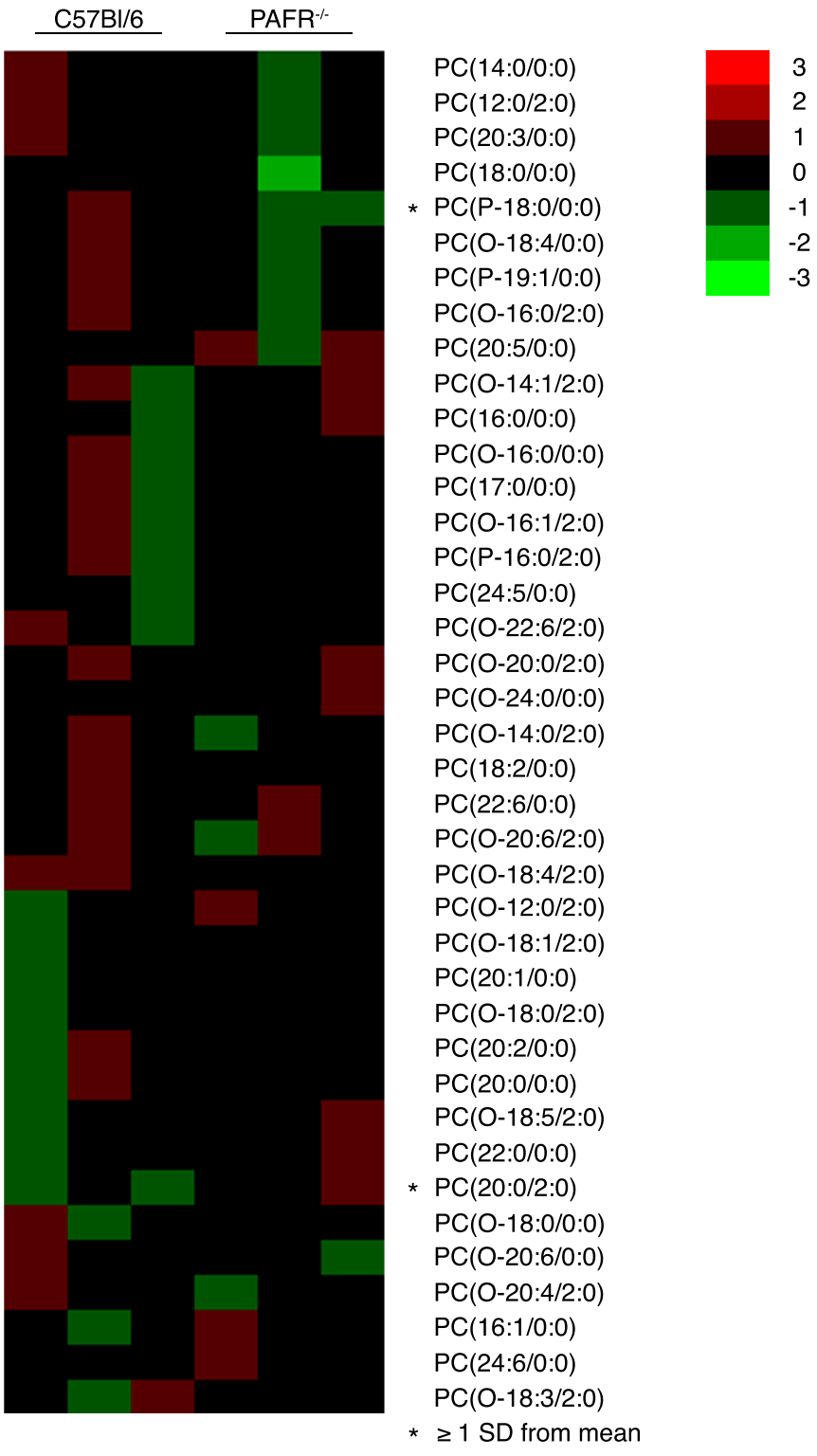
C57Bl/6
PAFR-/-
PC(14:0/0:0)
PC(12:0/2:0)
PC(20:3/0:0)
PC(18:0/0:0)
* PC(P-18:0/0:0)
PC(O-18:4/0:0)
PC(P-19:1/0:0)
PC(O-16:0/2:0)
PC(20:5/0:0)
PC(O-14:1/2:0)
PC(16:0/0:0)
PC(O-16:0/0:0)
PC(17:0/0:0)
PC(O-16:1/2:0)
PC(P-16:0/2:0)
PC(24:5/0:0)
PC(O-22:6/2:0)
PC(O-20:0/2:0)
PC(O-24:0/0:0)
PC(O-14:0/2:0)
PC(18:2/0:0)
PC(22:6/0:0)
PC(O-20:6/2:0)
PC(O-18:4/2:0)
PC(O-12:0/2:0)
PC(O-18:1/2:0)
PC(20:1/0:0)
PC(O-18:0/2:0)
PC(20:2/0:0)
PC(20:0/0:0)
PC(O-18:5/2:0)
PC(22:0/0:0)
* PC(20:0/2:0)
PC(O-18:0/0:0)
PC(O-20:6/0:0)
PC(O-20:4/2:0)
PC(16:1/0:0)
PC(24:6/0:0)
PC(O-18:3/2:0)
3
2
1
0
-1
-2
-3
* ≥ 1 SD from mean

Figure 3.5.4b. Differences in glycerophosphocholine lipid second messenger abundance in posterior striatum between uninjured wild-type and PAFR$^{-/-}$ mice and following MCAO. Small molecular weight glycerophosphocholine second messengers were identified by LC-ESI-MS. Data shown represent Log_2-transformed normalized peak area (Log_2PA_N) for species identified as significant by heatmap analysis, compared by paired 2-way ANOVA followed by *post-hoc* Bonferroni. *p<0.05. **p<0.01. ***p<0.005.

i. PC(P-18:0/0:0)

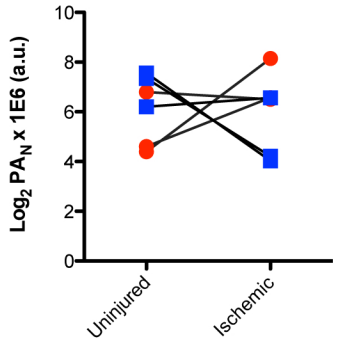

ii. PC(20:0/2:0)

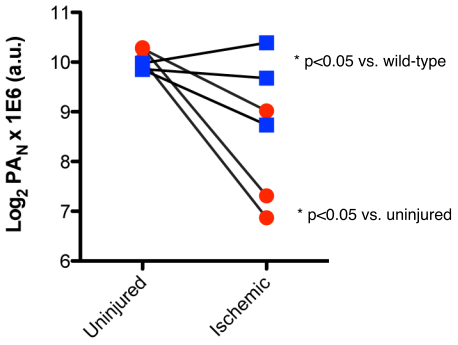



4. Discussion.

4.1 Summary

In this thesis, I sought to use a systems biology approach to address my overarching hypothesis that small molecular weight glycerophosphocholine second messenger lipids contribute to the expansion of ischemia/reperfusion injury following MCAO. By profiling glycerophosphocholine second messenger abundance in uninjured wild-type frontal cortex and striatum, I highlighted the potential of these lipids to be used to identify functional subdomains within anterior and posterior regions of cortex and striatum. Next, I showed that second messenger lipids have the potential to mediate crosstalk between neuroprotective and neurotoxic stimuli following MCAO *in vivo*. Finally, I highlighted the role of PAFR in mediating PAF metabolism, and proposed that microglia are the master regulators of this PAFR-mediated PAF metabolism, and are responsible for maintaining second messenger homeostasis in uninjured brain.

4.2 Defining functional domains in brain architecture through lipid topography

Based on the data presented in this thesis, I argue that the application of mass spectrometry to the study of discrete lipid species at the molecular level can be used to examine functionally heterogeneous domains within defined cerebral architectures. Just as regional and laminar architecture has been defined by cell morphology, cell type, and neurotransmitter profile (Fuxe et al., 2010; Moser and Moser, 1998), so to may it be possible to define new domains by their signature lipid profile. The finding, in this thesis, that discrete lipid second messengers display a

spatial gradient in cortex and striatum in uninjured mice demonstrates a specificity of lipid metabolism particular to different regions within “functional units.” Previous attempts to profile lipids in the brain, including both membrane phospholipids and their metabolites have considered individual brain regions (i.e., cortex and/or striatum) as homogenous tissue (see (Axelsen and Murphy, 2010), for example). The cerebral cortex is, however, a complex structure with intricate three-dimensional patterns of functional inputs and outputs. To illustrate this, the mouse homunculus, the representation of the regions of the mouse motor and somatosensory cortices that coordinate sensory inputs and motor outputs to different areas of the body, stretches the length of the cerebral cortex on the anterior/posterior axis. Similarly, the striatum, an important signaling centre of the basal ganglia, receives excitatory glutamatergic projections from layer V of the cortex, and sends primarily inhibitory dopaminergic projections to other regions of the basal ganglia (globus pallidus and substantia nigra) (Figure 4.1) (Gerfen, 2000). These two distinct forebrain structures represent common targets of stroke in human, and are the primary targets of experimental MCAO in rodents. Previous studies have demonstrated that neuronal subtypes, identified by their primary neurotransmitter, are selectively susceptible to focal ischemia in striatum (Katchanov et al., 2003). In this thesis, I found a gradient of lipid metabolites present in uninjured tissue that appears to be altered specifically following MCAO . I suggest that with the further validation describe below, these profiles begin to identify new domains or cellular grouping that define vulnerability, resistance, or cellular response (i.e., a change in cell ratios) to ischemia.

Figure 4.1. Dopamine signaling in the prefrontal cortex. A simplified representation of the cortico-striatal circuit of the basal ganglia. Layer V neurons of the prefrontal cortex send excitatory (green arrow) glutamatergic signals to the striatum, and receives inhibitory (red arrows) dopaminergic signals from the ventral tegmental area (VTA) via the nucleus accumbens (NAcc) area of the ventral striatum. The striatum also receives dopaminergic signals from the substantia nigra (SN).

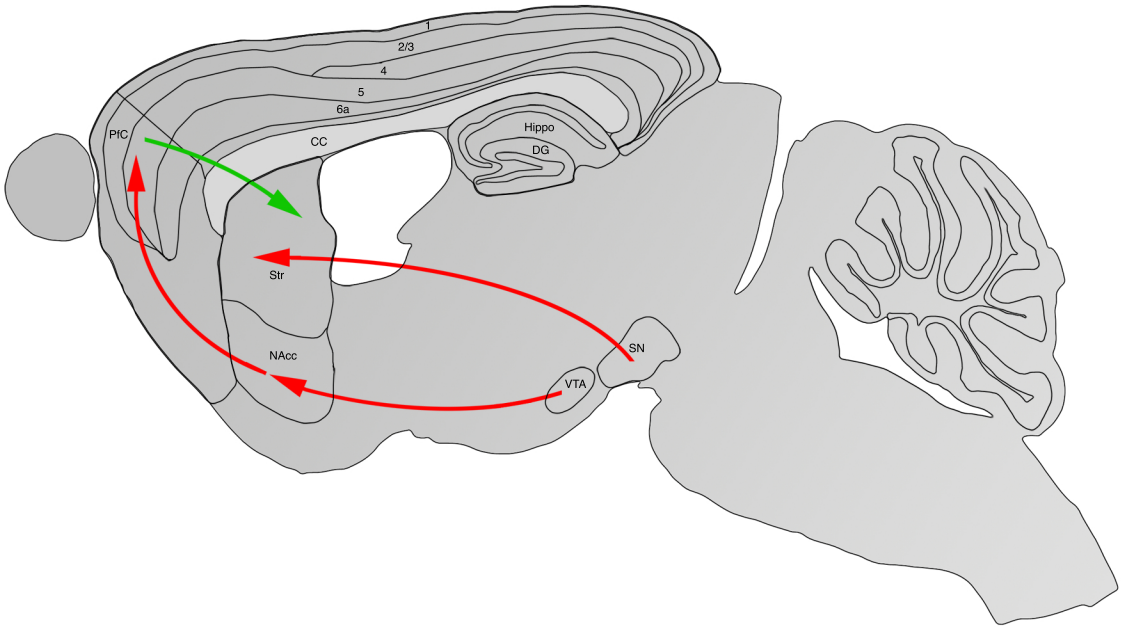
1
2/3
4
5
6a
PfC
CC
Hippo
DG
Str
NAcc
SN
VTA

Because many brain regions coordinate myriad different inputs and outputs comprising highly refined subsets of neuronal cell types, new emphasis has been placed on identifying landmarks defining distinct functional domains within the cytoarchitecture of specific regions. Recent studies have reported the presence of such functional subdomains in the hippocampus, identified using proteomic and transcriptomic approaches paired with cytoarchitectural analysis (Christensen et al., 2010; Dong et al., 2009). In this light, I hypothesized that these types of molecularly distinct subdomains may be present in the frontal cortex and striatum, and further, that they can be identified by unique patterns of glycerophosphocholine metabolism. To test this hypothesis, I profiled the small molecular weight choline-containing glycerophospholipid second messengers – a family of bioactive lipids that are the product of membrane phospholipid metabolism.

I identified twelve lipid species by LC-ESI-MS that displayed an anterior-posterior gradient of abundance in the frontal cortex of uninjured C57Bl/6 mice (Table 3.1.1). Of these, ten were more abundant posterior regions of cortex compared to anterior. Interestingly, the two lipid species with higher abundance in anterior regions of cortex – PC(O-18:1/2:0) and PC(O-22:6/2:0) – are PAF lipids containing two of the four most highly abundant fatty acid moieties in the C57Bl/6 brain (McNamara et al., 2009). A 22:6 fatty acid (DHA) deficiency in the prefrontal cortex has repeatedly been associated with major depressive disorder and other recurrent affective disorders (McNamara, 2010). One can hypothesize, then, that increased DHA incorporation into membrane lipids in anterior frontal cortex is required for proper function of neurons in the prefrontal cortex. Indeed, DHA

supplementation has been associated with increased prefrontal activation during periods of sustained attention (McNamara et al., 2010). In fact, both attention deficit hyperactivity disorder and major depressive disorder have been associated with depressed levels of dopamine. These data suggest that high levels of DHA in prefrontal cortical membranes may be required for proper dopamine signaling in the prefrontal cortex. This hypothesis is supported by evidence demonstrating a correlation between brain DHA levels and dopamine receptor (both D(1) and D(2) receptor families) concentration on the surface of dopaminergic neurons in the striatum (Davis et al., 2010). It follows, therefore, that high levels of DHA should be found in striatal tissue – the target areas of prefrontal dopaminergic projections.

In support of this hypothesis, we found levels of PC(O-22:6/2:0) even higher in anterior striatal regions compared to anterior cortex. It is important to note, however, that in both cases, these increases are specific to DHA-containing PAF lipids and not other species enriched in DHA. This imbalance is likely reflective of an overall higher level of DHA incorporation into membrane lipids in the prefrontal cortex compared to other regions. This hypothesis is further supported by evidence for preferential incorporation of dietary DHA into cortical plasma membrane (Lamaziere et al., 2011). However, while based on these data, I would have also expected an increase in DHA containing *lyso*-PAF, this lipid was either unaltered or below the level of detection of the mass spectrometer as it was not detected in either injured or uninjured tissue.

While the data presented in this thesis provide strong evidence for two metabolically distinct regions of cortex and two of striatum that can be defined by

their differing lipid profiles, it is important to note, however, that the tissue analyzed, while a subregion of both cortex and striatum defined by anterior-posterior position, was still quite large, and it is highly likely that yet more, smaller subdomains exist within these tissues. I argue that these lipid-defined domains may reflect the differences in neural networks to which they belong or alternatively the composition of cells and the afferents within these regions. To identify these subdomains more precisely, MALDI-ToF imaging would resolve lipid differences directly from tissue on a micrometer rather than millimeter scale – but to do so requires the identification of lead species, and here we have identified PC(O-22:6/2:0) as a prime candidate that should be pursued for more precise topographic mapping of potential functional domains.

4.3 Is crosstalk between neurotoxicity and neuroprotection mediated by specific lipid second messengers in the posterior frontal cortex following MCAO?

Under normoxic conditions, our data provide evidence for an intricate regulation of glycerophosphocholine lipid metabolism, leading to distinct gradients of abundance between anterior and posterior regions of frontal cortex and striatum. The MCAO model of transient focal ischemia produces sizeable lesions in both the cortex and striatum, and so I hypothesized that, after MCAO, the regulation of glycerophosphocholine metabolism would be disrupted, leading to alterations in this topography. To test this hypothesis, using LC-ESI-MS, I identified four main

patterns of dysregulation: (1) abrogation of a defined gradient, (2) exacerbation of a defined gradient, (3) reversal of a defined gradient, and (4) appearance a novel gradient. It remains to be determined whether these changes represent potentially deleterious effects of ischemic injury, or a concerted effort on behalf of the brain to protect itself from injury progression. Further, the source of these alterations in lipid abundance has yet to be established. It is conceivable that $cPLA_2$ and $iPLA_2$ activation, in response to rising levels of intracellular Ca^{2+} leads to increased membrane lipid metabolism and production of glycerophosphocholine second messenger lipids. Both lipases are known to be activated by the changes in calcium homeostasis accompanying ischemia/reperfusion (Sun et al., 2010). Alternatively, infiltrating glial and immune cell populations may contribute wholly, or in part, to these lipid imbalances (i.e. changes in lipid topography do not result from metabolic changes but rather a change in the ratio of cells present in target tissue). I submit, however, that a complex combination of these hypotheses underlies the dysregulation of glycerophosphocholine second messenger metabolism. To address these two hypotheses, I have collected a second cohort of animals processed for immunofluorescent analyses that can be used to identify the changes in cell type and degree of cell loss in the regions exhibiting lipid changes. These additional studies will provide needed insight into the changes in cell ratio and viability associated with the lipid imbalances described in this thesis.

As one example of lipid-defined subdomains, I found two PAF species exhibited novel gradients of abundance – PC(O-12:0/2:0) and PC(O-20:0/2:0) – in posterior regions of frontal cortex compared to anterior cortex and posterior striatum

respectively following MCAO. Recent evidence has indicated that PAF family members are able to induce blood-brain barrier permeability *in vitro* (Fang et al., 2011). In fact, compromised integrity of the blood brain barrier is a hallmark of ischemia/reperfusion injury (Sandoval and Witt, 2008). A compromised blood-brain barrier, in turn, is increasingly permeable to the passage of macromolecules, ions and fluid. This vasogenic edema, is thought to promote the progression of ischemic injury by exacerbating the immune response (Huang et al., 2006; Mehta et al., 2007). Further, as a potent chemoattractant (Luster et al., 2005), PAF lipids are capable of promoting infiltration of immune cells into the brain parenchyma – a process that requires a permeable blood-brain barrier (Garcia et al., 1994; Gelderblom et al., 2009), and occurs in a PAF receptor dependent manner (Rodrigues et al., 2011). Taken together, these findings point to the possibility that accumulation of PC(O-12:0/2:0) and PC(O-20:0/2:0) in posterior frontal cortex may contribute to neuronal injury by promoting the breakdown of the blood-brain barrier and attraction of immune cells, exacerbating the immune response. Both alterations would manifest as an increase in these two PAF species.

While accumulation of specific PAF lipids may promote the expansion of ischemia/reperfusion injury, there exists the possibility that other lipids may act to protect cells from cytotoxic stimuli. Indeed, PC(22:6/0:0), elevated in posterior frontal cortex, is the primary transport form of DHA to the brain (Bernoud et al., 1999; Lagarde et al., 2001). DHA is the parent fatty acid to the docosanoid family of potent anti-inflammatory mediators (Marcheselli et al., 2003). One of these docosanoid family members, NPD1 is capable of attenuating the progression of

ischemia resulting in smaller lesions. Recent reports indicate that pre-treatment with DHA promotes NPD1 biosynthesis in ischemic tissue following MCAO. Further, NPD1 provides more effective protection from cortical lesions compared to subcortical (Belayev et al., 2011). I hypothesize, then, that increased levels of DHA-containing LPC in posterior frontal cortex reflect an increase in transport to the brain and subsequent sequestration of DHA in ischemic cortical tissue in a concerted effort on behalf of the brain to protect itself from the expansion of ischemic injury. Further, transport into the brain from the vasculature is facilitated by accumulation of PAF lipids in posterior frontal cortex leading to compromised integrity of the blood-brain barrier.

4.4 PAFR null-mutant animals are deficient in PAF clearance.

To test whether accumulation of PAF lipids in ischemic posterior cortex leads to blood-brain barrier permeability as determined by PC(22:6/0:0) accumulation, I profiled the glycerophosphocholine second messenger lipidome of PAFR null-mutant mice. PAF-mediated activation of the PAF receptor promotes the activation of PLA_2 family members (Izumi and Shimizu, 1995), and hence, can contribute to the accumulation of glycerophosphocholine second messenger lipids. Based on these data, I hypothesized that the second messenger abundance gradients observed in frontal cortex and striatum of wild-type C57Bl/6 mice would be fundamentally altered or ablated in the brains PAFR null-mutant mice. Indeed, all, except four, of the gradients described in wild-type animals are absent in $PAFR^{-/-}$. These findings

highlight an important role for the PAF receptor in regulating the metabolism and biosynthesis of second messenger lipids. Preliminary data from our laboratory and others indicate that, in mice, PAFR is primarily expressed by microglia (unpublished data). These data are supported by an early study examining expression of PAFR transcript in rat glia and neurons (Mori et al., 1996). It is conceivable, then, that the chemotactic response elicited by the interaction of PAF lipids with the PAF receptor on microglia leads to regional differences in cell-type ratios. An extreme example of this phenomenon has been described in palmitoyl protein thioesterase-1 (PPT1) null-mutant mice. PPT1$^{-/-}$ mice display extensive loss of neurons in the cortex and hippocampus, and show localized microglial activation in specific cortical and subcortical regions (Bible et al., 2004). While no such extensive neuronal loss has been demonstrated in uninjured PAFR$^{-/-}$ animals, the localization and concentration of microglia in cortical and striatal tissue has yet to be determined. Microglia, then, may play important roles in PAF lipid homeostasis in the uninjured brain.

Interestingly, three of the four gradients conserved between uninjured wild-type and PAFR$^{-/-}$ animals (i.e., increased abundance of PC(O-18:0/0:0) and PC(O-18:1/2:0) in anterior striatum and of PC(O-18:0/2:0) in posterior striatum) correspond to lipids containing ether-linked octadecyl alkyl chains, suggesting that the metabolism of these lipid species is tightly regulated, in a *sn*-1 chain length and linkage PAFR-independent manner. Although the functional significance of this regulation remains elusive, one can hypothesize that these lipids contribute to the proper function of specific subdomains in frontal cortex and striatum. To answer this, MALDI-ToF imaging again would provide insight into the specific location of

these domains, and the identity of the population of cells within focused on the target lipids identified in this thesis.

Following MCAO, I found a marked imbalance in the number of PAF lipids displaying significantly altered abundance between two regions in wild-type (4 PAF lipids) and $PAFR^{-/-}$ animals (9 PAF lipids). This does not appear to support the idea that PAF-PAFR interaction leads to the activation of PLA_2 resulting in the accumulation of more PAF species, but is more consistent with a model whereby PAF-PAFR interaction promotes the consumption of PAF lipids by activating PAF-AH. The activation of PAFR by binding of PC(O-16:0/2:0) has been shown to trigger the secretion of PAF-AH in murine macrophages in an attempt to decrease local concentrations of PAF at inflammatory sites (Ohshima et al., 2002). Given that PAFR appears to be restricted to microglia in murine brain, these findings support the notion that PAF accumulation following MCAO acts as a chemottractant – attracting microglia and other non-resident immune cells to inflammatory sites. At these sites, PAF-PAFR interaction leads to the internalization of receptor bound PAF and the hydrolysis of free PAF by secreted PAF-AH resulting in the decrease in PAF lipids seen in $PAFR^{+/+}$ but not $PAFR^{-/-}$ following MCAO.

Finally, I hypothesized that these increased levels of PAF lipids in specific brain regions would lead to increased blood-brain barrier permeability, as was seen in wild-type animals. Indeed, I found a specific accumulation of three PAF species (PC(O-14:1/2:0), PC(O-14:0/2:0) and PC(O-20:0/2:0)) in posterior frontal cortex compared to posterior striatum, along with a correspondingly increased abundance of PC(22:6/0:0). It is important to note, however, that because PC(22:6/0:0) levels

are increased in both genotypes, it is unknown whether blood-brain barrier permeability is required for PC(22:6/0:0) passage, and further, the extent to which PAF contributes to this blood-brain barrier permeability is unclear. In this light, I directly compared glycerophosphocholine second messenger profiles between wild-type and $PAFR^{-/-}$ animals. Only two different lipids - PC(O-20:1/0:0) and PC(O-20:0/0:0) – showed significantly altered abundance between wild-type and $PAFR^{-/-}$ in posterior regions of ischemic cortex and striatum respectively. The finding that almost all lipids are found in equal abundance within a region between both genotypes supports a model in which the PAF receptor is capable of, but not required for blood-brain barrier permeability, and that the contribution of infiltrating immune cells and activated microglia to local lipid profiles may mask any differences in lipid abundance from ischemic neurons. Further studies will require direct assessment of blood-brain barrier permeability in $PAFR^{+/+}$ and $PAFR^{-/-}$ mice. This tissue has been collected and can be analyzed by immunohistochemistry for infiltration of mouse IgG into compromised tissue as described previously (Bennett et al., 1995).

4.5 Conclusion

Using a lipidomic approach to profile regional differences in glycerophosphocholine lipid second messenger metabolism, I have revealed the potential of lipid topography as a tool to define functional subdomains defined by specific subpopulations of cells within brain regions. Further, I have outlined a

model in which the accumulation of PAF lipids in specific regions could lead to the activation and migration of microglia and non-resident immune cells to inflammatory sites through a mechanism facilitated by PAF-PAFR interaction (Figure 4.2). PAF accumulation may also contribute to the permeabilization of the blood-brain barrier, leading to the facilitated transport of PC(22:6/0:0) to the brain where DHA is converted to NDP1 in an attempt to attenuate the progression of ischemic injury. While these hypotheses will require direct assessment, they represent two possible mechanistic outcomes of changes in glycerophosphocholine second messenger metabolism following MCAO.

Figure 4.2. PAF accumulation in ischemic tissue promotes a PAFR-dependent response leading to increased inflammation. PAF homeostasis is maintained by resident microglia in uninjured frontal cortex (left panel). Increased PAF production and accumulation following ischemia leads to microglial activation, blood-brain barrier permeability, and immune cell infiltration, all through PAF receptor-dependent mechanisms (right panel).

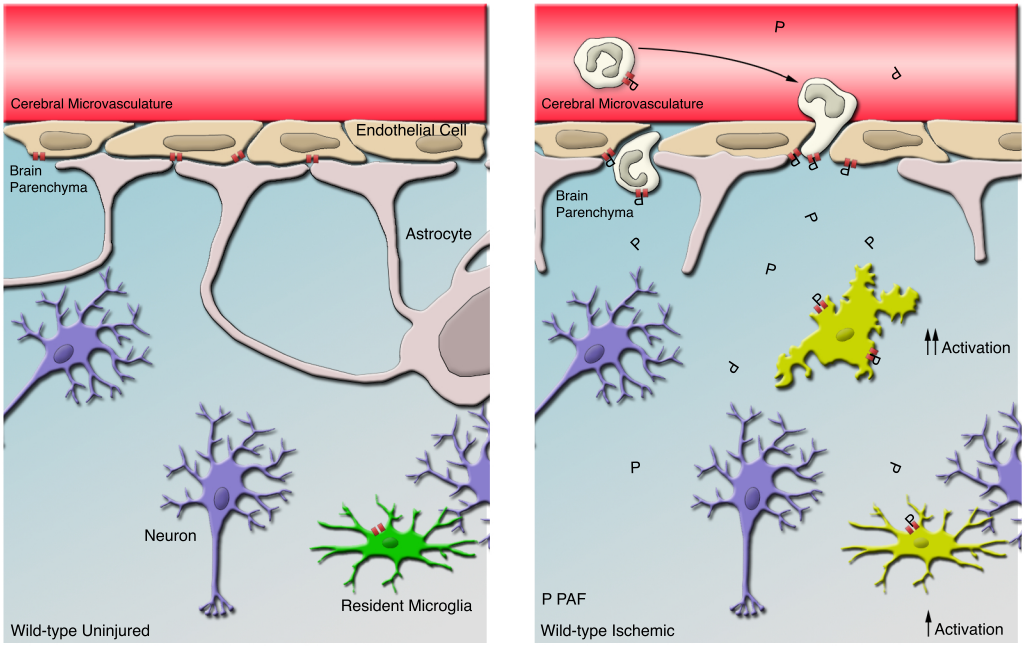
Cerebral Microvasculature
Endothelial Cell
Brain Parenchyma
Astrocyte
Neuron
Resident Microglia
Wild-type Uninjured
P
Cerebral Microvasculature
Brain Parenchyma
Activation
P PAF
Wild-type Ischemic
Activation

5. References.

Adibhatla, R.M., and Hatcher, J.F. (2007). Secretory phospholipase A2 IIA is up-regulated by TNF-alpha and IL-1alpha/beta after transient focal cerebral ischemia in rat. Brain Res *1134*, 199-205.

Arai, K., Ikegaya, Y., Nakatani, Y., Kudo, I., Nishiyama, N., and Matsuki, N. (2001). Phospholipase A2 mediates ischemic injury in the hippocampus: a regional difference of neuronal vulnerability. Eur J Neurosci *13*, 2319-2323.

Axelsen, P.H., and Murphy, R.C. (2010). Quantitative analysis of phospholipids containing arachidonate and docosahexaenoate chains in microdissected regions of mouse brain. J Lipid Res *51*, 660-671.

Banik, N.L., Matzelle, D.C., Gantt-Wilford, G., Osborne, A., and Hogan, E.L. (1997). Increased calpain content and progressive degradation of neurofilament protein in spinal cord injury. Brain Res *752*, 301-306.

Bazan, N.G., and Allan, G. (1996). Platelet-activating factor in the modulation of excitatory amino acid neurotransmitter release and of gene expression. J Lipid Mediat Cell Signal *14*, 321-330.

Bazan, N.G., Squinto, S.P., Braquet, P., Panetta, T., and Marcheselli, V.L. (1991). Platelet-activating factor and polyunsaturated fatty acids in cerebral ischemia or convulsions: intracellular PAF-binding sites and activation of a fos/jun/AP-1 transcriptional signaling system. Lipids *26*, 1236-1242.

Bazan, N.G., Tu, B., and Rodriguez de Turco, E.B. (2002). What synaptic lipid signaling tells us about seizure-induced damage and epileptogenesis. Prog Brain Res *135*, 175-185.

Belayev, L., Busto, R., Zhao, W., Fernandez, G., and Ginsberg, M.D. (1999). Middle cerebral artery occlusion in the mouse by intraluminal suture coated with poly-L-lysine: neurological and histological validation. Brain Res *833*, 181-190.

Belayev, L., Khoutorova, L., Atkins, K.D., Eady, T.N., Hong, S., Lu, Y., Obenaus, A., and Bazan, N.G. (2011). Docosahexaenoic Acid Therapy of Experimental Ischemic Stroke. Transl Stroke Res *2*, 33-41.

Belousov, A.B., Godfraind, J.M., and Krnjevic, K. (1995). Internal Ca2+ stores involved in anoxic responses of rat hippocampal neurons. J Physiol *486 (Pt 3)*, 547-556.

Bennett, S.A., Stevenson, B., Staines, W.A., and Roberts, D.C. (1995). Periodic acid-Schiff (PAS)-positive deposits in brain following kainic acid-induced seizures: relationships to fos induction, neuronal necrosis, reactive gliosis, and blood-brain barrier breakdown. Acta Neuropathol *89*, 126-138.

Benveniste, H., Drejer, J., Schousboe, A., and Diemer, N.H. (1984). Elevation of the extracellular concentrations of glutamate and aspartate in rat hippocampus during transient cerebral ischemia monitored by intracerebral microdialysis. J Neurochem *43*, 1369-1374.

Bernoud, N., Fenart, L., Moliere, P., Dehouck, M.P., Lagarde, M., Cecchelli, R., and Lecerf, J. (1999). Preferential transfer of 2-docosahexaenoyl-1-lysophosphatidylcholine through an in vitro blood-brain barrier over unesterified docosahexaenoic acid. J Neurochem *72*, 338-345.

Bible, E., Gupta, P., Hofmann, S.L., and Cooper, J.D. (2004). Regional and cellular neuropathology in the palmitoyl protein thioesterase-1 null mutant mouse model of infantile neuronal ceroid lipofuscinosis. Neurobiol Dis *16*, 346-359.

Bito, H., Kudo, Y., and Shimizu, T. (1993). Characterization of platelet-activating factor (PAF) receptor in the rat brain. J Lipid Mediat *6*, 169-174.

Bligh, E.G., and Dyer, W.J. (1959). A rapid method of total lipid extraction and purification. Can J Biochem Physiol *37*, 911-917.

Brand, A., Crawford, M.A., and Yavin, E. (2010). Retailoring docosahexaenoic acid-containing phospholipid species during impaired neurogenesis following omega-3 alpha-linolenic acid deprivation. J Neurochem *114*, 1393-1404.

Braquet, P., Paubert-Braquet, M., Koltai, M., Bourgain, R., Bussolino, F., and Hosford, D. (1989). Is there a case for PAF antagonists in the treatment of ischemic states? Trends Pharmacol Sci *10*, 23-30.

Brown, H.A., and Murphy, R.C. (2009). Working towards an exegesis for lipids in biology. Nat Chem Biol *5*, 602-606.

Callender, H.L., Forrester, J.S., Ivanova, P., Preininger, A., Milne, S., and Brown, H.A. (2007). Quantification of diacylglycerol species from cellular extracts by electrospray ionization mass spectrometry using a linear regression algorithm. Anal Chem *79*, 263-272.

Carpenter, C.R., Keim, S.M., Milne, W.K., Meurer, W.J., and Barsan, W.G. (2011). Thrombolytic therapy for acute ischemic stroke beyond three hours. J Emerg Med *40*, 82-92.

Christensen, T., Bisgaard, C.F., Nielsen, H.B., and Wiborg, O. (2010). Transcriptome differentiation along the dorso-ventral axis in laser-captured microdissected rat hippocampal granular cell layer. Neuroscience *170*, 731-741.

Clark, G.D., Zorumski, C.F., McNeil, R.S., Happel, L.T., Ovella, T., McGuire, S., Bix, G.J., and Swann, J.W. (2000). Neuronal platelet-activating factor receptor signal transduction involves a pertussis toxin-sensitive G-protein. Neurochem Res *25*, 603-611.

Connolly, E.S., Jr., Winfree, C.J., Stern, D.M., Solomon, R.A., and Pinsky, D.J. (1996). Procedural and strain-related variables significantly affect outcome in a murine model of focal cerebral ischemia. Neurosurgery *38*, 523-531; discussion 532.

Cuadrado, E., Rosell, A., Colome, N., Hernandez-Guillamon, M., Garcia-Berrocoso, T., Ribo, M., Alcazar, A., Ortega-Aznar, A., Salinas, M., Canals, F.*, et al.* (2010). The proteome of human brain after ischemic stroke. J Neuropathol Exp Neurol *69*, 1105-1115.

Davis, P.F., Ozias, M.K., Carlson, S.E., Reed, G.A., Winter, M.K., McCarson, K.E., and Levant, B. (2010). Dopamine receptor alterations in female rats with diet-induced decreased brain docosahexaenoic acid (DHA): interactions with reproductive status. Nutr Neurosci *13*, 161-169.

Dayon, L., Turck, N., Garci-Berrocoso, T., Walter, N., Burkhard, P.R., Vilalta, A., Sahuquillo, J., Montaner, J., and Sanchez, J.C. (2011). Brain extracellular fluid protein changes in acute stroke patients. J Proteome Res *10*, 1043-1051.

Dennis, E.A. (2009). Lipidomics joins the omics evolution. Proc Natl Acad Sci U S A *106*, 2089-2090.
Dingledine, R., Borges, K., Bowie, D., and Traynelis, S.F. (1999). The glutamate receptor ion channels. Pharmacol Rev *51*, 7-61.
Dirnagl, U., Iadecola, C., and Moskowitz, M.A. (1999). Pathobiology of ischaemic stroke: an integrated view. Trends Neurosci *22*, 391-397.
Dong, H.W., Swanson, L.W., Chen, L., Fanselow, M.S., and Toga, A.W. (2009). Genomic-anatomic evidence for distinct functional domains in hippocampal field CA1. Proc Natl Acad Sci U S A *106*, 11794-11799.
Doyle, K.P., Simon, R.P., and Stenzel-Poore, M.P. (2008). Mechanisms of ischemic brain damage. Neuropharmacology *55*, 310-318.
Ejsing, C.S., Sampaio, J.L., Surendranath, V., Duchoslav, E., Ekroos, K., Klemm, R.W., Simons, K., and Shevchenko, A. (2009). Global analysis of the yeast lipidome by quantitative shotgun mass spectrometry. Proc Natl Acad Sci U S A *106*, 2136-2141.
Fang, W., Geng, X., Deng, Y., Li, Y., Shang, E., Cen, J., and Lv, P. (2011). Platelet activating factor induces blood brain barrier permeability alteration in vitro. J Neuroimmunol *230*, 42-47.
Farooqui, A.A., and Horrocks, L.A. (2001). Plasmalogens: workhorse lipids of membranes in normal and injured neurons and glia. Neuroscientist *7*, 232-245.
Farooqui, A.A., and Horrocks, L.A. (2006). Phospholipase A2-generated lipid mediators in the brain: the good, the bad, and the ugly. Neuroscientist *12*, 245-260.
Farooqui, A.A., Horrocks, L.A., and Farooqui, T. (2000). Deacylation and reacylation of neural membrane glycerophospholipids. J Mol Neurosci *14*, 123-135.
Farooqui, A.A., Horrocks, L.A., and Farooqui, T. (2007a). Interactions between neural membrane glycerophospholipid and sphingolipid mediators: a recipe for neural cell survival or suicide. J Neurosci Res *85*, 1834-1850.
Farooqui, A.A., Horrocks, L.A., and Farooqui, T. (2007b). Modulation of inflammation in brain: a matter of fat. J Neurochem *101*, 577-599.
Farooqui, A.A., Ong, W.Y., and Horrocks, L.A. (2006). Inhibitors of brain phospholipase A2 activity: their neuropharmacological effects and therapeutic importance for the treatment of neurologic disorders. Pharmacol Rev *58*, 591-620.
Fenn, J.B., Mann, M., Meng, C.K., Wong, S.F., and Whitehouse, C.M. (1989). Electrospray ionization for mass spectrometry of large biomolecules. Science *246*, 64-71.
Fischer, I., Romano-Clarke, G., and Grynspan, F. (1991). Calpain-mediated proteolysis of microtubule associated proteins MAP1B and MAP2 in developing brain. Neurochem Res *16*, 891-898.
Fuchs, B., and Schiller, J. (2009). Recent developments of useful MALDI matrices for the mass spectrometric characterization of apolar compounds. Current Organic Chemistry *13*, 1664-1681.
Fuchs, B., Suss, R., and Schiller, J. (2010). An update of MALDI-TOF mass spectrometry in lipid research. Prog Lipid Res *49*, 450-475.

Fuxe, K., Dahlstrom, A.B., Jonsson, G., Marcellino, D., Guescini, M., Dam, M., Manger, P., and Agnati, L. (2010). The discovery of central monoamine neurons gave volume transmission to the wired brain. Prog Neurobiol *90*, 82-100.

Garcia, J.H., Liu, K.F., Yoshida, Y., Lian, J., Chen, S., and del Zoppo, G.J. (1994). Influx of leukocytes and platelets in an evolving brain infarct (Wistar rat). Am J Pathol *144*, 188-199.

Gelderblom, M., Leypoldt, F., Steinbach, K., Behrens, D., Choe, C.U., Siler, D.A., Arumugam, T.V., Orthey, E., Gerloff, C., Tolosa, E.*, et al.* (2009). Temporal and spatial dynamics of cerebral immune cell accumulation in stroke. Stroke *40*, 1849-1857.

Gerfen, C.R. (2000). Molecular effects of dopamine on striatal-projection pathways. Trends Neurosci *23*, S64-70.

Gerlai, R. (1996). Gene-targeting studies of mammalian behavior: is it the mutation or the background genotype? Trends Neurosci *19*, 177-181.

Gomez-Munoz, A., O'Brien, L., Hundal, R., and Steinbrecher, U.P. (1999). Lysophosphatidylcholine stimulates phospholipase D activity in mouse peritoneal macrophages. J Lipid Res *40*, 988-993.

Gorelick, P.B., Scuteri, A., Black, S.E., Decarli, C., Greenberg, S.M., Iadecola, C., Launer, L.J., Laurent, S., Lopez, O.L., Nyenhuis, D.*, et al.* (2011). Vascular Contributions to Cognitive Impairment and Dementia: A Statement for Healthcare Professionals From the American Heart Association/American Stroke Association. Stroke.

Han, X., Holtzman, D.M., and McKeel, D.W., Jr. (2001). Plasmalogen deficiency in early Alzheimer's disease subjects and in animal models: molecular characterization using electrospray ionization mass spectrometry. J Neurochem *77*, 1168-1180.

Hara, H., Huang, P.L., Panahian, N., Fishman, M.C., and Moskowitz, M.A. (1996). Reduced brain edema and infarction volume in mice lacking the neuronal isoform of nitric oxide synthase after transient MCA occlusion. J Cereb Blood Flow Metab *16*, 605-611.

Hillenkamp, F., Karas, M., Beavis, R.C., and Chait, B.T. (1991). Matrix-assisted laser desorption/ionization mass spectrometry of biopolymers. Anal Chem *63*, 1193A-1203A.

Hossmann, K.A. (1996). Periinfarct depolarizations. Cerebrovasc Brain Metab Rev *8*, 195-208.

Hostettler, M.E., and Carlson, S.L. (2002). PAF antagonist treatment reduces pro-inflammatory cytokine mRNA after spinal cord injury. Neuroreport *13*, 21-24.

Hou, W., Zhou, H., Elisma, F., Bennett, S.A., and Figeys, D. (2008). Technological developments in lipidomics. Brief Funct Genomic Proteomic *7*, 395-409.

HSF (2006). Tipping the Scales of Progress: Heart Disease In Canada 2006, H.a.S.F.o. Canada, ed.

Huang, J., Upadhyay, U.M., and Tamargo, R.J. (2006). Inflammation in stroke and focal cerebral ischemia. Surg Neurol *66*, 232-245.

Huang, Y.H., Schafer-Elinder, L., Wu, R., Claesson, H.E., and Frostegard, J. (1999). Lysophosphatidylcholine (LPC) induces proinflammatory cytokines by a

platelet-activating factor (PAF) receptor-dependent mechanism. Clin Exp Immunol *116*, 326-331.
Igbavboa, U., Hamilton, J., Kim, H.Y., Sun, G.Y., and Wood, W.G. (2002). A new role for apolipoprotein E: modulating transport of polyunsaturated phospholipid molecular species in synaptic plasma membranes. J Neurochem *80*, 255-261.
Ivanova, P.T., Milne, S.B., Forrester, J.S., and Brown, H.A. (2004). LIPID arrays: new tools in the understanding of membrane dynamics and lipid signaling. Mol Interv *4*, 86-96.
Izumi, T., and Shimizu, T. (1995). Platelet-activating factor receptor: gene expression and signal transduction. Biochim Biophys Acta *1259*, 317-333.
Jiang, S.X., Whitehead, S., Aylsworth, A., Slinn, J., Zurakowski, B., Chan, K., Li, J., and Hou, S.T. (2010). Neuropilin 1 directly interacts with Fer kinase to mediate semaphorin 3A-induced death of cortical neurons. J Biol Chem *285*, 9908-9918.
Johnson, G.V., Jope, R.S., and Binder, L.I. (1989). Proteolysis of tau by calpain. Biochem Biophys Res Commun *163*, 1505-1511.
Katchanov, J., Waeber, C., Gertz, K., Gietz, A., Winter, B., Bruck, W., Dirnagl, U., Veh, R.W., and Endres, M. (2003). Selective neuronal vulnerability following mild focal brain ischemia in the mouse. Brain Pathol *13*, 452-464.
Katchman, A.N., and Hershkowitz, N. (1993). Early anoxia-induced vesicular glutamate release results from mobilization of calcium from intracellular stores. J Neurophysiol *70*, 1-7.
Kitagawa, K., Matsumoto, M., Yang, G., Mabuchi, T., Yagita, Y., Hori, M., and Yanagihara, T. (1998). Cerebral ischemia after bilateral carotid artery occlusion and intraluminal suture occlusion in mice: evaluation of the patency of the posterior communicating artery. J Cereb Blood Flow Metab *18*, 570-579.
Koizumi, S., Yamamoto, S., Hayasaka, T., Konishi, Y., Yamaguchi-Okada, M., Goto-Inoue, N., Sugiura, Y., Setou, M., and Namba, H. (2010). Imaging mass spectrometry revealed the production of lyso-phosphatidylcholine in the injured ischemic rat brain. Neuroscience *168*, 219-225.
Krishnaswamy, A., Klein, J.P., and Kapadia, S.R. (2010). Clinical cerebrovascular anatomy. Catheter Cardiovasc Interv *75*, 530-539.
Kumar, R., Harvey, S.A., Kester, M., Hanahan, D.J., and Olson, M.S. (1988). Production and effects of platelet-activating factor in the rat brain. Biochim Biophys Acta *963*, 375-383.
Lagarde, M., Bernoud, N., Brossard, N., Lemaitre-Delaunay, D., Thies, F., Croset, M., and Lecerf, J. (2001). Lysophosphatidylcholine as a preferred carrier form of docosahexaenoic acid to the brain. J Mol Neurosci *16*, 201-204; discussion 215-221.
Lamaziere, A., Richard, D., Barbe, U., Kefi, K., Bausero, P., Wolf, C., and Visioli, F. (2011). Differential distribution of DHA-phospholipids in rat brain after feeding: A lipidomic approach. Prostaglandins Leukot Essent Fatty Acids *84*, 7-11.
Lambeau, G., Barhanin, J., Schweitz, H., Qar, J., and Lazdunski, M. (1989). Identification and properties of very high affinity brain membrane-binding sites

for a neurotoxic phospholipase from the taipan venom. J Biol Chem *264*, 11503-11510.
Lees, K.R., Bluhmki, E., von Kummer, R., Brott, T.G., Toni, D., Grotta, J.C., Albers, G.W., Kaste, M., Marler, J.R., Hamilton, S.A.*, et al.* (2010). Time to treatment with intravenous alteplase and outcome in stroke: an updated pooled analysis of ECASS, ATLANTIS, NINDS, and EPITHET trials. Lancet *375*, 1695-1703.
Lin, P., and Ye, R.D. (2003). The lysophospholipid receptor G2A activates a specific combination of G proteins and promotes apoptosis. J Biol Chem *278*, 14379-14386.
Lin, T.N., Wang, Q., Simonyi, A., Chen, J.J., Cheung, W.M., He, Y.Y., Xu, J., Sun, A.Y., Hsu, C.Y., and Sun, G.Y. (2004). Induction of secretory phospholipase A2 in reactive astrocytes in response to transient focal cerebral ischemia in the rat brain. J Neurochem *90*, 637-645.
Lindsberg, P.J., Yue, T.L., Frerichs, K.U., Hallenbeck, J.M., and Feuerstein, G. (1990). Evidence for platelet-activating factor as a novel mediator in experimental stroke in rabbits. Stroke *21*, 1452-1457.
Lohmann, C., Schachmann, E., Dandekar, T., Villmann, C., and Becker, C.M. (2010). Developmental profiling by mass spectrometry of phosphocholine containing phospholipids in the rat nervous system reveals temporo-spatial gradients. J Neurochem *114*, 1119-1134.
Lowry, O.H., Passonneau, J.V., Hasselberger, F.X., and Schulz, D.W. (1964). Effect of Ischemia on Known Substrates and Cofactors of the Glycolytic Pathway in Brain. J Biol Chem *239*, 18-30.
Luster, A.D., Alon, R., and von Andrian, U.H. (2005). Immune cell migration in inflammation: present and future therapeutic targets. Nat Immunol *6*, 1182-1190.
Maclennan, K.M., Smith, P.F., and Darlington, C.L. (1996). Platelet-activating factor in the CNS. Prog Neurobiol *50*, 585-596.
Majno, G., and Joris, I. (1995). Apoptosis, oncosis, and necrosis. An overview of cell death. Am J Pathol *146*, 3-15.
Marathe, G.K., Silva, A.R., de Castro Faria Neto, H.C., Tjoelker, L.W., Prescott, S.M., Zimmerman, G.A., and McIntyre, T.M. (2001). Lysophosphatidylcholine and lyso-PAF display PAF-like activity derived from contaminating phospholipids. J Lipid Res *42*, 1430-1437.
Marcheselli, V.L., Hong, S., Lukiw, W.J., Tian, X.H., Gronert, K., Musto, A., Hardy, M., Gimenez, J.M., Chiang, N., Serhan, C.N.*, et al.* (2003). Novel docosanoids inhibit brain ischemia-reperfusion-mediated leukocyte infiltration and pro-inflammatory gene expression. J Biol Chem *278*, 43807-43817.
Martin, R.L., Lloyd, H.G., and Cowan, A.I. (1994). The early events of oxygen and glucose deprivation: setting the scene for neuronal death? Trends Neurosci *17*, 251-257.
Matsuzawa, A., Murakami, M., Atsumi, G., Imai, K., Prados, P., Inoue, K., and Kudo, I. (1996). Release of secretory phospholipase A2 from rat neuronal cells and its possible function in the regulation of catecholamine secretion. Biochem J *318 (Pt 2)*, 701-709.

Mayevsky, A., and Chance, B. (1975). Metabolic responses of the awake cerebral cortex to anoxia hypoxia spreading depression and epileptiform activity. Brain Res *98*, 149-165.
McNamara, R.K. (2010). DHA deficiency and prefrontal cortex neuropathology in recurrent affective disorders. J Nutr *140*, 864-868.
McNamara, R.K., Able, J., Jandacek, R., Rider, T., and Tso, P. (2009). Inbred C57BL/6J and DBA/2J mouse strains exhibit constitutive differences in regional brain fatty acid composition. Lipids *44*, 1-8.
McNamara, R.K., Able, J., Jandacek, R., Rider, T., Tso, P., Eliassen, J.C., Alfieri, D., Weber, W., Jarvis, K., DelBello, M.P.*, et al.* (2010). Docosahexaenoic acid supplementation increases prefrontal cortex activation during sustained attention in healthy boys: a placebo-controlled, dose-ranging, functional magnetic resonance imaging study. Am J Clin Nutr *91*, 1060-1067.
Mehta, S.L., Manhas, N., and Raghubir, R. (2007). Molecular targets in cerebral ischemia for developing novel therapeutics. Brain Res Rev *54*, 34-66.
Mies, G., Iijima, T., and Hossmann, K.A. (1993). Correlation between peri-infarct DC shifts and ischaemic neuronal damage in rat. Neuroreport *4*, 709-711.
Mori, M., Aihara, M., Kume, K., Hamanoue, M., Kohsaka, S., and Shimizu, T. (1996). Predominant expression of platelet-activating factor receptor in the rat brain microglia. J Neurosci *16*, 3590-3600.
Moser, M.B., and Moser, E.I. (1998). Functional differentiation in the hippocampus. Hippocampus *8*, 608-619.
Nakamura, M., Honda, Z., Izumi, T., Sakanaka, C., Mutoh, H., Minami, M., Bito, H., Seyama, Y., Matsumoto, T., Noma, M.*, et al.* (1991). Molecular cloning and expression of platelet-activating factor receptor from human leukocytes. J Biol Chem *266*, 20400-20405.
Network, C.S. (2011). The Quality of Stroke Care in Canada.
Nishida, K., and Markey, S.P. (1996). Platelet-activating factor in brain regions after transient ischemia in gerbils. Stroke *27*, 514-518; discussion 518-519.
Ohshima, N., Ishii, S., Izumi, T., and Shimizu, T. (2002). Receptor-dependent metabolism of platelet-activating factor in murine macrophages. J Biol Chem *277*, 9722-9727.
Perry, S.W., Hamilton, J.A., Tjoelker, L.W., Dbaibo, G., Dzenko, K.A., Epstein, L.G., Hannun, Y., Whittaker, J.S., Dewhurst, S., and Gelbard, H.A. (1998). Platelet-activating factor receptor activation. An initiator step in HIV-1 neuropathogenesis. J Biol Chem *273*, 17660-17664.
Pike, L.J., Han, X., Chung, K.N., and Gross, R.W. (2002). Lipid rafts are enriched in arachidonic acid and plasmenylethanolamine and their composition is independent of caveolin-1 expression: a quantitative electrospray ionization/mass spectrometric analysis. Biochemistry *41*, 2075-2088.
Pinard, E., Nallet, H., MacKenzie, E.T., Seylaz, J., and Roussel, S. (2002). Penumbral microcirculatory changes associated with peri-infarct depolarizations in the rat. Stroke *33*, 606-612.
Piomelli, D., Astarita, G., and Rapaka, R. (2007). A neuroscientist's guide to lipidomics. Nat Rev Neurosci *8*, 743-754.

Potter, D.A., Tirnauer, J.S., Janssen, R., Croall, D.E., Hughes, C.N., Fiacco, K.A., Mier, J.W., Maki, M., and Herman, I.M. (1998). Calpain regulates actin remodeling during cell spreading. J Cell Biol *141*, 647-662.

Pulsinelli, W.A., and Brierley, J.B. (1979). A new model of bilateral hemispheric ischemia in the unanesthetized rat. Stroke *10*, 267-272.

Qin, Z.X., Zhu, H.Y., and Hu, Y.H. (2009). Effects of lysophosphatidylcholine on beta-amyloid-induced neuronal apoptosis. Acta Pharmacol Sin *30*, 388-395.

Raichle, M.E. (1983). The pathophysiology of brain ischemia. Ann Neurol *13*, 2-10.

Rehncrona, S., Westerberg, E., Akesson, B., and Siesjo, B.K. (1982). Brain cortical fatty acids and phospholipids during and following complete and severe incomplete ischemia. J Neurochem *38*, 84-93.

Rink, C., and Khanna, S. (2011). Significance of brain tissue oxygenation and the arachidonic acid cascade in stroke. Antioxid Redox Signal *14*, 1889-1903.

Rodrigues, D.H., Lacerda-Queiroz, N., de Miranda, A.S., Fagundes, C.T., Campos, R.D., Arantes, R.E., Vilela Mde, C., Rachid, M.A., Teixeira, M.M., and Teixeira, A.L. (2011). Absence of PAF receptor alters cellular infiltrate but not rolling and adhesion of leukocytes in experimental autoimmune encephalomyelitis. Brain Res *1385*, 298-306.

Rodriguez De Turco, E.B., Jackson, F.R., DeCoster, M.A., Kolko, M., and Bazan, N.G. (2002). Glutamate signalling and secretory phospholipase A2 modulate the release of arachidonic acid from neuronal membranes. J Neurosci Res *68*, 558-567.

Rothwell, P.M., Algra, A., and Amarenco, P. (2011). Medical treatment in acute and long-term secondary prevention after transient ischaemic attack and ischaemic stroke. Lancet *377*, 1681-1692.

Rothwell, P.M., and Warlow, C.P. (2005). Timing of TIAs preceding stroke: time window for prevention is very short. Neurology *64*, 817-820.

Ryan, S.D., Harris, C.S., Carswell, C.L., Baenziger, J.E., and Bennett, S.A. (2008). Heterogeneity in the sn-1 carbon chain of platelet-activating factor glycerophospholipids determines pro- or anti-apoptotic signaling in primary neurons. J Lipid Res *49*, 2250-2258.

Ryan, S.D., Harris, C.S., Mo, F., Lee, H., Hou, S.T., Bazan, N.G., Haddad, P.S., Arnason, J.T., and Bennett, S.A. (2007). Platelet activating factor-induced neuronal apoptosis is initiated independently of its G-protein coupled PAF receptor and is inhibited by the benzoate orsellinic acid. J Neurochem *103*, 88-97.

Ryan, S.D., Whitehead, S.N., Swayne, L., Moffat, T.C., Hou, W., Ethier, M., Bourgeois, A.J.G., Rashidian, J., P. Blanchard, A., Fraser, P.E.*, et al.* (2009). Disruption of alkylacylglycerophosphocholines by amyloid-{Beta}42 signals tau hyperphosphorylation and compromises neuronal viability. Proc Natl Acad Sci U S A *106*, 20936-20941.

Samuelsson, B. (1983). Leukotrienes: mediators of immediate hypersensitivity reactions and inflammation. Science *220*, 568-575.

Sanchez-Mejia, R.O., Newman, J.W., Toh, S., Yu, G.Q., Zhou, Y., Halabisky, B., Cisse, M., Scearce-Levie, K., Cheng, I.H., Gan, L.*, et al.* (2008). Phospholipase A2 reduction ameliorates cognitive deficits in a mouse model of Alzheimer's disease. Nat Neurosci *11*, 1311-1318.

Sandoval, K.E., and Witt, K.A. (2008). Blood-brain barrier tight junction permeability and ischemic stroke. Neurobiol Dis *32*, 200-219.
Saver, J.L. (2006). Time is brain--quantified. Stroke *37*, 263-266.
Schilling, T., Lehmann, F., Ruckert, B., and Eder, C. (2004). Physiological mechanisms of lysophosphatidylcholine-induced de-ramification of murine microglia. J Physiol *557*, 105-120.
Sharkey, J., and Butcher, S.P. (1995). Characterisation of an experimental model of stroke produced by intracerebral microinjection of endothelin-1 adjacent to the rat middle cerebral artery. J Neurosci Methods *60*, 125-131.
Sicard, K.M., and Fisher, M. (2009). Animal models of focal brain ischemia. Exp Transl Stroke Med *1*, 7.
Silver, I.A., and Erecinska, M. (1990). Intracellular and extracellular changes of [Ca2+] in hypoxia and ischemia in rat brain in vivo. J Gen Physiol *95*, 837-866.
Sun, G.Y., Shelat, P.B., Jensen, M.B., He, Y., Sun, A.Y., and Simonyi, A. (2010). Phospholipases A2 and inflammatory responses in the central nervous system. Neuromolecular Med *12*, 133-148.
Sun, G.Y., Xu, J., Jensen, M.D., and Simonyi, A. (2004). Phospholipase A2 in the central nervous system: implications for neurodegenerative diseases. J Lipid Res *45*, 205-213.
Tillman, T.S., and Cascio, M. (2003). Effects of membrane lipids on ion channel structure and function. Cell Biochem Biophys *38*, 161-190.
Traystman, R.J. (2003). Animal models of focal and global cerebral ischemia. ILAR J *44*, 85-95.
van Meeteren, L.A., and Moolenaar, W.H. (2007). Regulation and biological activities of the autotaxin-LPA axis. Prog Lipid Res *46*, 145-160.
Wang, Q., Tang, X.N., and Yenari, M.A. (2007). The inflammatory response in stroke. J Neuroimmunol *184*, 53-68.
Wassall, S.R., and Stillwell, W. (2008). Docosahexaenoic acid domains: the ultimate non-raft membrane domain. Chem Phys Lipids *153*, 57-63.
Weaver, J.G., Tarze, A., Moffat, T.C., Lebras, M., Deniaud, A., Brenner, C., Bren, G.D., Morin, M.Y., Phenix, B.N., Dong, L.*, et al.* (2005). Inhibition of adenine nucleotide translocator pore function and protection against apoptosis in vivo by an HIV protease inhibitor. J Clin Invest *115*, 1828-1838.
Whitehead, S.N., Chan, K.H., Gangaraju, S., Slinn, J., Li, J., and Hou, S.T. (2011). Imaging Mass Spectrometry Detection of Gangliosides Species in the Mouse Brain following Transient Focal Cerebral Ischemia and Long-Term Recovery. PLoS One *6*, e20808.
Whitehead, S.N., Gangaraju, S., Slinn, J., and Hou, S.T. (2010). Transient and bilateral increase in Neuropilin-1, Fer kinase and collapsin response mediator proteins within membrane rafts following unilateral occlusion of the middle cerebral artery in mouse. Brain Res *1344*, 209-216.
Whitehead, S.N., Hou, W., Ethier, M., Smith, J.C., Bourgeois, A., Denis, R., Bennett, S.A., and Figeys, D. (2007). Identification and quantitation of changes in the platelet activating factor family of glycerophospholipids over the course of neuronal differentiation by high-performance liquid chromatography

electrospray ionization tandem mass spectrometry. Anal Chem *79*, 8539-8548.
Williams, V., and Grossman, R.G. (1970). Ultrastructure of cortical synapses after failure of presynaptic activity in ischemia. Anat Rec *166*, 131-141.
Wojda, U., Salinska, E., and Kuznicki, J. (2008). Calcium ions in neuronal degeneration. IUBMB Life *60*, 575-590.

6. Appendix 1

A1.1 Lipid differences between anterior and posterior regions of uninjured frontal cortex of PAFR$^{-/-}$ mice.

Heatmap analyses, as outlined in 3.1.1, revealed two glycerophosphocholine lipid second messenger species, PC(O-18:4/0:0) and PC(P-18:0/0:0) that show altered abundance between anterior and posterior regions of uninjured cortex in PAFR null-mutant mice (Fig. A1.1a). Four species (Table 3.3.1), including one identified by heatmap analysis (PC(O-18:4/0:0)), show statistically significant alterations in abundance between these tissues as identified by paired t-test (Fig A1.1b).

Lipid Species	Mean Log_2PA_N x 10^6		Paired t-test p-value
	Anterior	Posterior	
PC(14:0/0:0)	5.60E+00	7.29E+00	0.0381
PC(O-18:4/0:0)	5.60E+00	3.87E+00	0.0243
PC(20:5/0:0)	4.71E+00	3.87E+00	0.0071
PC(O-18:0/2:0)	7.28E+00	6.07E+00	0.0357

Table A1.1. Lipid species that show significantly altered abundance between anterior and posterior regions of uninjured PAFR$^{-/-}$ frontal cortex by paired t-test.

A1.2 Lipid differences between anterior and posterior regions of uninjured striatum in the forebrain of PAFR$^{-/-}$ mice.

Heatmap analysis revealed no changes in glycerophosphocholine second messenger lipid levels between anterior and posterior regions of uninjured striatum in PAFR-/- brain (Fig. A1.2a), but eight lipids with statistically significant changes were revealed by paired t-test Table 3.3.2, Fig. A1.2b).

Figure A1.1a. Heatmap clustering of relative glycerophosphocholine lipid second messenger abundance between anterior and posterior regions of uninjured PAFR$^{-/-}$ frontal cortex. Small molecular weight glycerophosphocholine second messengers were identified by LC-ESI-MS. Data represent the number of standard deviations (Log_2A^*) by which the abundance of a given species in a given animal differs from the mean abundance of the whole population. * denotes species that show at least 1 standard deviation from the mean. These were considered significant and were prioritized for a second level of statistical analysis.

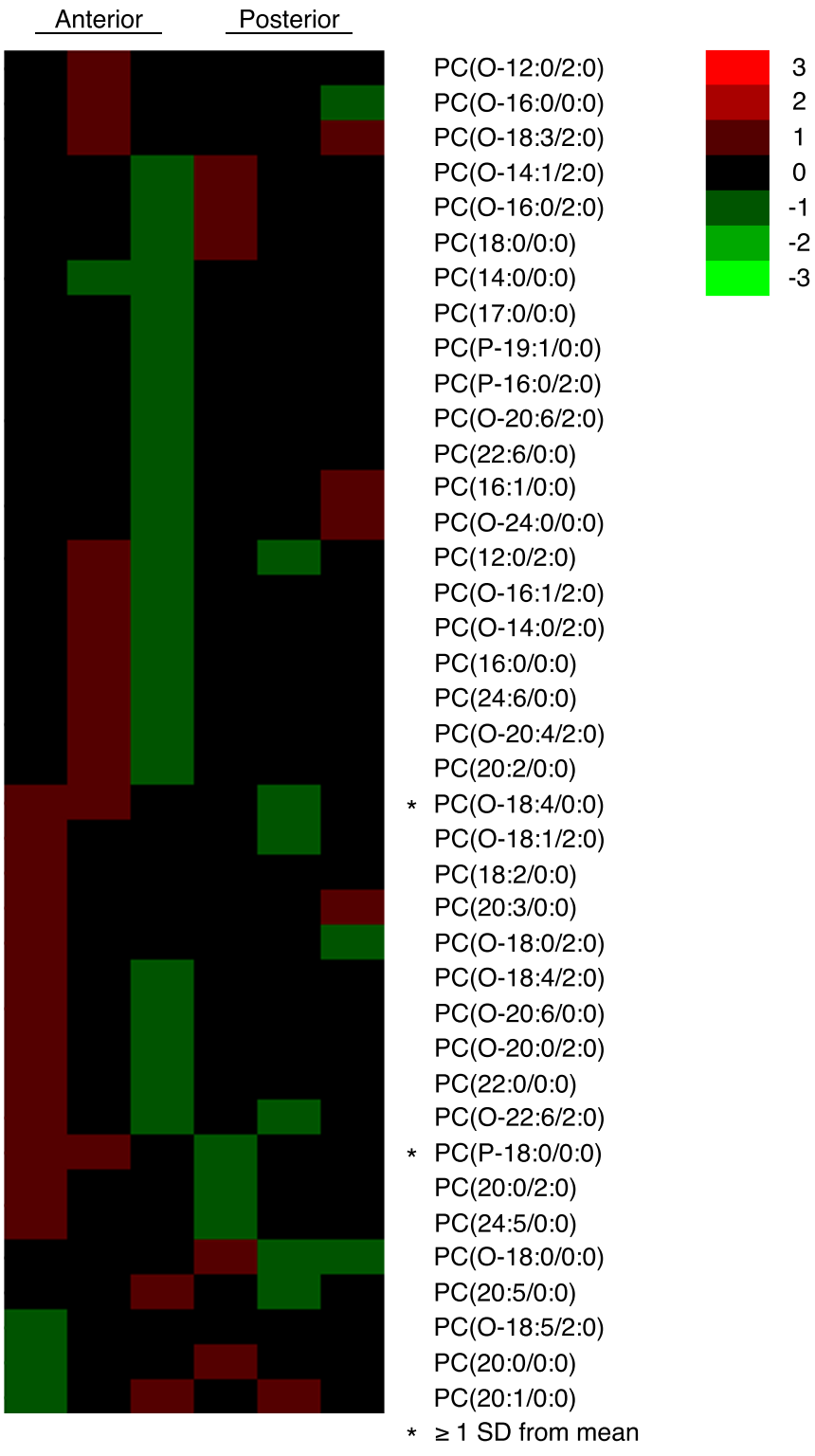
Anterior
Posterior
PC(O-12:0/2:0)
PC(O-16:0/0:0)
PC(O-18:3/2:0)
PC(O-14:1/2:0)
PC(O-16:0/2:0)
PC(18:0/0:0)
PC(14:0/0:0)
PC(17:0/0:0)
PC(P-19:1/0:0)
PC(P-16:0/2:0)
PC(O-20:6/2:0)
PC(22:6/0:0)
PC(16:1/0:0)
PC(O-24:0/0:0)
PC(12:0/2:0)
PC(O-16:1/2:0)
PC(O-14:0/2:0)
PC(16:0/0:0)
PC(24:6/0:0)
PC(O-20:4/2:0)
PC(20:2/0:0)
* PC(O-18:4/0:0)
PC(O-18:1/2:0)
PC(18:2/0:0)
PC(20:3/0:0)
PC(O-18:0/2:0)
PC(O-18:4/2:0)
PC(O-20:6/0:0)
PC(O-20:0/2:0)
PC(22:0/0:0)
PC(O-22:6/2:0)
* PC(P-18:0/0:0)
PC(20:0/2:0)
PC(24:5/0:0)
PC(O-18:0/0:0)
PC(20:5/0:0)
PC(O-18:5/2:0)
PC(20:0/0:0)
PC(20:1/0:0)
* ≥ 1 SD from mean
3
2
1
0
-1
-2
-3

Figure A1.1b. Anterior-posterior gradients of glycerophosphocholine lipid second messenger abundance in uninjured PAFR$^{-/-}$ frontal cortex. Small molecular weight glycerophosphocholine second messengers were identified by LC-ESI-MS. Log_2-transformed normalized peak areas (Log_2PA_N) for lipid species exhibiting a regional difference by heatmap analysis were further analyzed in the anterior and posterior regions of frontal cortex by paired t-test. *p<0.05. **p<0.01. ***p<0.005.

i. PC(14:0/0:0)

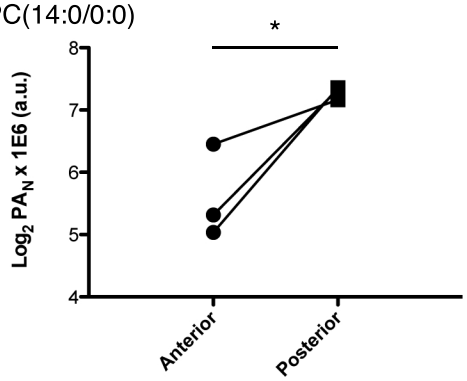

ii. PC(O-18:4/0:0)

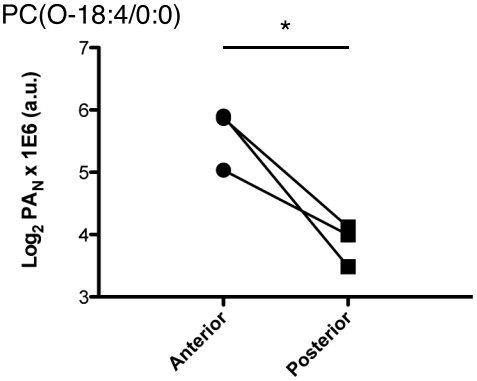

iii. PC(20:5/0:0)

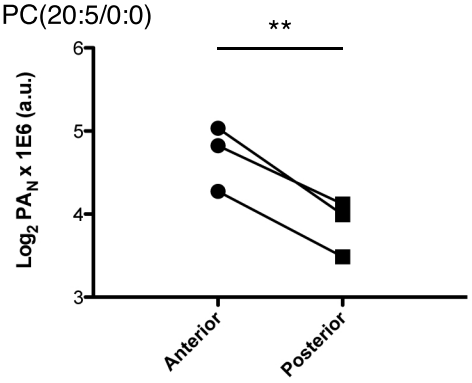

iv. PC(O-18:0/2:0)

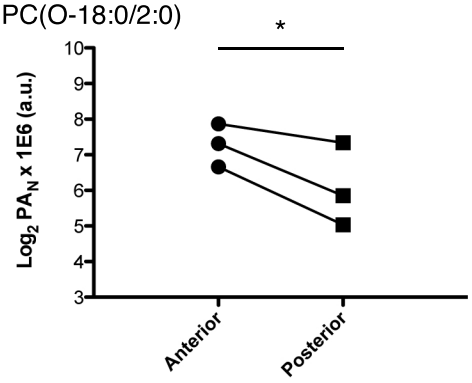

Figure A1.2a. Heatmap clustering of relative glycerophosphocholine lipid second messenger abundance between anterior and posterior regions of uninjured PAFR$^{-/-}$ striatum. Small molecular weight glycerophosphocholine second messengers were identified by LC-ESI-MS. Data represent the number of standard deviations (Log_2A^*) by which the abundance of a given species in a given animal differs from the mean abundance of the whole population. * denotes species that show at least 1 standard deviation from the mean. These were considered significant and were prioritized for a second level of statistical analysis.

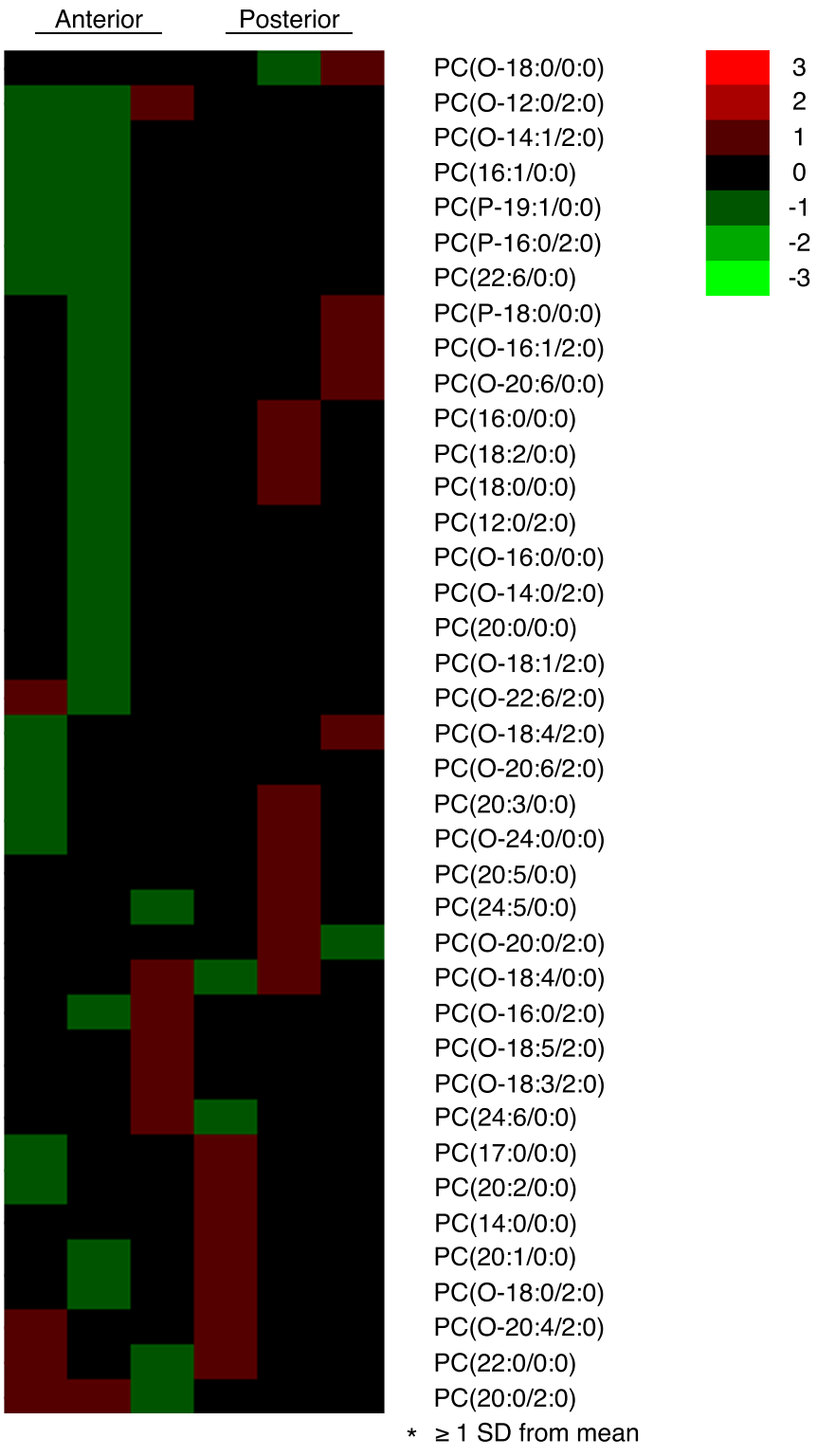
Anterior
Posterior
PC(O-18:0/0:0)
PC(O-12:0/2:0)
PC(O-14:1/2:0)
PC(16:1/0:0)
PC(P-19:1/0:0)
PC(P-16:0/2:0)
PC(22:6/0:0)
PC(P-18:0/0:0)
PC(O-16:1/2:0)
PC(O-20:6/0:0)
PC(16:0/0:0)
PC(18:2/0:0)
PC(18:0/0:0)
PC(12:0/2:0)
PC(O-16:0/0:0)
PC(O-14:0/2:0)
PC(20:0/0:0)
PC(O-18:1/2:0)
PC(O-22:6/2:0)
PC(O-18:4/2:0)
PC(O-20:6/2:0)
PC(20:3/0:0)
PC(O-24:0/0:0)
PC(20:5/0:0)
PC(24:5/0:0)
PC(O-20:0/2:0)
PC(O-18:4/0:0)
PC(O-16:0/2:0)
PC(O-18:5/2:0)
PC(O-18:3/2:0)
PC(24:6/0:0)
PC(17:0/0:0)
PC(20:2/0:0)
PC(14:0/0:0)
PC(20:1/0:0)
PC(O-18:0/2:0)
PC(O-20:4/2:0)
PC(22:0/0:0)
PC(20:0/2:0)
3
2
1
0
-1
-2
-3
* ≥ 1 SD from mean

Figure A1.2b. Anterior-posterior gradients of glycerophosphocholine lipid second messenger abundance in uninjured PAFR$^{-/-}$ striatum. Small molecular weight glycerophosphocholine second messengers were identified by LC-ESI-MS. Log_2-transformed normalized peak areas (Log_2PA_N) for lipid species exhibiting a regional difference by heatmap analysis were further analyzed in the anterior and posterior regions of striatum by paired t-test. *$p<0.05$. **$p<0.01$. ***$p<0.005$.

i. PC(O-16:1/2:0)

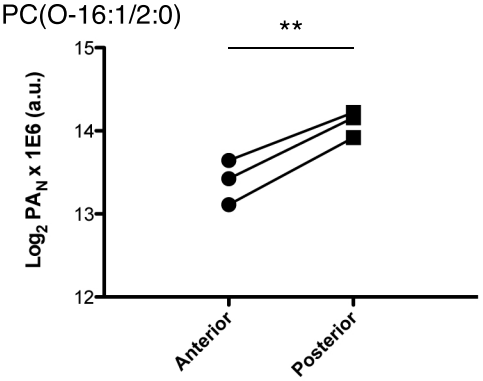

ii. PC(18:0/0:0)

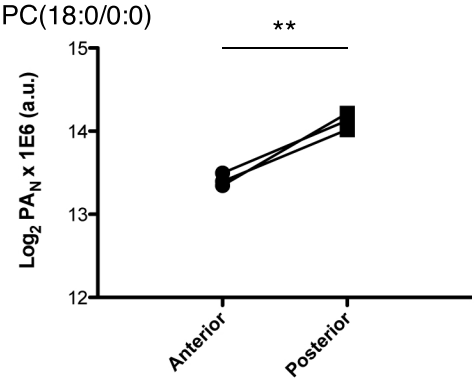

iii. PC(O-18:5/2:0)

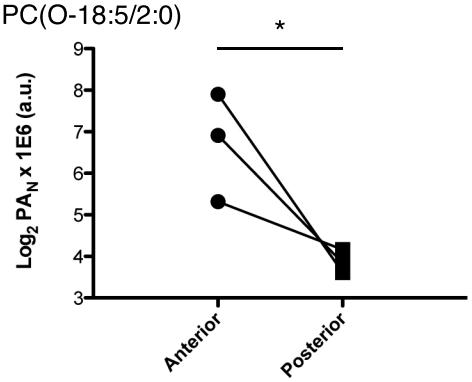

iv. PC(O-18:4/2:0)

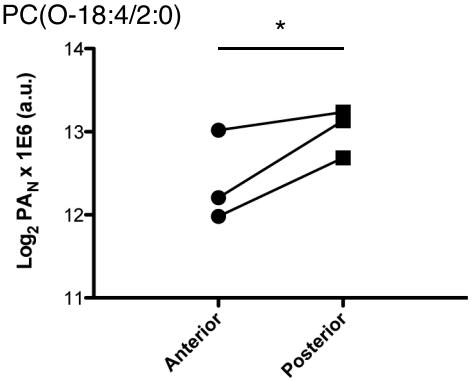

v. PC(20:3/0:0)

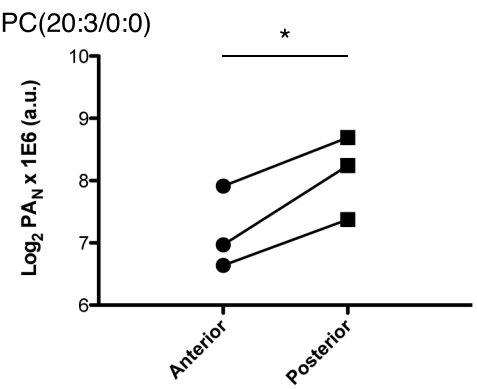

vi. PC(20:1/0:0)

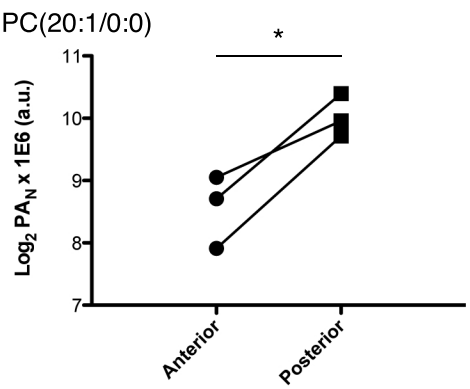

vii. PC(O-20:6/2:0)

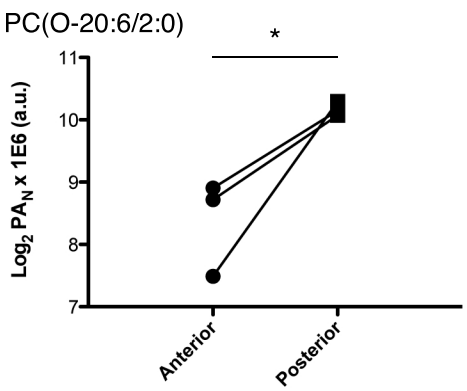

viii. PC(24:5/0:0)

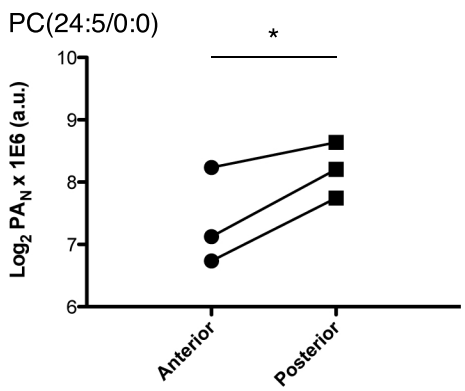

Lipid Species	Mean Log_2PA_N x 10^6		Paired t-test p-value
	Anterior	Posterior	
PC(O-16:1/2:0)	1.34E+01	1.41E+01	0.0046
PC(18:0/0:0)	1.34E+01	1.41E+01	0.0063
PC(O-18:5/2:0)	6.71E+00	3.87E+00	0.0449
PC(O-18:4/2:0)	1.24E+01	1.30E+01	0.0496
PC(20:3/0:0)	7.17E+00	8.10E+00	0.0163
PC(20:1/0:0)	8.56E+00	1.00E+01	0.0175
PC(O-20:6/2:0)	8.37E+00	1.02E+01	0.0350
PC(24:5/0:0)	7.36E+00	8.20E+00	0.0304

Table A1.2. Lipid species that show significantly altered abundance between anterior and posterior regions of uninjured $PAFR^{-/-}$ frontal striatum by paired t-test.

A1.3 Lipid differences between anterior regions of uninjured cortex and striatum in the forebrain of $PAFR^{-/-}$ mice.

Heatmap analysis revealed no changes in glycerophosphocholine second messenger lipid levels between anterior and posterior regions of uninjured striatum in PAFR-/- brain (Fig. A1.3a), but three lipids with statistically significant changes were revealed by paired t-test Table 3.3.3, Fig. A1.3b).

Lipid Species	Mean Log_2PA_N x 10^6		Paired t-test p-value
	Cortex	Striatum	
PC(O-18:0/0:0)	6.48E+00	4.64E+00	0.0089
PC(O-18:1/2:0)	1.11E+01	8.06E+00	0.0233
PC(20:0/2:0)	1.19E+01	9.98E+00	0.0353

Table A1.3. Lipid species that show significantly altered abundance between anterior regions of uninjured $PAFR^{-/-}$ frontal cortex and striatum by paired t-test.

Figure A1.3a. Heatmap clustering of relative glycerophosphocholine lipid second messenger abundance between anterior regions of uninjured PAFR$^{-/-}$ frontal cortex and striatum. Small molecular weight glycerophosphocholine second messengers were identified by LC-ESI-MS. Data represent the number of standard deviations (Log_2A^*) by which the abundance of a given species in a given animal differs from the mean abundance of the whole population. * denotes species that show at least 1 standard deviation from the mean. These were considered significant and were prioritized for a second level of statistical analysis.

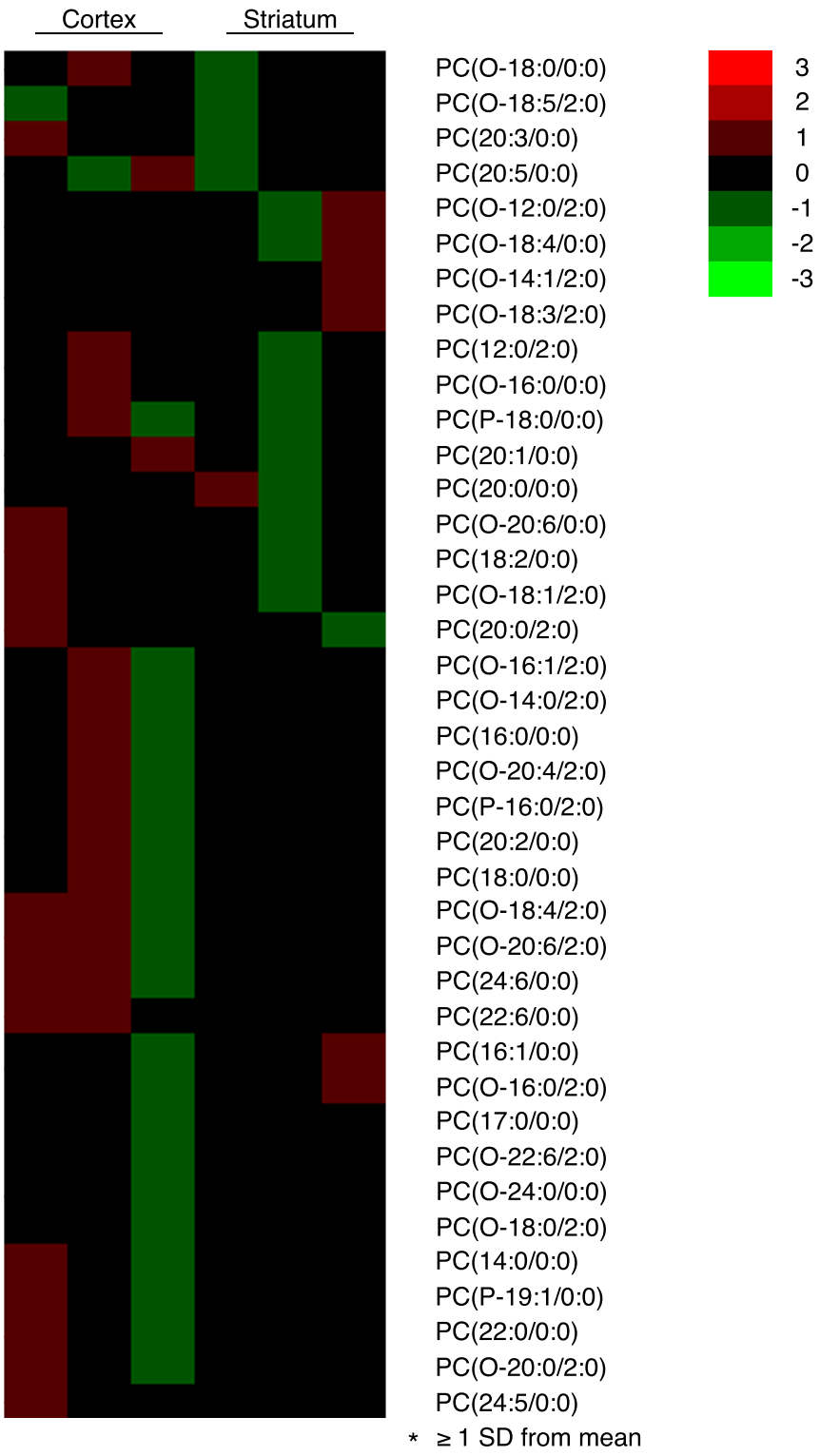
Cortex
Striatum
PC(O-18:0/0:0)
PC(O-18:5/2:0)
PC(20:3/0:0)
PC(20:5/0:0)
PC(O-12:0/2:0)
PC(O-18:4/0:0)
PC(O-14:1/2:0)
PC(O-18:3/2:0)
PC(12:0/2:0)
PC(O-16:0/0:0)
PC(P-18:0/0:0)
PC(20:1/0:0)
PC(20:0/0:0)
PC(O-20:6/0:0)
PC(18:2/0:0)
PC(O-18:1/2:0)
PC(20:0/2:0)
PC(O-16:1/2:0)
PC(O-14:0/2:0)
PC(16:0/0:0)
PC(O-20:4/2:0)
PC(P-16:0/2:0)
PC(20:2/0:0)
PC(18:0/0:0)
PC(O-18:4/2:0)
PC(O-20:6/2:0)
PC(24:6/0:0)
PC(22:6/0:0)
PC(16:1/0:0)
PC(O-16:0/2:0)
PC(17:0/0:0)
PC(O-22:6/2:0)
PC(O-24:0/0:0)
PC(O-18:0/2:0)
PC(14:0/0:0)
PC(P-19:1/0:0)
PC(22:0/0:0)
PC(O-20:0/2:0)
PC(24:5/0:0)
3
2
1
0
-1
-2
-3
* ≥ 1 SD from mean

Figure A1.3b. Medial-lateral gradients of glycerophosphocholine lipid second messenger abundance in anterior regions of uninjured PAFR$^{-/-}$ frontal cortex and striatum. Small molecular weight glycerophosphocholine second messengers were identified by LC-ESI-MS. Log_2-transformed normalized peak areas (Log_2PA_N) for lipid species exhibiting a regional difference by heatmap analysis were further analyzed in the anterior regions of frontal cortex and striatum by paired t-test. *p<0.05. **p<0.01. ***p<0.005.

i. PC(O-18:0/0:0)

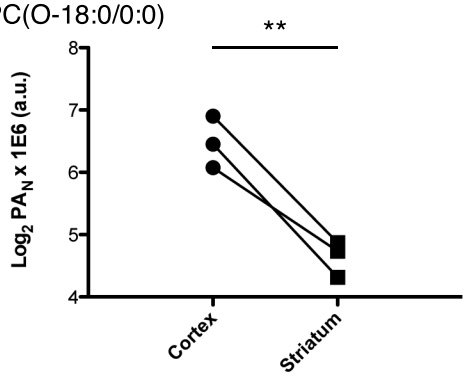

ii. PC(O-18:1/2:0)

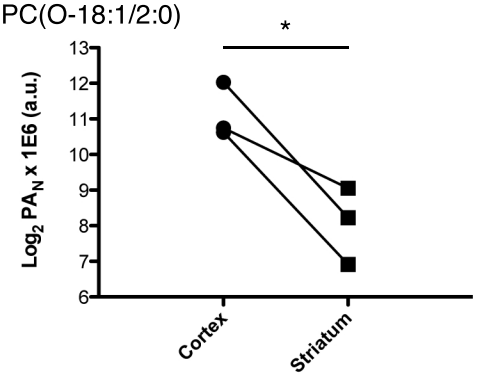

iii. PC(20:0/2:0)

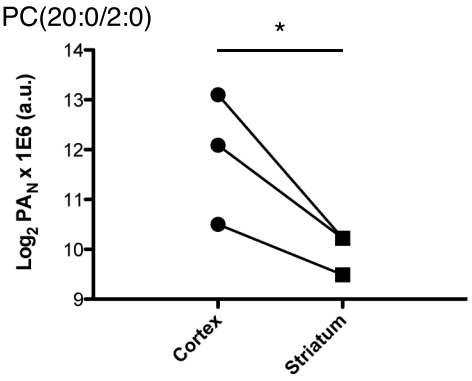

A1.4 Lipid differences between posterior regions of uninjured cortex and striatum in the forebrain of PAFR$^{-/-}$ mice.

Two glycerophosphocholine lipid second messenger species – PC(O-12:0/2:0) and PC(O-14:0/2:0) show differences in abundance between posterior regions of cortex and striatum in PAFR$^{-/-}$ brain by heatmap analysis (Fig. A1.4a). Eight different lipid species show statistically significant differences in abundance in these tissues by paired t-test analysis (Table 3.3.4, Fig. A1.4b).

Lipid Species	Mean Log_2PA_N x 10^6		Paired t-test p-value
	Cortex	Striatum	
PC(O-16:0/0:0)	5.54E+00	6.11E+00	0.0045
PC(O-14:1/2:0)	9.69E+00	1.03E+01	0.0083
PC(16:1/0:0)	1.05E+01	1.01E+01	0.0347
PC(P-18:0/0:0)	5.20E+00	7.04E+00	0.0145
PC(P-19:1/0:0)	9.60E+00	9.76E+00	0.0480
PC(O-18:5/2:0)	6.81E+00	3.87E+00	0.0265
PC(O-18:0/2:0)	6.07E+00	8.65E+00	0.0187
PC(20:0/0:0)	7.13E+00	8.86E+00	0.0010

Table A1.4. Lipid species that show significantly altered abundance between posterior regions of uninjured PAFR$^{-/-}$ frontal cortex and striatum by paired t-test.

Figure A1.4a. Heatmap clustering of relative glycerophosphocholine lipid second messenger abundance between posterior regions of uninjured PAFR$^{-/-}$ frontal cortex and striatum. Small molecular weight glycerophosphocholine second messengers were identified by LC-ESI-MS. Data represent the number of standard deviations (Log_2A^*) by which the abundance of a given species in a given animal differs from the mean abundance of the whole population. * denotes species that show at least 1 standard deviation from the mean. These were considered significant and were prioritized for a second level of statistical analysis.

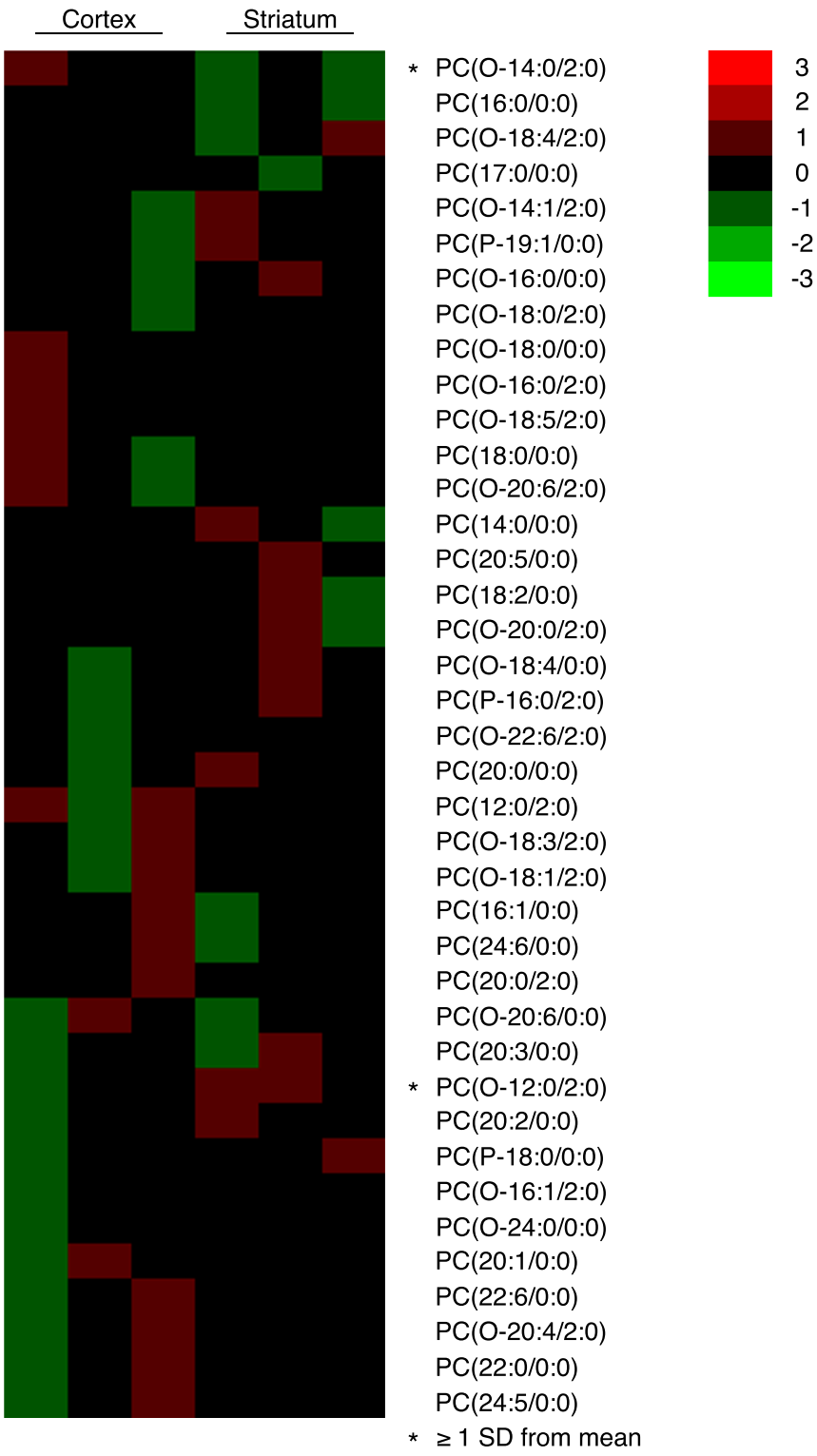
Cortex
Striatum
* PC(O-14:0/2:0)
PC(16:0/0:0)
PC(O-18:4/2:0)
PC(17:0/0:0)
PC(O-14:1/2:0)
PC(P-19:1/0:0)
PC(O-16:0/0:0)
PC(O-18:0/2:0)
PC(O-18:0/0:0)
PC(O-16:0/2:0)
PC(O-18:5/2:0)
PC(18:0/0:0)
PC(O-20:6/2:0)
PC(14:0/0:0)
PC(20:5/0:0)
PC(18:2/0:0)
PC(O-20:0/2:0)
PC(O-18:4/0:0)
PC(P-16:0/2:0)
PC(O-22:6/2:0)
PC(20:0/0:0)
PC(12:0/2:0)
PC(O-18:3/2:0)
PC(O-18:1/2:0)
PC(16:1/0:0)
PC(24:6/0:0)
PC(20:0/2:0)
PC(O-20:6/0:0)
PC(20:3/0:0)
* PC(O-12:0/2:0)
PC(20:2/0:0)
PC(P-18:0/0:0)
PC(O-16:1/2:0)
PC(O-24:0/0:0)
PC(20:1/0:0)
PC(22:6/0:0)
PC(O-20:4/2:0)
PC(22:0/0:0)
PC(24:5/0:0)
* ≥ 1 SD from mean
3
2
1
0
-1
-2
-3

Figure A1.4b. Medial-lateral gradients of glycerophosphocholine lipid second messenger abundance in posterior regions of uninjured PAFR$^{-/-}$ frontal cortex and striatum. Small molecular weight glycerophosphocholine second messengers were identified by LC-ESI-MS. Log_2-transformed normalized peak areas (Log_2PA_N) for lipid species exhibiting a regional difference by heatmap analysis were further analyzed in the posterior regions of frontal cortex and striatum by paired t-test. *p<0.05. **p<0.01. ***p<0.005.

i. PC(O-16:0/0:0)

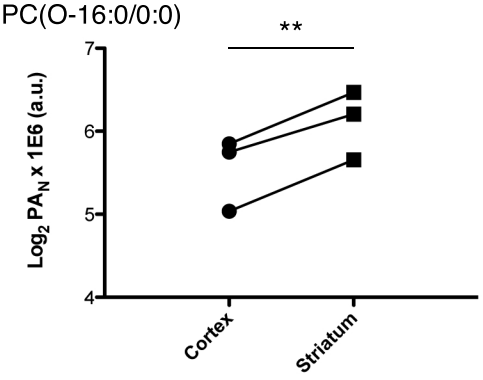

ii. PC(O-14:1/2:0)

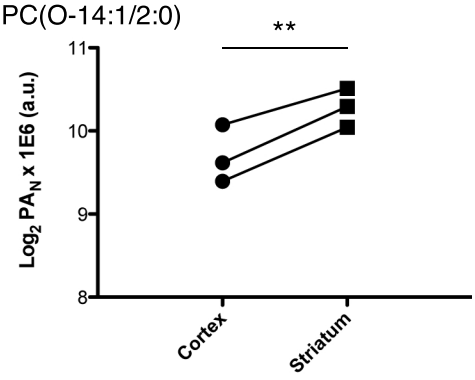

iii. PC(16:1/0:0)

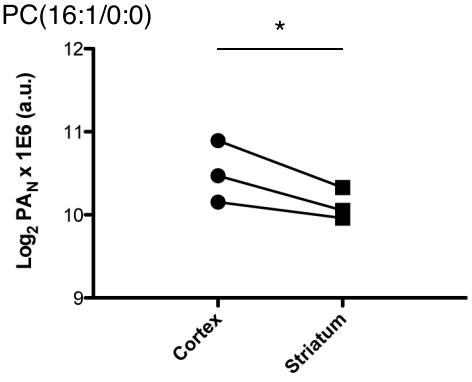

iv. PC(P-18:0/0:0)

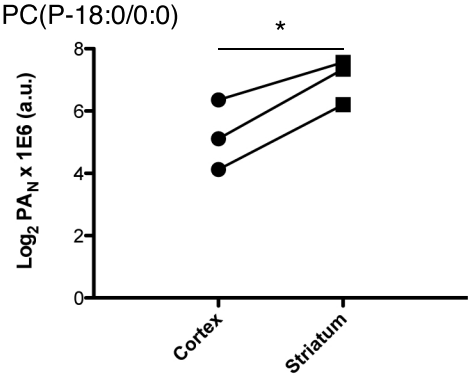

v. PC(P-19:1/0:0)

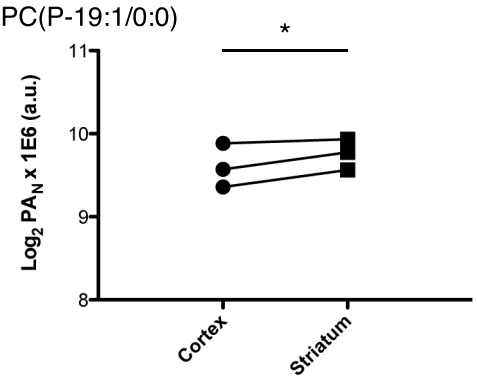

vi. PC(O-18:5/2:0)

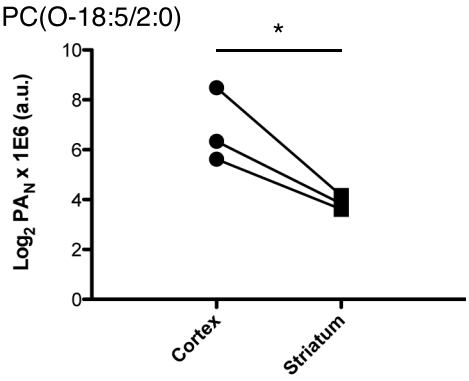

vii. PC(O-18:0/2:0)

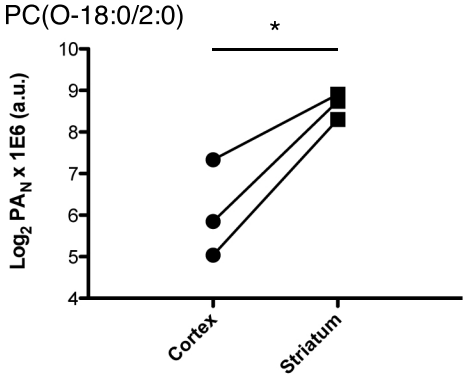

viii. PC(20:0/0:0)

